

**Ministry of Higher Education and Scientific Research  
University of Baghdad  
Institute of Laser for Postgraduate Studies**



# **Design and Analysis of All-Optical Plasmonic Logic Gates in C-Band Systems**

**A Thesis Submitted to the Institute of Laser for  
Postgraduate Studies, University of Baghdad in Partial  
Fulfillment of the Requirements for the Degree of  
Doctor of Philosophy in Laser / Electronic and  
Communication Engineering**

**By**

**Hassan Falah Mohsin Fakhruideen**

B.Sc. Communication Engineering - 2010

M.Sc. Electronic and Communication Engineering - 2014

**Supervisor**

**Asst. Prof. Dr. Tahreer Safa'a Mansour**

**2020 AD**

**1441 AH**

## Certification

I certify that this thesis was prepared under my supervision at the Institute of Laser for Postgraduate Studies, University of Baghdad, in a partial fulfillment of requirements for the degree of a Doctor of Philosophy in Laser/ Electronic and Communication Engineering.

Signature: 

Name: **Dr. Tahreer Safa'a Mansour**

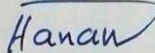
Title: **Asst. Professor**

Address: Institute of Laser for Postgraduate Studies,  
University of Baghdad.

Date: *18/4* / 2020

(Supervisor)

In view of the available recommendation, I forward this thesis for debate by examining committee.

Signature: 

Name: **Dr. Hanan Jaafar Taher**

Title: **Asst. Professor**

Address: Head of the Scientific Committee,  
Institute of laser for postgraduate studies,  
University of Baghdad.

Date: *18/4* / 2020

*Dedication*

*To*

*My beloved mother*

*Hassan*

*2020*

## Acknowledgments

Firstly, I would like to express my sincere gratitude to my supervisor, **Asst. Prof. Dr. Tahreer S. Mansour**, for her support, guidance, advice, and patience during my Ph.D. research.

My grateful thanks go to **Asst. Prof. Dr. Hussein A. Jawad**, Dean of the Institute of Laser for Postgraduate Studies, for his unlimited encouragement and support during my Ph.D. journey.

Special thanks are gone to **Asst. Prof. Dr. Mohammed K. Thaher**, head of the Engineering and Industrial Applications Department, for his continuous advice and support.

My special thanks go to all the faculty members of the Institute, especially to **Prof. Dr. Abdul Hadi M. Al-Janabi**, **Asst. Prof. Dr. Shelan K. Tawfeeq**, and **Asst. Prof. Dr. Zaineb F. Mahdi**, for their valuable suggestions and advice during my study time.

It would never have been possible for me to take this work to completion without their incredible support and encouragement.

Two persons deserve a very special word of gratitude they are; **Dr. Yousif Ibrahim Hammadi**, College of Engineering, University of Diyala, and **Dr. Saif Hassan Abdalnabi**, College of Engineering, University of Kufa, for their valuable support, insightful comments, suggestions, and constructive criticism in this work, they helped me dealing with the bureaucracies of doing a PhD.

I am truly grateful to my family for their immeasurable love and care. They have always encouraged me to explore my potential and pursue my dreams. They helped me a lot to reach this stage in my life.

## ABSTRACT

All optical nanoscale signal processing is the most important techniques that used to realize the plasmonic logic gates in the nowadays optical nanowire network system, after manipulating the limitation of photonic device in terms of diffraction limit. In this work, all-optical logic gates was achieved using Insulator-Metal-Insulator (IMI) configuration which contained Nano-rings with two and multiple input ports with laser bimodal waveguide at the two most common communication bands (1310 and 1550) nm, after enhancing the performance of the designed gates by maximizing the index contrast ratio (CR) between the ON and FF states which is the figure of merit of our work. The fundamental design contains a single Nano-ring structure with two straight waveguides, it's proposed to realize the function of all-optical NOT logic gate only. Based on the fundamental design structure, all the proposed logic gates are designed and developed by employing new nano-rings and straight waveguides to the fundamental structure with the same dimensions.

NOT gate at C-band is designed with (180 nm × 200 nm), while the NOT gate at L-band is designed with (350 nm × 350 nm), the transmission threshold is (0.5) for both structures. Then, all-optical logic gates are simulated to operate at C-band with dimensions of (350 nm × 350 nm) and transmission threshold of (0.5). Multiple inputs all-optical logic gates at C-band are simulated and investigated in the last stage which is dedicated to design and simulate three inputs plasmonic gates with dimensions of (400 nm × 400 nm) and transmission threshold of (0.26).

The performance of the designed all-optical plasmonic logic gates is analyzed and investigated based on the normalized transmission and the contrast ratio between opposite states of the specific gate. The simulation results show a transmission in some designed cases such as the OR gate,

where the normalized transmission in this gate is (127%) exceeds (100%) due the nonlinearity effects of DFWM. On the other hand, some designed gates show a contrast ratio (CR) of the specific gate which gives an indicator about the performance of the gate, the Maximum contrast ratio is achieved in multiple input NAND gate which equals to 14.6 dB.

<b>Abstract</b>		i
<b>Contents</b>		iii
<b>LIST OF ABBREVIATIONS</b>		v
<b>LIST OF SYMBOLS</b>		vii
<b>LIST OF TABLES</b>		viii
<b>LIST OF FIGURES</b>		ix
<b>CHAPTER ONE: Introduction and Basic Concepts</b>		
1.1	Introduction	1
1.2	Principles of Plasmonic Technology	2
1.3	Limitations of Electronics	6
1.4	Limitation of Photonics Devices	8
1.5	Features of Plasmonics	11
1.6	Surfaces Plasmon Polariton at Insulator-Metal -Interfaces	12
1.7	Excitation of Surface Plasmon Polaritons (SPPs)	13
1.8	Properties Surface Plasmon Polaritons (SPPs)	13
1.9	Plasmonic Waveguides	14
	1.9.1 Insulator-Metal-Insulator (IMI) Plasmonic Waveguided	15
	1.9.2 Metal-Insulator-Metal Plasmonic (MIM) Waveguided	17
1.10	Coupled Mode Theory for Modeling Nanoring Resonators	18
1.11	Nonlinear Surface Plasmon-Polaritons at Metal Surfaces	22
1.12	Applications of Plasmonic Technology	25
1.13	Aim of the Works	27
1.14	Literature Survey	27
1.15	Thesis Organization	34
<b>CHAPTER TWO: Design of The Plasmonic Logic Gates</b>		
2.1	The Structures of all-optical NOT gate	35
2.2	The Structure of All-Optical Logics Gates	37
2.3	Distribution of Structure Ports	40
2.4	The Structure of Multiple Inputs Ally-Optical Logics Gates	42
2.5	Ports Distribution of Multiple Inputs Logic Gates Proposed Structure	43
2.6	Optical Transmission Based on Structure Parameters	45

	2.6.1	Optical Transmission as a Function of Spacing Distance	46
	2.6.2	Optical Transmission as a Function of Waveguide Length	47
	2.6.3	Optical Transmission as a Function of Outer Ring Radius	48
	2.6.4	Optical Transmission as a Function of Inner Ring Radius	49
	2.6.5	Optical Transmission as a Function of Structure Metal	50
<b>CHAPTER THREE: Simulation Results and Discussions</b>			
3.1	The All-Optical NOT Logic Gate		51
3.2	All-Optical Logic Gates		55
	3.2.1	All-Optical NOT Logic Gate	56
	3.2.2	All-Optical OR Logic Gate	58
	3.2.3	All-Optical AND Logic Gate	61
	3.2.4	All-Optical NOR Logic Gate	64
	3.2.5	All-Optical NAND Logic Gate	67
	3.2.6	All-Optical EX-OR Logic Gate	70
	3.2.7	All-Optical EX-NOR Logic Gate	73
3.3.	Comparison between the Proposed Structure and the Previous Related Works.		75
3.4.	The Multiple Inputs All-Optical Logic Gates		76
	3.4.1	Three Inputs All-Optical NOT Logic Gate	77
	3.4.2	Three Inputs All-Optical AND Logic Gate	79
	3.4.3	Three Inputs All-Optical NAND Logic Gate	83
	3.4.4	Three Inputs All-Optical NOR Logic Gate	87
	3.4.5	Three Inputs All-Optical EX-NOR Logic Gate	91
<b>CHAPTER FOUR: Conclusions and Future Works</b>			
4.1	Conclusion		96
4.2	Future Works		96
<b>References</b>			98
<b>Appendices</b>			

## LIST OF ABBREVIATIONS

ABBREVIATION	DESCRIPTION
2-D	TwoDimensions
3-D	Three Dimensions
AD	Anno Domini
ALU	Arithmetic Logic Unit
CMOS	Complementary Metal Oxide Semiconductor
CPML	Convolutional Perfectly Matched Layer
DMD	Dielectric-Metal-Dielectric
DWs	Dielectric Waveguides
EM	Electromagnetic
FDTD	Finite Difference Time Domain
FEM	Finite Element Method
FoM	Figure of Merit
ICs	Integrated Circuits
ILT	Inequality Less Than
IMI	Insulator-Metal-Insulator
IMT	Inequality More Than
LRSPPs	Long-Range Surface Plasmon Polaritons
LSP	Localized Surface Plasmon
LSPRs	Localized Surface Plasmon Resonances
MZI	Mach-Zehnder Interferometer
NIR	Near-Infrared
NSOM	Near Field Scanning Optical Microscopy
PEC	Perfect Electric Conductor
PWs	Plasmonic Waveguide
Q-factor	Quality Factor
TIR	Total Internal Reflection
TM	Transverse Magnetic
SOI	Silicon-On-Insulator
SPs	Surface Plasmons
SPP	Surface Plasmon Polariton
SPPs	Surface Plasmon Polaritons
SRSPPs	Short-Range Surface Plasmon Polaritons
MDM	Metal-Dielectric-Metal
MIM	Metal-Insulator-Metal
MZI	Mach-Zehnder Interferometer
BER	Bit error rate

C-band	Conventional band
L-band	Long band
O-band	Original band
PC	Polarization controller
PD	Photodiode
OSA	Optical spectrum analyzer
OSC	Oscilloscope
AC	Auto-correlator
dB	Decibel
dBm	Decibel per mill watt
Gbit/s	Giga bit per second
Tbit/s	Tera bit per second
GHz	Giga Hertz
G symbol/s	Giga symbol/second
m	Meter
km	Kilometer
nm	Nanometer
ps	Picosecond
fs	Femtosecond
rad	Radian
W	Watt
V	Voltage

## LIST OF SYMBOLS

SYMBOL	DESCRIPTION
$a$	Period of grating surface in grating coupling mechanism
$r$	Inner radius of Nano-ring
$R$	Outer radius of Nano-ring
$L_T$	Total length of the waveguide
$c$	Speed of light
$d$	Coupling distance between stripes and Nano-rings
$E$	Electric field
$F$	Gate function
$H$	Magnetic field
$K$	Wave number
$l$	Length of plate
$L$	Length of the waveguide
$m$	Mode number
$m$	Interference order
$M$	Magnetization
$n$	Integer number more than 1
$P$	Polarization
$R$	Resistance of conductor
$T$	Normalized Transmission
$w$	Width of stripes
$\beta$	Propagation Constant
$\sigma$	Conductivity
$\rho$	Electric resistivity
$\omega$	Angular frequency
$\theta$	Phase of incident wave
$\beta_x$	Propagation constant in x-direction
$\epsilon_0$	Permittivity of free space
$\epsilon_2$	Permittivity of the second material
$\epsilon(\omega)$	Complex dielectric function
$\lambda_0$	Wavelength in vacuum
$\lambda_{inc}$	Incident wavelength
$\lambda_{SPP}$	Surface plasmon polariton resonance wavelength
$\omega_p$	Plasma frequency

## LIST OF TABLE

Table 3.1.	The operation details of the first proposed all-optical NOT logic gate	54
Table 3.2	The Operation Details of the Proposed All-Optical NOT Logic Gate	55
Table 3.3	The Operation Details of the Proposed All-Optical NOT Logic Gate	58
Table 3.4	The operation details of the proposed all-optical OR logic gate	60
Table 3.5	The operation details of the proposed all-optical AND logic gate	63
Table 3.6	The Operation Details of the Proposed All-Optical NOR Logic Gate	66
Table 3.7	The operation details of the proposed all-optical NAND logic gate	69
Table 3.8	The operation details of the proposed all-optical EX-OR logic gate	72
Table 3.9	The operation details of the proposed all-optical EX-NOR logic gate	75
Table 3.10	Comparison between the proposed structure and related works	76
Table 3.11	The operation details of the proposed all-optical three inputs NOT logic gate	79
Table 3.12	The operation details of the proposed all-optical three inputs AND logic gate	83
Table 3.13	The operation details of the proposed all-optical three inputs NAND logic gate	87
Table 3.14	The operation details of the proposed all-optical three inputs NOR logic gate	91
Table 3.15	The Operation Details of the Proposed All-Optical Three Inputs EX-NOR Logic Gate	95

## LIST OF FIGURES

Fig.1.1	Incident electromagnetic wave on a dielectric-metal interface [31].	3
Fig.1.2	Schematic describing surface plasmon resonance of metallic nanoparticle [35].	4
Fig.1.3	The propagation of surface plasmon polariton (spp) waves [32].	4
Fig. 1.4	Operation Speed of Optical Devices as a Function of Their Dimensions [54].	10
Fig. 1.5	Dispersion Relation for SPPs on a Single Interface for Ag metal [42].	12
Fig. 1.6	Schematic Diagram of The IMI Structure. The Red Lines in The Two Panels are The Characteristic Electric Field Profile in The Two Metal Slab Waveguides With a Core Thickness of $z = dm$ The Anti-Symmetric Mode, Corresponding to The Solution of $L+$ ; The Symmetric Mode, Corresponding to The Solution of $L-$ . [47].	16
Fig. 1.7	The Propagation Length and The Modal Index of The IMI Waveguide Mode [61].	16
Fig. 1.8	Schematic Diagram of The MIM Structure [41].	17
Fig. 1.9	The propagation length and the modal index off the MIM waveguide mode as a function of the insulators thickness $d$ [61].	18
Fig.1.10	Waveguide coupled nano cavity resonator [90]	19
Fig.1.11	Nonlinear excitation of surface plasmon polaritons at metal surfaces. (a) the SPP wave at the FWM [96] (b) coupling the surface FWM wave with a nano-grating efficiently converts the FWM emission to outgoing waves in free space [97] (c) a nano-patterned metal surface strongly scattering the SPP waves at the FWM frequency enables a nonlinear dark-field microscopy [98].	24
Fig.1.12	Main areas of applications of plasmonic [62].	25
Fig.1.13	Cascaded logic gates for NOR gates (a) schematic illustrations of logic gates NOR built by cascaded NOR and NOT gates (b) optical images of the designed Ag nanowire structures [24].	26
Fig.1.14	The proposed structures for [21]	28
Fig.1.15	The proposed structures for [12].	29
Fig.1.16	The proposed structure for [25].	29
Fig.1.17	The proposed structure for [11].	31

Fig.1.18	The proposed structures fore [27].	31
Fig.1.19	The proposed structure fore [29].	32
Fig.1.20	The proposed structure for [99].	33
Fig.1.21	The proposed structure for [100].	34
Fig.2.1	All-optical NOT gate at C-band.	35
Fig.2. 2	All-optical NOT gate at L-band	36
Fig.2. 3	The structure all-optical logic gates	37
Fig.2. 4	NOT logic gate ports distribution	40
Fig.2.5	OR, AND, and EX-OR logic gates ports distribution.	41
Fig.2.6	NOR, NAND, and EX-NOR logic gates ports distribution.	41
Fig. 2.7	The proposed structure of multiple inputs all-optical logic gates.	42
Fig. 2.8	The proposed structure of multiple inputs ally-optical AND logics gates.	44
Fig. 2.9	The proposed structures of multiple inputs ally-optical NAND, NOR, and EX-NOR logic gates.	44
Fig.2.10	The proposed structure all-optical NOT logic gate.	45
Fig.2.11	The optical transmission as a function of coupling distance (d).	46
Fig.2.12	The optical transmission as a function of waveguide length (L).	47
Fig.2.13	The optical transmission as a function of bigger ring radius (R).	48
Fig.2.14	The optical transmission as a function of smaller ring radius (r).	49
Fig.2.15	The optical transmission as a function of structure metal.	50
Fig.3. 1	Normalized transmission of the first proposed all-optical NOT logic gate as a function of wavelength for different input states	52
Fig.3. 2	The magnetic field distribution of the first proposed all-optical NOT logic gate at the different input states; (a) off input state, and (b) on input state.	53
Fig.3. 3	Normalized transmission of the proposed all-optical not logic gate as a function of wavelength for different input states.	54
Fig. 3. 4	The magnetic field distribution of the proposed all-optical NOT logic gate at the different input states; (a) off input state, and (b) on input state.	55

Fig.3. 5	Normalized transmission of the proposed all-optical NOT logic gate as a function of wavelength for different input states.	57
Fig.3. 6	The magnetic field distribution of the proposed all-optical NOT logic gate at the different input states; (a) off input state, and (b) on input state.	57
Fig.3. 7	Normalized transmission of the proposed all-optical OR logic gate as a function of wavelength for different input states.	59
Fig.3. 8	The magnetic field distribution of the proposed all-optical OR logic gate at the different input states; (a) (off-off) input states, (b) (off-on) input states, (c) (on-off) input states, and (d) (on-on) input states.	60
Fig.3. 9	Normalized transmission of the proposed all-optical AND logic gate as a function of wavelength for different input states.	62
Fig.3.10	The magnetic field distribution of the proposed all-optical AND logic gate at different input states; (a) (off-off) input states, (b) (off-on) input states, (c) (on-off) input states, and (d) (on-on) input states.	63
Fig.3.11	Normalized transmission of the proposed all-optical NOR logic gate as a function of wavelength for different input states.	65
Fig.3.12	The magnetic field distribution of the proposed all-optical NOR logic gate at different input states; (a) (off-off) input states, (b) (off-on) input states, (c) (on-off) input states, and (d) (on-on) input states.	66
Fig.3.13	Normalized transmission of the proposed all-optical NAND logic gate as a function of wavelength for different input states.	68
Fig.3.14	The magnetic field distribution of the proposed all-optical NAND logic gate at different input states; (a) (off-off) input states, (b) (off-on) input states, (c) (on-off) input states, and (d) (on-on) input states.	69
Fig.3.15	Normalized transmission of the proposed all-optical EX-OR logic gate as a function of wavelength for different input states.	71
Fig.3.16	The magnetic field distribution of the proposed all-optical EX-OR logic gate at different input states; (a) (off-off) input states, (b) (off-on) input states, (c) (on-off) input states, and (d) (on-on) input states.	72

Fig.3.17	Normalized transmission of the proposed all-optical EX-NOR logic gate as a function of wavelength for different input states.	74
Fig.3.18	The magnetic field distribution of the proposed all-optical EX-NOR logic gate at different input states; (a) (off-off) input states, (b) (off-on) input states, (c) (on-off) input states, and (d) (on-on) input states.	74
Fig.3.19	Normalized transmission of the proposed all-optical three inputs NOT logic gate as a function of wavelength for different input states.	78
Fig.3.20	The magnetic field distribution of the proposed all-optical three inputs NOT logic gate at the different input states; (a) off input state, and (b) on input state.	78
Fig.3.21	Normalized Transmission of The Proposed All-Optical Three Inputs AND Logic Gate as a Function of Wavelength for Different Input States.	80
Fig.3.22	The magnetic field distribution of the proposed all-optical three inputs AND logic gate at the different inputs states; (a) (off-off-off), (b) (off-off-on), (c) (off-on-off), (d) (off-on-on), (e) (on-off-off), (f) (on-off-on), (g) (on-on-off), and (h) (on-on-on) inputs states.	81
Fig.3.23	Normalized transmission of the proposed all-optical three inputs NAND logic gate as a function of wavelength for different input states	84
Fig.3.24	The magnetic field distribution of the proposed all-optical three inputs NAND logic gate at the different inputs states; (a) (off-off-off), (b) (off-off-on), (c) (off-on-off), (d) (off-on-on), (e) (on-off-off), (f) (on-off-on), (g) (on-on-off), and (h) (on-on-on) inputs states.	85
Fig.3.25	Normalized transmission of the proposed all-optical three inputs NOR logic gate as a function of wavelength for different input states	88
Fig.3.26	The Magnetic Field Distribution of The Proposed All-Optical Three Inputs NOR Logic Gate at the Different Inputs States; (a) (OFF-OFF-OFF), (b) (OFF-OFF-ON), (c) (OFF-ON-OFF), (d) (OFF-ON-ON), (e) (ON-OFF-OFF), (f) (ON-OFF-ON), (g) (ON-ON-OFF), and (h) (ON-ON-ON) Inputs States.	89
Fig.3.27	Normalized transmission of the proposed all-optical three inputs EX-NOR logic gate as a function of wavelength for different input states.	92
Fig.3.28	The magnetic field distribution of the proposed all-optical three inputs EX-NOR logic gate at the different	93

	inputs states; (a) (off-off-off), (b) (off-off-on), (c) (off-on-off), (d) (off-on-on), (e) (on-off-off), (f) (on-off-on), (g) (on-on-off), and (h) (on-on-on) inputs states.	
--	--	--

# **Chapter One**

**Introduction and Basic Concepts**

## 1.1 Introduction

Recently, bandwidth and bitrate of data transmission have more attention. One way of increasing these parameters is by using all-optical signal processing. Guiding the optical signal through the optical waveguides is an essential part of realizing the all-optical signal processing. Many research studies have explored the applications of using optical waveguides, especially in optical communications systems, photonics systems, and optical integrated circuits. Utilizing the compact optical devices in all-optical signal processing applications has many advantages such as large bandwidth, high transmission speed, overcoming the diffraction limit problem, ultrahigh-speed processing, high security, immunity to external interference, and low power consumption. In recent years, all-optical devices based on Surface Plasmon Polaritons (SPP) (plasmonic devices) have been extensively investigated and explored. Plasmonic devices motivated new techniques to overcome the delay, heat, and diffraction limit, which occur in electronic and photonic devices. Plasmonic devices also called subwavelength devices because the usage of such devices enables light manipulation in subwavelength scales [1, 2]. SPPs are defined as the interaction of electromagnetic waves and the free electrons of metals; they were propagating on the boundary between the metal-dielectric or dielectric-metal interfaces [3]. It is a collective wave where billions of electrons oscillate in synchronization at optical frequencies. Plasmon waves can propagate through nanoscale dimension wires. Many types of plasmonic devices have been realized, such as resonators [4], Nano-cavities [5], splitters [6], couplers [7], modulators [8], demultiplexers [9], waveguides [6], hybrid plasmonic waveguides [10], switches [11, 12], and logic gates [13-18]. On the field of all-optical universal gates, several studies and investigations have been proposed, such as single semiconductor optical amplifiers [19], hybrid plasmonic-photonic crystal nanobeam cavities [18],

two-photon absorption in silicon waveguides [20], silicon micro-ring resonators [21, 22], cross-phase modulation [23], and nanophotonic plasmonics [24]. Recently, many structures of all-optical plasmonic devices proposed nanoscale logic gates [25-29]. This thesis offers all the basic all-optical gates obtained using the same structure and the most significant number of multiple-input logic gates (five three-input logic gates), also using the same structure. The structures are designed and constructed using Nanorings resonator and Insulator-Metal-Insulator (IMI) plasmonic waveguides. NOT, OR, AND, NOR, NAND, XOR, and XNOR plasmonic logic gates are proposed, analyzed, and realized. The simulation results obtained using COMSOL Multiphysics package software (version 5.3 a) are based on the Finite Element Method (FEM). In the future, these devices will be the gateway to the Nanophotonic integrated circuits applications and all-optical signal processing systems.

## **1.2 Limitations of Electronics**

It is without a doubt that the requirement for faster processing and data transmission is ageless. As a result of our consistent requirement for more rapid, smaller, and progressively productive devices, electronic devices have pushed toward Nano scale devices. It is standard to create ultra-quick transistors in the Nano scale range, and a distinguished case of that is the Intel chips [40, 41]. The significant part in Integrated Circuits (ICs) is interconnected because they give out signs, force, and clock to different segments on the IC. As the size of the parts is diminished to the Nano scale, the exhibition of the IC turns out to be exceptionally reliant on interconnects. Be that as it may, in contrast to transistors, where usefulness improves with decreasing size, interconnect proficiency diminishes, in this manner restricting the speed of electronic circuits and electronic devices [42]. Since the interconnectors are made of copper material and their size reductions to the nanometer, defers increment because of an expansion in the successful opposition, capacitance, cross talk,

and radiation [40-42]. Far beyond, the time steady influences the interconnect line, which is the result of the opposition and capacitance of the line [43]. It was evident from the obstruction and capacitance are given in Equations (1.2) and (1.3), individually, that the size of the conductor diminishes its opposition increments [43].

$$R = \frac{\rho L}{WT_c} \quad (1.1)$$

$$C = \frac{\varepsilon_0 \varepsilon_d l w_p}{dp} \quad (1.2)$$

Where  $\rho$  is the electrical resistivity,  $\varepsilon_0$  and  $\varepsilon_d$  are the permittivities of free space and the dielectric material, individually.  $L$  and  $l$  are the lengths of the conductor and plate, separately. and are the width of the conductor and plate, individually. Also, the thickness of the conductor and separation between the plates, individually. It is demonstrated that when an interconnector is downsized to the Nano scale, R increments because of its backward proportionality connection with, and C increments because of the decreasing in. In this manner, a copper interconnects are constrained by their transmission capacity and limit. In this manner, this will put an imperative on the number of segments that can be put on a chip. Since electronics manage charge stream (electrons), when the recurrence of electronic pulse expands, the electronic device gets hot and the wires become free. Hence, the rule of 'high frequency, high information move rate' can't be applied and can't transmit an immense measure of information. What's more, the subsequent hindrance is the point at which the size of electronic wires diminishes, expanding obstruction. This causes the postpone time impact. Instead of using a chip with a processing core, multiple processing cores chips were introduced to increase the performance [44]. However, as these chips are reduced in size to the nanometer, and the number of cores is increased, the wires connecting these cores kinked the connection since they

take a large area of the chip. Moreover, a large fraction of power gets lost in the connecting wires, leading to reduction. This happens, especially in low power devices. From this, it is known that there are limits to how far cores are placed. Then again, the basic structure square of the Arithmetic Logic Unit (ALU) is logic gates. These logic gates become problematic inactivity because of the lower speed experiencing significant change between logic 0 and logic 1 in electronics. Hence an elective strategy must be utilized, particularly when the speed and information rate are very high. Nonetheless, the appearance of the coordinated photonic circuit has tackled this issue significantly, which can manage the capacity of every component optically. For instance, dielectric photonic interconnects because of their similarity with Complementary Metal Oxide Semiconductor (CMOS) gadgets [44, 45]. The photonic offers different answers for obstructions referenced in devices. These give as high data transfer capacity, and low misfortune interconnects among optics and hardware [45], prompting a superior handling of conveyed segments and centers, better execution inactivity, higher speed, and transmission capacity, and lower misfortunes than electronic interconnects.

#### **1.4 Limitation of Photonics Devices**

Photonics is the science that joins optics and electronics and includes the generation, outflow, transmission, regulation, intensification, recognition, and all types of controlling light [45]. Dielectric optical interconnects have higher speed and data transfer capacity at least power utilization contrasted with electronic interconnects. Notwithstanding, this includes some significant pitfalls of multiple times bigger optical interconnects than their electronic partner [45]. Massive optical devices have invigorated the need for scaled-down devices in the size of sub-micrometer and nanometer to take advantage of their high limit. It is proposed to utilize scaled-down optical devices and interfaces due to their capacity to convey

multiple times the limit of electronic circuits [40, 41, 43-48]. It appears that optical systems are established for massive scale electric signal correspondence. The adaptability of these systems has upset the cutting edge integrated-on-chip optical communications [42]. The advances in cutting edge innovation and the improvement of manufacture strategies disentangled the acknowledgment of optical devices. Various silicon-on-insulator devices (SOI) have been proposed for high-thickness photonic incorporated circuits. This is incomplete because of their high refractive list differentiate and for their excellent optical properties at optic fiber correspondence frequencies [42]. A Mach-Zehnder electro-optic modulator is a sort of SOI device. The capacity of this optical device is changed over to the electrical sign to an optical sign. This is cultivated by encoding an optical wave with a fast electronic sign. It is exhibited that optical adjustment rates up to 10 Gbps are acquired with low force utilization [42]. A grating coupler utilizing the traditional SOI has been proposed in [49]. This device guarantees a coupling misfortune beneath 1 dB, and simplicity of coordination in photonic circuits [42]. Another device, the ring resonator channel utilizing photonic wires [50], was tried tentatively and created. Also, in [51], a resonant coupling type polarization splitter is illustrated. It uses photonic crystals utilizing the photonic band-gap effect and micro-cavities. It is difficult to design a waveguide using photonic crystals due to their reduced size and high index contrast. Moreover, these crystals incur high losses compared to photonic wires [52]. The signal interconnects represent the target defiance that limits the speed of the digital system. Nonetheless, the size mismatch between Nano scale electronic circuits and optical devices has limited electronic and optical integration [46, 47]. When the dimensions of optical components become close to half the wavelength of light, optical diffraction occurs, limiting the propagation of light and limiting the scalability and dimensions of the optical devices [40, 46, 47]. This is due to the three dimensions (3D)

nature of waves propagating in a dielectric material. It is derived from Equation (1.4) below [53].

$$\beta^2 + K_x^2 + K_y^2 = \varepsilon_c \frac{\omega^2}{c^2} \quad (1.3)$$

where  $\beta$  is propagation constant,  $k_x$  and  $k_y$  are wave number in  $x$  and  $y$  directions, respectively,  $\varepsilon_c$  is dielectric constant of the core material,  $\omega$  is angular frequency, and  $c$  is speed of the light which is  $3 \times 10^8$  m/sec. This makes the dielectric photonic parts on more than one occasion requests, of extent more significant than their electronic partners. Besides, photonic devices rely upon recurrence and have a restricted transmission capacity, contingent upon the gadget design, constraining their use and effectiveness. These impediments originate from as far as possible wonder, which came about because of utilizing photonic devices with a size smaller than the request for working. This marvel brings about more power dispersed. Hence, an immense measure of information can't be sent alongside scaling down. Therefore, scaling down the procedure to nanometer measurements of the photonic device is wasteful and confusing to acknowledge practically speaking mainly when the photonic device working in terahertz frequencies goes (is more than 1000 nm). Along these lines, it is essential to discover an innovation or a circuit at the Nano scale measurements that fill the hole between the two advancements (Electronics and Photonics), and convey both optical and electrical signs, subsequently improving proficiency and eliminating the chip's capacity dispersal. Plasmonic or SPPs is the answer to this issue. Accordingly, plasmonic can go about as the bridge between photonics (expansive transmission capacity) and electronics (nanometer scaling down) for correspondence as appeared in Figure (1.4) [54].

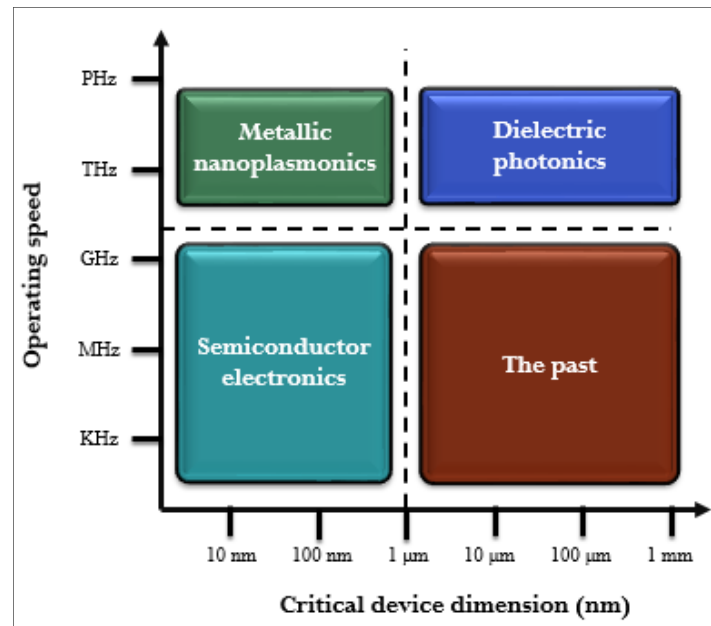


**Fig. 1.1 Operation Speed of Optical Devices as a Function of Their Dimensions [54].**

Plasmonics has a high information rate capacity offered by optics. They work at frequencies in the light and approach infrared districts, consequently giving them the high limit managed by optics. Moreover, plasmonics satisfies the scaling down of device size measurements offered by electronics, which makes it perfect with the present planar assembling strategies, for example, silicon-on-insulator (SOI) and complementary metal-oxide-semiconductor (CMOS) advances. Thus, plasmonics has the capability of giving a wide exhibit of sub-wavelength optical parts coordinated together on a similar structure or chip to clear and create the future contract of PCs "every single optical PC". Subsequently, this answers the topic of why we need plasmonics.

## 1.2 Principles of Plasmonic

The term Plasmonic is derived from (*plasma of electronic*), but the term Plasmonics refers to (*applications of plasmonic*). The plasmonic technology describes how the light field can be confined in waveguides, which is smaller than the applied wavelength in dimensions. Thus the plasmonic technology also called a sub-wavelength technique. It is a new

area of interest, which couples the powers of both electronics and photonics technologies. The rapid development of nanofabrication techniques such as optical lithography, help to improve the applications of nanoscale plasmonic structures [30]. Plasmonic are semi particles or an aggregate wave where billions of electrons waver in synchronization at optical frequencies coming about because of the reliable trade of vitality between an electromagnetic wave and excitation in material, for example, photon-electron coupling. At the point when electromagnetic waves are occurrence on a dielectric-metal or metal-dielectric interface (as appeared in Figure 1.2), it will accelerate the electrons and lead to induce polarization, which makes reestablishing, the power which causes an oscillation of the free electron of the metal as appeared in Figure 1.3. This oscillation is quantized, and free electrons oscillation is the quantization of plasma oscillations, and it's known as a plasmon [31]. In this case, electromagnetic surface waves are excited and propagate along with the interface, as shown in Figure 1.4 [32].

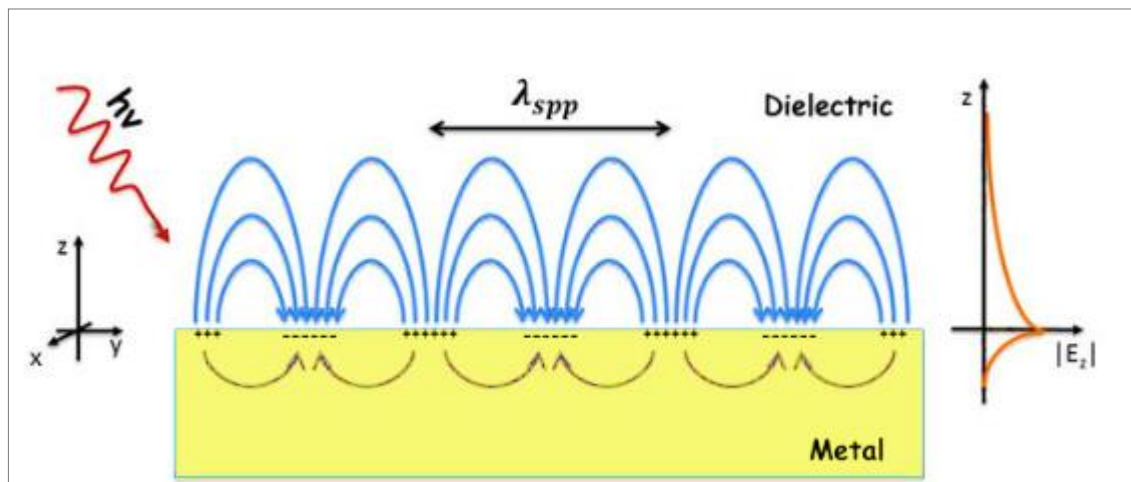


**Fig. 1.2 Incident electromagnetic wave on a dielectric-metal interface [31].**

These surface waves are evanescently propagated in the perpendicular direction and are known as Surface Plasmon Polariton (SPP) waves [33]. SPP waves in metallic waveguides and metal nanostructures open the likelihood to bind and guide optical waves on the nanometer scale

[32].The term plasmonic defines the basics of nanophotonics, which has been given to the investigation of optical wonders coming about because of the communication of electromagnetic fields with the conduction electrons in metals [34]. The resonance wavelength of SPP can be determined by Equation (1.3) [27]:

$$\lambda_{ssp} = \frac{4\pi n_{eff}R}{m} \quad (1.3)$$

Where  $n_{eff}$  is the effective refractive index,  $R$  is the dimension of the nano structure in nanoring structure  $R$  is the radius of the ring structure, and  $m$  is an integer number refer to the mode number ( $m = 1, 2, 3, \dots$ ).

As indicated by Eq. (2.1), the structure parameters and the type of metal and insulator materials play a big role in tuning the resonance wavelength.

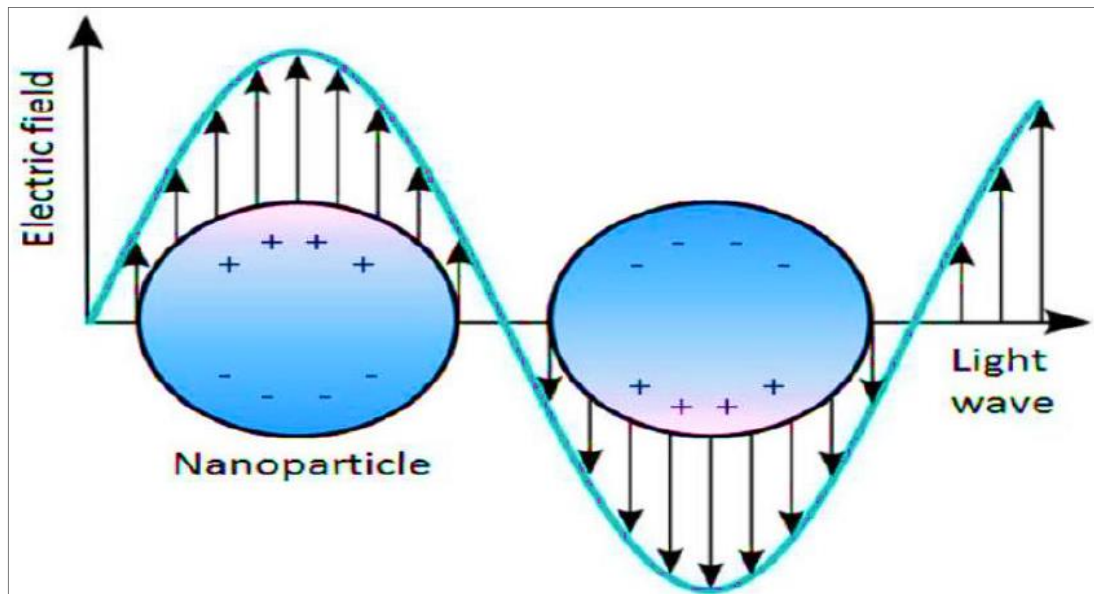


**Fig.1.3 Schematic describing surface plasmon resonance of metallic nanoparticle**

[35].

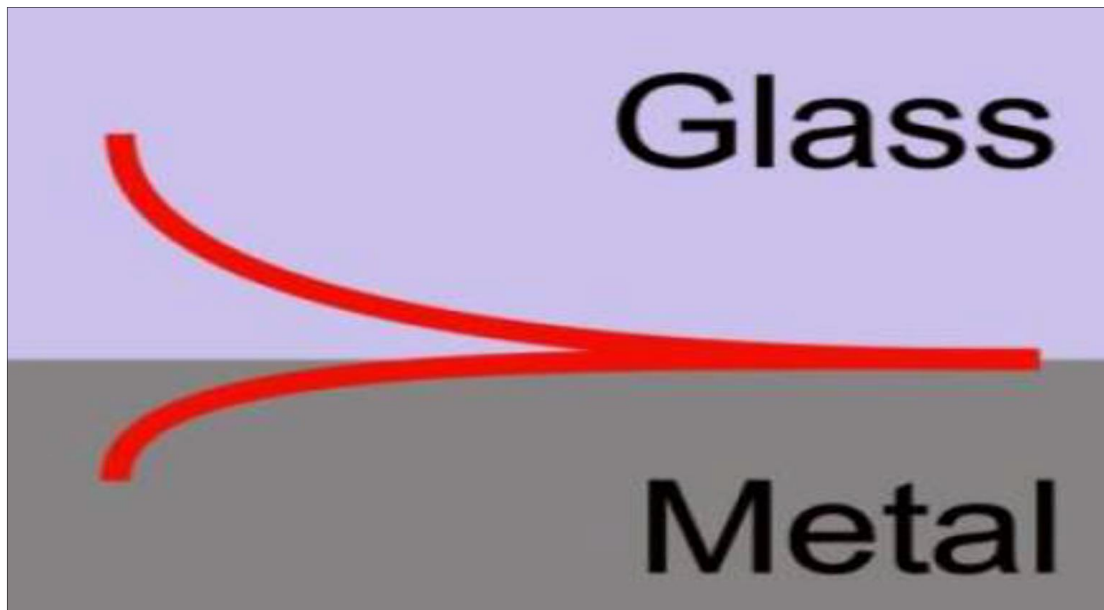


**Fig. 1.4 The propagation of surface plasmon polariton (spp) waves [32].**

The term plasmonic is a sub-section from nanophotonics, which has been given to the investigation of optical wonders coming about because of the communication of electromagnetic fields with the conduction electrons in metals [34]. Two advantages of photon-electron associations at surface metal interfaces are sub-diffraction field confinement and field improvement. This requires nanoscale structures with plasmon oscillations at various ranges in the electromagnetic spectrum. Besides, to accomplish high upgrade levels, plasmonic components must have a top-notch factor (Q-factor). Gold, silver, and copper meet these prerequisites in the unmistakable and near infrared range. Silver and gold are the most widely recognized materials in plasmon affirmed optics and spectroscopy [36]. At times, electromagnetic waves can't be transmitted through metal when their frequencies are smaller than the Plasmon frequency. The plasmons that bind at the metal-dielectric interface are called Surface Plasmons (SPs). At the point when light is coupled to these SPs under specific conditions, it improves transitory electromagnetic fields, called surface plasmon polaritons (SPPs). This is the primary kind of SPs whose longitudinal waves at the metal-dielectric interface and exponentially rot away from the limit into the encompassing materials. These waves make a trip corresponding to

the course of spread, so a transverse wave can't energize them. The best method to stimulate a plasmon is to utilize electrons. For example, at the point when light excites the particles, they will go through a thin metal layer and lose some vitality. This misfortune in energy is utilized to energize SPP [37]. The second type of SPs is a Localized Surface Plasmon (LSP). LSP is non-propagating waves resulting when the electron oscillation is confined in three dimensions [38]. These waves induce resonances that can be observed as peaks in dispersion in the scattering and absorption cross-sections spectra. The spectral position of the resonances depends on several factors: the metal permittivity, the permittivity of the surrounding dielectric, and the size and shape of the metallic nanostructure [34]. On account of a circular nanoparticle, the curved surface of the nanoparticle makes a reestablishing power on the electrons to bring about a limited oscillation. This sort of vibration can be energized by direct light illumination [39]. The association of metallic nanostructures with electromagnetic fields and attributes of SPPs can be portrayed by an old-style type of Maxwell's conditions, which help to acquire the wave condition and all the optical properties of SPPs.

### **1.5 Features of Plasmonics**

The highlights of plasmonics technology are exhibited underneath [58]:

- Several orders of extent field improvement (Enhanced Transmission).
- Field repression in a few nanometers.
- It is viewed as a Nano photonic device (Reduced Device Footprint).
- Dependent on condition.
- Tunable.
- Efficient coupling.
- Highly dispersive.

- Short-territory proliferation length (greatest spread length compasses to certain millimeters)
- Lossy.
- Thermal impact.
- Nanofabrication methods limit structure measurements (a few structures illogical).
- Difficult to mimic.

### **1.6 Surface Plasmon Polariton at Insulator-Metal -Interface**

Surface plasmon polaritons (SPPs) are transitory electromagnetic waves spreading alongside the interface of metal and insulator materials because of collective electron oscillations alongside an outer optical field. SPPs exceptional sort of electromagnetic waves alongside electron thickness motions permit Nano scale imprisonment of electromagnetic radiation. Surface plasmon polaritons spread around a metal point with a constrained bend sweep, utilizing a one-dimensional model like the dispersing of a potentially limited significance well. They acquired articulations of reflection and transmission coefficients in the short wavelength limit, just as an upper destined for the transmittance. Now and again, the proliferation of non-planar surfaces may bring about lower misfortunes than level surfaces, in spite of desires [55]. In view of the linearity of the homogeneous Helmholtz's conditions [Appendix A], the issue of the wave occurrence can be isolated into a two-section planar surface an S- enamored wave and an enchanted P-wave [56] [Appendix B]. Figure (1.5) shows the scattering qualities of SPPs utilizing the marvelous dielectric permittivity of the silver metal got from [57].

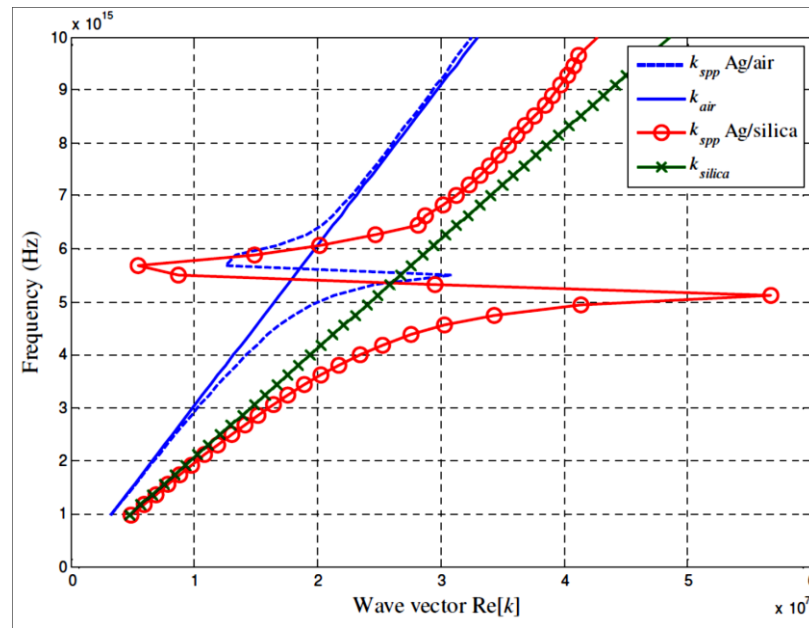


**Fig. 1.1 Dispersion Relation for SPPs on a Single Interface for Ag metal [42].**

### 1.7 Excitation of Surface Plasmon Polaritons (SPPs)

The SPP scattering bend lies totally down that of free space light in the dielectric, with the end goal that  $> K$ . Consequently, direct excitation of SPPs by light bars is inconceivable except if unique coupling system to accomplish stage coordinating is utilized. Right now, it is conceivable to excite SPPs. Numerous techniques are found to excite SPPs [Appendix C].

### 1.8 Properties Surface Plasmon Polaritons (SPPs)

The accompanying focuses give the fundamental properties of SPPs that are [58]:

- SPPs are Electromagnetic (EM) waves that have an infrared or visible frequency, which can proliferate alongside a metal-protector or surface metal interface.
- SPP contains the longitudinal and transverse segments of the EM field.
- SPPs contain the parts of the electric and magnetic field, likewise as a plane EM wave.
- SPP spreads at the same time in two materials, to be specific dielectric and metal.

- SPP's electric field is related to electrical conduction (free) charges.
- The electric field of SPP is normal, and its magnetic field is parallel to the surface metal interface for high conductivity metals.
- Force lines of the electric field are intended to meet limit conditions; that is, the electric field is ordinary for flawless metals.
- Oscillations of surface conduction charges in thick surfaces give a critical improvement of close to optical field thought close to the metal surface.
- Plasmon's conduct shifts from the standard principles of photons.
- Plasmons are dynamic for controlling the electromagnetic waves on a nanometer scale.
- The power transferred by the SPP is gathered in the ultra-flimsy region in the nanometers scale, and the wonders can surpass as far as possible.

### **1.9 Plasmonic Waveguides**

Fiber optics communications have changed data transmission because of their excellent functionality to transmit monstrous information over long separations with enormous transfer speed [32]. Notwithstanding, the short-distance information transmission on chip-incorporated electronic hardware was limited in speed because of the time postponement of Nano scale metal associations. The utilization of light waves as data transporters on Nano-chip circuits can address the issue of decreasing the pace of information transmission of electronic circuits [42]. The traditional dielectric waveguides (DWs) that guide light inside a high refractive list zone encompassed by a low-power bar are dependent upon the rule of total inner reflection through Snell's law [47]. In any case, the diffraction furthest reaches of light in optical photonic waveguides has obstructed scaled-down photonic waveguides; this implies light waves can't be compacted into space with a measurement smaller than a large portion of their wavelength in that medium [50]. Luckily, Nano-plasmonics had the option to neglect the diffraction furthest reaches of light by utilizing SPPs waves that recently

talked about. One of the SPPs-based applications that have gotten superb research consideration over the previous decade is plasmonic waveguides (PWs), which empower the change of light on the sub-wavelength scale into SPPs at the metal-dielectric or dielectric-metal interface conquering as far as possible. PWs are an excellent possibility to build up the up and coming age of ultra-little gadgets that have the upsides of both the enormous data transmission activity of photonics and true Nano scale, making ready for the future reconciliation of high-limit photonics and electronic devices on a scale like electronics [50, 53]. Diverse waveguide structures and geometries have been proposed for SPPs with the end goal of misusing the novel highlights of SPPs waveguides in the nanometer scale. Disregarding the intriguing highlights of PWs, there is one primary issue confronting them, which is the tradeoff among misfortune and imprisonment. The two types of PWs generally utilized in late applications: Insulator-Metal-Insulator (IMI), or Dielectric-Metal-Dielectric (DMD) plasmonic waveguide and Metal-Insulator-Metal (MIM) or Metal-Dielectric-Metal (MDM) plasmonic waveguide are shown right now [59]. Additionally, their points of interest, hindrances, and correlation between them are presented in this chapter.

### **1.9.1 Insulator-Metal-Insulator (IMI) Plasmonic Waveguided**

IMI or DMD is framed by setting a thin metallic film with a width of under 50 nm between two dielectric materials of the equivalent or distinctive refractive files. This is like a blend of two dielectric/metal interfaces, where the field debases vigorously inside the metal, starting with one interface then onto the next. This results in the guiding of two leaky waves [53, 59].

The dispersion relation Equations 1.5 (a) and 1.5 (b) for Transverse Magnetic (TM) mode in the waveguide is given by [32, 60]. IMI structures incorporate metal movies or stripes, which are utilized to manage long range symmetrical SPP (LRSPPs). The spread separation is in several

microns or even millimeters [42]. In any case, reducing the thickness or width of the stripe of the metal outcomes in diminished confinement of the mode [47], and an abbreviated proliferation length [50], individually. Then again, short-extend hostile to even SPPs (SRSPPs) have higher confinement; however, shorter spread separations and are more qualified for coordinated circuits [47]. IMI PWs, including their proliferation length and modular file of the IMI waveguide mode, are appeared in Figures (1.6) and (1.7), individually. IMI arrangement was utilized to understand a Mach-Zehnder interferometer, a polarization splitter, and micro-ring cavities.

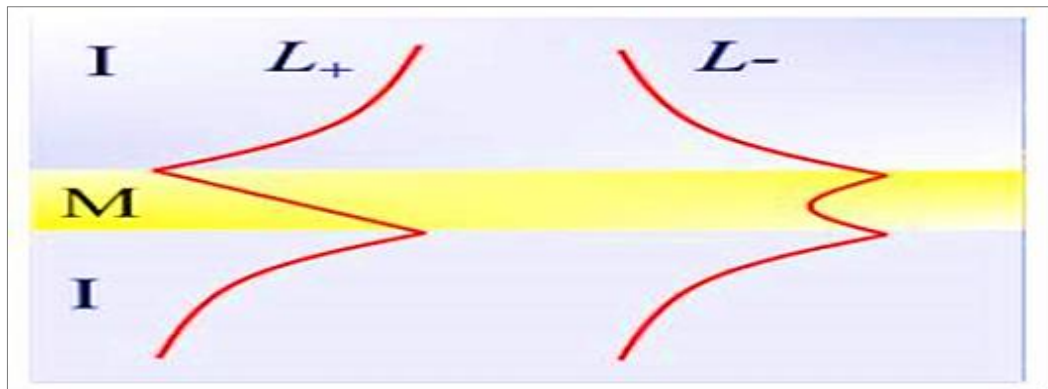


**Fig. 1.2 Schematic Diagram of The IMI Structure. The Red Lines in The Two Panels are The Characteristic Electric Field Profile in The Two Metal Slab Waveguides With a Core Thickness of  $z = d_m$  The Anti-Symmetric Mode, Corresponding to The Solution of  $L_+$ ; The Symmetric Mode, Corresponding to The Solution of  $L_-$ . [47].**

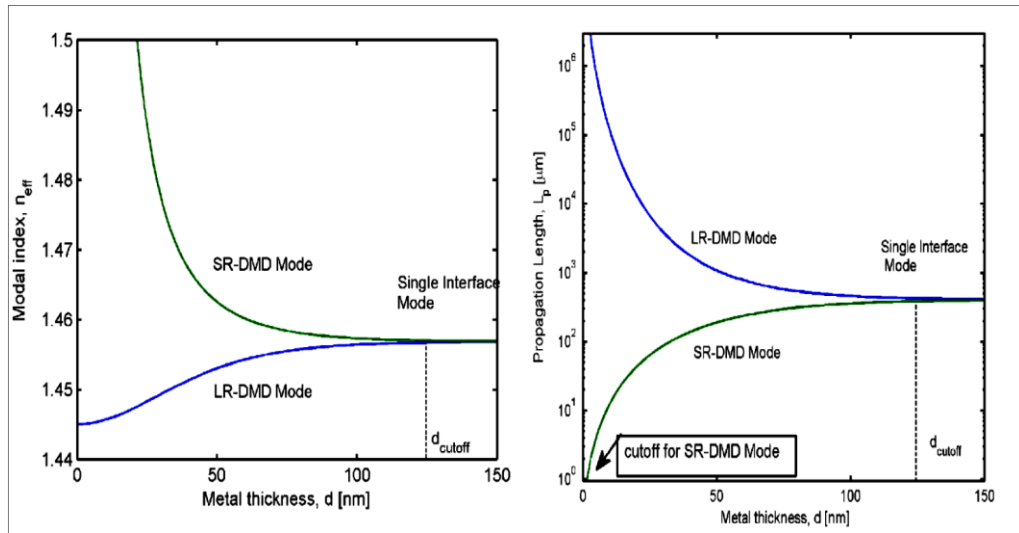


**Fig. 1.3 The Propagation Length and The Modal Index of The IMI Waveguide Mode [61].**

The dispersion relation Equations 1.5 (a) and 1.5 (b) for Transverse Magnetic (TM) mode in the waveguide is given by [32, 60].

$$\varepsilon_m k_d + \varepsilon_d k_m \tanh\left(\frac{k_m}{2} d_m\right) = 0 \quad (1.5 a)$$

$$\varepsilon_m k_d + \varepsilon_d k_m \coth\left(\frac{k_m}{2} d_m\right) = 0 \quad (1.5 b)$$

Where  $d_m$  is thin metal thickness.

$$k_d = (\beta^2 + \varepsilon_d k_0^2)^{1/2} \text{ (Dielectric wave number)}$$

$$k_m = (\beta^2 + \varepsilon_m k_0^2)^{1/2} \text{ (Metal wave number)}$$

$$k_0 = \frac{2\pi}{\lambda_0} \text{ (free space wave number)}$$

$\beta$ : Propagation constant that is represented by an effective refractive index of the waveguide (SPP).

### 1.9.2 Metal-Insulator-Metal Plasmonic Waveguide

The second setup that permits sub-wavelength confinement and coordination is the MIM or MDM geometry, as appeared in Figure (1.8).

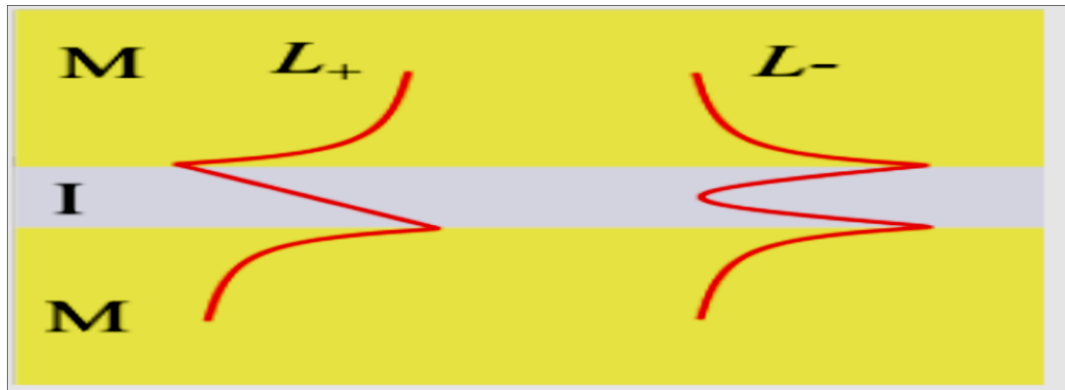


**Fig. 1.4 Schematic Diagram of The MIM Structure [41].**

As the metal hole diminishes, the causing consistent increments, inferring a progressively kept mode. Even though this structure has short spread lengths contrasted with IMI, it is described by solid mode confinement, which can be effortlessly coordinated into photonics chips. It isn't influenced by radiation or cross-talk [59, 60]. At a couple of nanometers of encasing thickness  $d$ , the modular list of the MIM guided mode has a considerable worth, and it diminishes as the cover thickness increments until it arrives at the cutoff dielectric thickness, where the modular list of the MIM mode moves toward the single interface SPP modular while the proliferation length expanded with expanding the width of dielectric. The dispersion relation for MIM structures is given by Equation (1.6) [60].

$$\varepsilon_d k_m + \varepsilon_m k_d \tanh\left(\frac{k_d}{2} d_i\right) = 0 \quad (1.6)$$

Figure (1.9) shows the spread length and the modular record of the MIM waveguide mode versus the encasing thickness  $d$ .

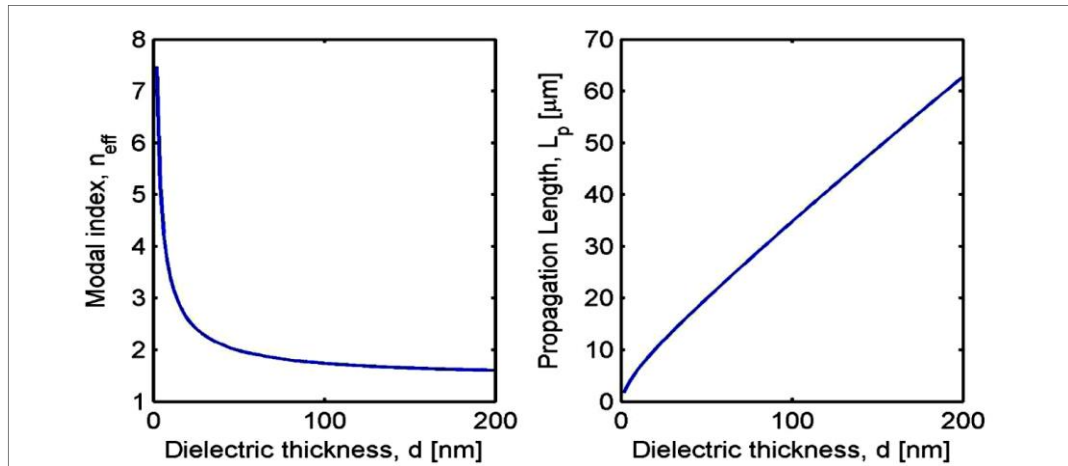


**Fig. 1.5** The propagation length and the modal index of the MIM waveguide mode as a function of the insulator thickness  $d$  [61].

### 1.10 Coupled Mode Theory for Modeling Nanoring Resonators

The modified coupled mode theory considers planar waveguides, addressing only two dimensions rather than three. Specifically, the optical field propagation vectors are constrained to propagate in a plane we denote this plane the  $x$ - $z$  plane; the sheet waveguides are infinite in extent perpendicular to that plane in the  $y$  direction. The fields do not vary in this  $y$  direction in our model no diffraction [90]. Circular waveguide nanoring resonator with two attendant bus waveguides diametrically opposed, as shown in Fig. 1.10 [90]. None absorbing and gain-free non scattering media are considered in a configuration in which bending losses are negligible. Also, the bus waveguide and the ring waveguide is each of constant although possibly differing thickness and refractive index, chosen such that only one TE mode is supported in each. The general coupled mode theory approach assumes that the perturbing polarizability influences only one mode sufficiently to modify its amplitude [90].

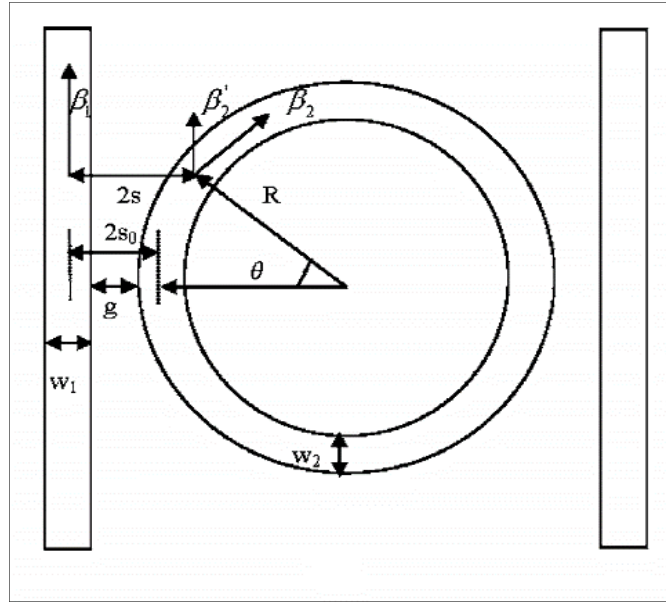


**Fig. 1.6 Waveguide coupled nano cavity resonator [90]**

For real fabricated structures, the propagation constant in the  $x$ - $z$  plane is determined in part by confinement in the  $y$  direction, but here only the  $x$ - $z$  component of the propagation constant ( $\beta$ ) pertains. Consequently, we assert that these concepts have validity in other waveguide configurations e.g., ridge structures for which the  $y$  component of  $\beta$  is constant along the waveguide. In our present analysis, no gradient refractive index structures are explicitly considered, although only characterization by the in-plane longitudinal propagation constant  $\beta_{xz}$  is required to include this case. The evaluation of integral expressions becomes challenging. Likewise, no tapered waveguides are considered, since these have inconstant that introduces extraneous difficulties [90]. A general expression for the coupling coefficient  $\kappa$  is given by Equations (1.7) and (1.8) [91]

$$\kappa_{ab} = \frac{\omega \epsilon_0 \int_{-\infty}^{\infty} (N^2 - N_b^2) E_a^* \cdot E_b dx}{\int_{-\infty}^{\infty} u_z \cdot (E_a^* \times H_a + E_a \times H_a^*) dx} \quad (1.7)$$

$$= \frac{\omega^2 \epsilon_0 \mu_0 (n_a^2 - n_0^2) \int_{-w_1}^{w_1} E_{1y}^* \cdot E_{2y} dx}{2\beta \int_{-\infty}^{\infty} |E_{1y}|^2 dx} \quad (1.8)$$

where  $N=N_{(x,z)}$  denotes the refractive index distribution throughout the entire problem space, and  $N_j$  denotes the refractive index distribution of each waveguide in the absence of any perturbing structure i.e., the other waveguide. The subscript pair  $(a, b) = (1, 2)$  or  $(2, 1)$  indicates coupling to waveguide a from waveguide b. Over the region of perturbing polarizability (i.e., across waveguide 1), it can be seen that  $(N^2 - N_b^2) = (n_a^2 - n_0^2)$ , where  $n_a$  and  $n_0$  are the customary variables used to represent the refractive indices of waveguide a and of the substrate, respectively [91]. Although this expression appears symmetric in  $(a, b)$ , other evidence indicates that  $\kappa_{12}$  is not equal to  $\kappa_{21}$  for unequal waveguide curvatures. Only the TE mode is considered, since the method of analysis is similar for the TM mode. The electrical field components associated with an independent (uncoupled) planar waveguide 1 are expressed in Equations (1.9) and (1.10) [91]

$$E_{1y} \begin{cases} A \cos(k_{x1}x) & (|x| \leq w_1/2) \\ A \cos(k_{x1} w_1/2) \exp[-\alpha_1(|x| - w_1/2)] & (|x| > w_1/2) \end{cases} \quad (1.9)$$

$$E_{2y} = A \cos(k_{x2} w_2/2) \exp[\alpha_2(x - 2s_0 + w_2/2)] \quad (|x| \leq w_1/2) \quad (1.10)$$

where  $k_{x1}$  and  $k_{x2}$ , transverse propagation constants inside the planar waveguides 1 and 2, satisfy  $k_{xi} = (n_i^2 k^2 - \beta_i^2)^{1/2}$ , where  $k$  is the free-space wave vector. Similarly,  $\alpha_1$  and  $\alpha_2$ , transverse decay constants of the field amplitude, are given by  $\alpha_i = (\beta_i^2 - n_0^2 k^2)^{1/2}$ . The widths of waveguides 1 and 2 are  $w_1$  and  $w_2$ , and their refractive indices are  $n_1$  and  $n_2$ , respectively.  $n_0$  represents the substrate refractive index. The waveguides are separated, center to center, by the distance  $2s_0$  ( $2s_0 > w_1 + w_2$ ).

Substituting Equations (1.9) and (1.10) into Equation (1.8) and performing the integration results after several algebraic steps in the explicit expression for the coupling coefficient between two planar optical

waveguides with dissimilar refractive indices and arbitrary widths and separation is expressed in Equation (1.11) [91].

$$\begin{aligned} \kappa_{12}(s_0) = & \frac{\omega^2 \varepsilon_0 \mu_0 (n_1^2 - n_0^2) \cos(k_{x2} w_2) \exp[a_2(w_2 - 2_{s0})]}{\beta_1 (k_{x1}^2 + \alpha_2^2) (w_1 + \frac{1}{\alpha_1})} \\ & \times [\alpha_2 \cos(k_{x1} w_1) \sinh(\alpha_2 w_1) \\ & + k_{x1} \sin(k_{x1} w_1) \cosh(\alpha_2 w_1)] \end{aligned} \quad (1.11)$$

To extend the relations described above, developing coupled mode theory to apply to a curved waveguide such as the nanoring resonator shown in Fig. 1.10 is required. However, in this case, the coupling coefficient is no longer a constant, since the coupling distance the bus-to-ring gap changes along the propagation path. Therefore, it is appropriate to redefine  $\kappa$  as the coupling efficiency instead of the coupling coefficient. In addition, the effect of accumulating phase mismatch of the two coupled modes one from each of the two waveguide regions should be taken into account. To illustrate the new theory, an input bus and a nanoring is depicted in Fig. 1.10 with the minimal gap spacing, measured at the point of closest proximity, indicated by  $g$ . The widths of the bus and ring are  $w_1$  and  $w_2$ ;  $\beta_1$  and  $\beta_2$  denote, respectively, their propagation constants. The smallest separation between the center points of the bus and ring waveguide is  $2_{s0}$ , increasing to  $2_s$  along the  $z$  direction as indicated in Fig. 1.10. The net coupling efficiency can be obtained by integrating over the entire region in which the waveguided fields interact and taking into account the phase mismatch of the waveguide modes as described in Equation (1.12) [90].

$$\kappa = \int_{-\infty}^{\infty} \kappa[s(z)] \exp(-j\Delta\beta) dz \quad (1.12)$$

The gap spacing as a function of  $z$  is described by simple geometrical considerations in Equation (1.13) [90]

$$2_s = 2_{s0} + \left( R - \sqrt{R^2 - z^2} \right) \cong 2_{s0} + z^2/2R \quad (1.13)$$

Also, the parallel component of propagation constant  $\beta'_2$  is described in Equation (1.14) [90]

$$\beta'_2(z) = \cos(\arcsin \theta) \cdot \beta_2 \cong \left( 1 - z^2/2R^2 \right) \cdot \beta_2 \quad (1.14)$$

The phase mismatch  $\Delta\beta(z)$  is described in Equation (1.15) [90]

$$\Delta\beta(z) = \beta_1 - \beta'_2 \quad (1.15)$$

Substituting Equations (1.12)-(1.14) in Equation (1.11) results in

$$\kappa_{12} = \kappa_{12(2s0)} \int_{-\infty}^{\infty} \exp \left[ -\frac{\alpha_2}{2R} z^2 - j \left( \beta_{1z} - \beta_{2z} + \frac{z^3}{2R^2} \beta_2 \right) \right] dz \quad (1.16)$$

where  $\kappa_{12(2s0)}$  is a constant representing the coupling coefficient for two parallel waveguides, which is separated by a distance  $2s_0$ .

### 1.11 Nonlinear Surface Plasmon-Polaritons at Metal Surfaces

Compared to conventional bulk nonlinear crystals, metals with considerably lower optical nonlinearities are seemingly not a suitable choice for nonlinear optics research and applications. In addition, the shallow penetration of electromagnetic waves in metals leads to the optical response of bulk metals mainly governed by the weak light–matter interaction in the region near the metal–dielectric interface. At the nanoscale, however, the light–matter interaction can be significantly enhanced in the presence of surface plasmons, which can leverage various nonlinear optical processes. Because of the centrosymmetric lattice structure of metals, the second-order nonlinear response of metals vanishes for the bulk and the dominant contribution originates from the lattice-constants thick layer near the surface. In contrast, the third-order nonlinear response of metals is allowed in the bulk region and originates predominantly from the oscillating nonlinear dipoles in a surface layer with thickness of the order  $\lambda/2\pi$ , which is evidently much larger than the lattice constant. Importantly, excitation of SPPs can create surface waves traveling along the metal surface

[92] and thus confine the free-space waves into the subwavelength-thick surface layer for enhanced nonlinear response. Surface plasmon-polariton induced nonlinear polarization in metals was first reported for second harmonic generation in 1974, where by exciting the surface mode at an Ag-air interface enhanced the overall nonlinear polarization [93]. It has been found that the SPPs can modify the SHG response of the metal film in two different ways. First, the SPP excitation at the pump wavelength results in an enhanced electric field near the interface, which can significantly increase the nonlinear polarization in the interfacial region [94]. Second, the surface waves can be launched at the second-harmonic wavelength under the right phase-matching conditions [94]. This harmonic surface waves can then constructively interfere with other interfacial second-harmonic radiation, leading to an enhanced overall SH emission into the far-field [95]. Except for SHG, optical excitation of surface polaritons and SPPs at semiconductor and metal surfaces has also been demonstrated to affect the third-order nonlinear optical processes, such as FWM and THG. For instance, simultaneously exciting the surface polaritons in GaP at the pump frequencies  $\omega_1$  and  $\omega_2$  dramatically enhanced the nonlinear emission signal at the FWM frequency  $2\omega_1 - \omega_2$  [91]. In addition, launching surface polaritons at the FWM frequency can also be expected to generate strong nonlinear optical interaction if the wave-vector matching condition is fulfilled at the interface. Different from the SHG process, which only occurs at the metal surface, the surface polaritons mediated FWM emission can extend over the penetration depth of surface modes into the materials, which enables a sensitive spectroscopy probe for the third-order bulk nonlinear susceptibility  $\chi^3$ . In addition to the surface FWM waves, the intrinsic FWM originating from the metal bulk also contributes to the total emission, although the SPP-enhanced FWM can be dominant in proper experimental configurations [96]. Similar phenomena have also been observed for third-harmonic generation. More specifically, it has been demonstrated in recent

experiments [94] that launching SPP modes at the FWM frequency was achievable by carefully selecting the incidence angles of the pump beams, as per Fig. (1.11 a) [96] In this experimental configuration, the incidence waves were not directly coupled to the surface waves and thus enabled freespace excitation of SPP modes at the metal surface. In particular, the FWM signal can be further increased by coupling surface FWM waves with a nanostructured metal surface which is capable of more efficiently transferring the surface waves into outgoing, free-space propagating waves, as indicated in Fig. (1.11 b) [97]. Finally, the metal surface with locally structured features can dramatically enhance FWM, which has consequently inspired the development of nonlinear dark field microscopes as depicted in Fig (1.11 c) [98].

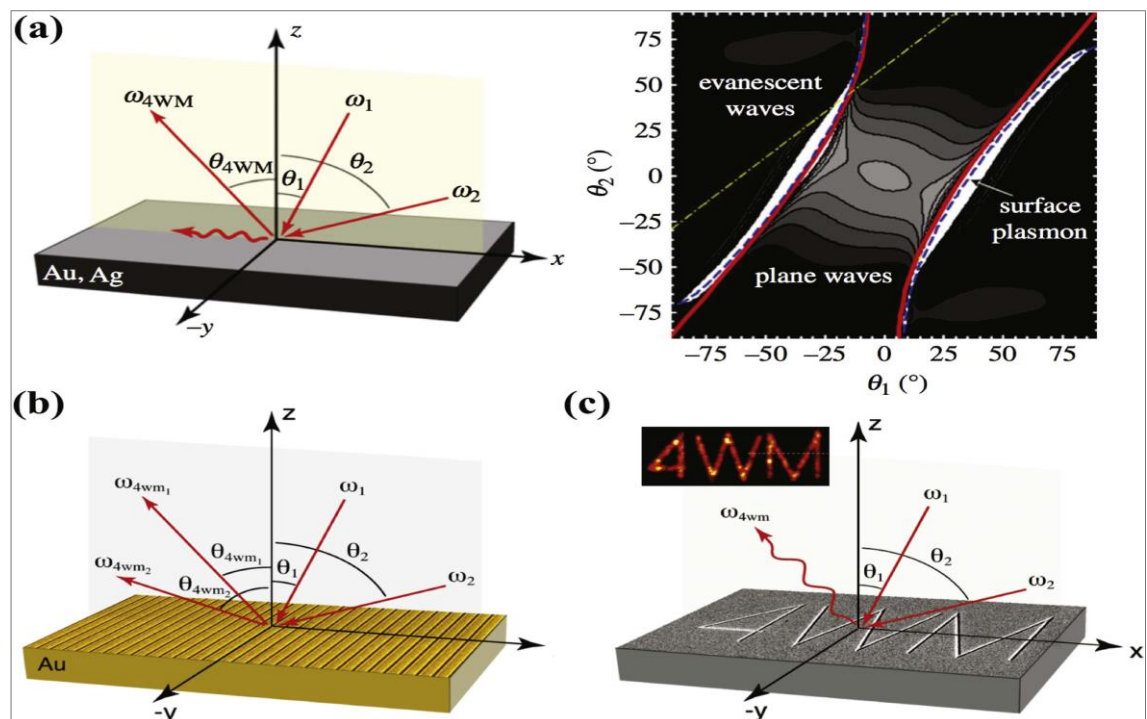


**Fig. 1.7 Nonlinear excitation of surface plasmon polaritons at metal surfaces. (a) the SPP wave at the FWM [96] (b) coupling the surface FWM wave with a nano-grating efficiently converts the FWM emission to outgoing waves in free space [97] (c) a nano-patterned metal surface strongly scattering the SPP waves at the FWM frequency enables a nonlinear dark-field microscopy [98].**

## 1.12 Applications of Plasmonic Technology

Plasmonics is one of the most dynamic regions of nanophotonic research, and it has been known as 'the following chip empowering innovation' and 'the following enormous thing in nanotechnology' as a result of its capability to be helpful for some applications [62]. Figure (1.12) exhibits a few territories where SPP can be useful.

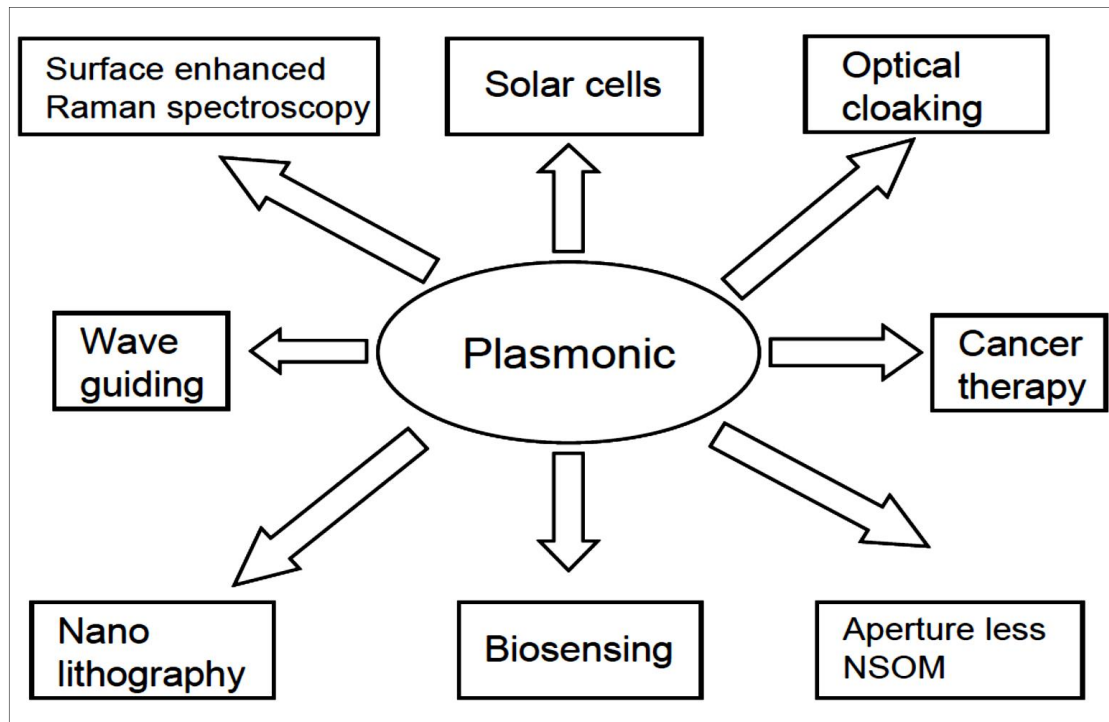


**Fig. 1.8 Main areas of applications of plasmonic [62].**

This postulation quickly centers on the plasmonic waveguide applications to feature the pre-owned structure (Plasmonic Gates) in this work. SPP waveguides have an exceptional ability to focus and manipulate light in locales with profound wavelengths, making them especially helpful for the future design of nanophotonics ICs and devices. Specific utilitarian plasmonic segments and extras use SPP waveguides to apply their ideal function(s), for example, plasmonic sensor and plasmonic modulators [62]. This thesis centers on the plasmonic logic gates application for the criticalness of this application in future integrated circuits. For integrated plasmonic circuits or devices, which include electronic and SPP parts, the

switch (plasmonic logic gates) is fundamental as a transport for signal handling. In the electronic circuit, alongside the on/off states, a third state is required without input, so signals can be traded without upsetting different parts. The reasonable choices for the switch in plasmonic circuits are the metal nanowires because they can all the while bolster distinctive SPP wavelengths and can deal with them autonomously [63]. For the most part, by changing the light polarization, the status components and field appropriations can be managed inside nanowires, giving an approach to control the steering of plasmons in nanowires, for example, Figure (1.13 a) and (1.13 b).

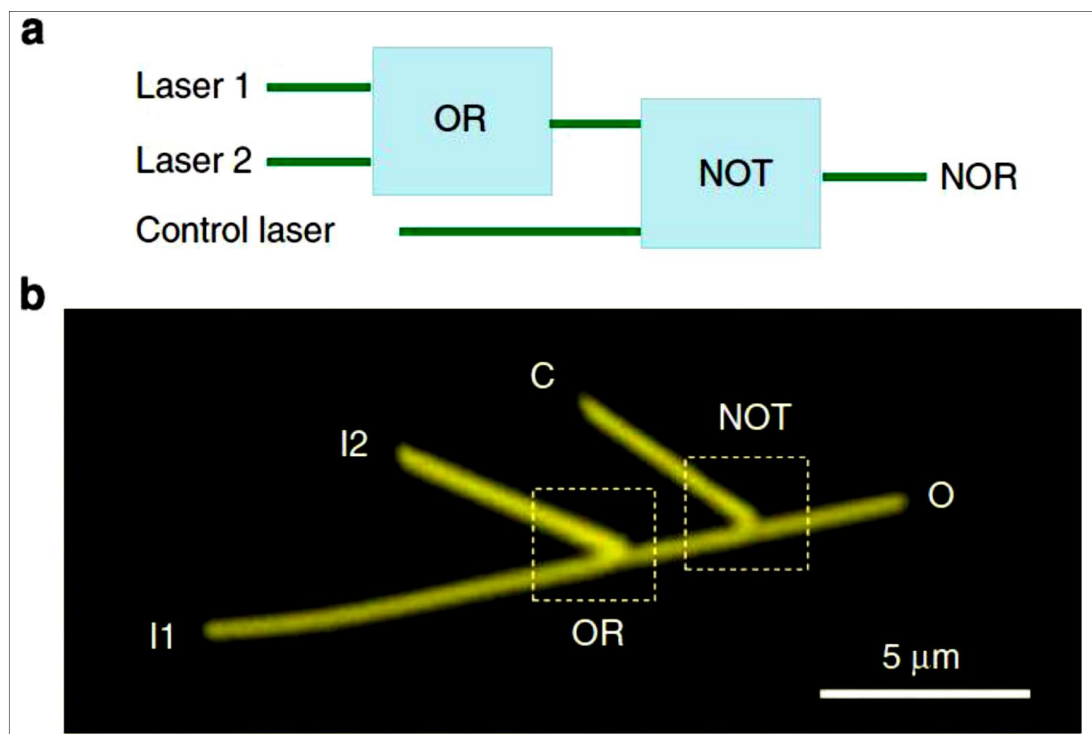


**Fig. 1.9** Cascaded logic gates for NOR gates (a) schematic illustrations of logic gates NOR built by cascaded OR and NOT gates (b) optical images of the designed nanowire structures[24].

The SPP switch can be actualized with a nanowire arrangement by utilizing the diverse stage variety of SPP impedance [24, 64].

### 1.13 Aim of the Work

This thesis aims to design and analyze two and multiple inputs all-optical NOT, OR, AND, NOR, NAND, EX-OR, and EX-NOR logic gates using; the same structure, resonance frequency, transmission threshold, materials, and structure dimensions based on Nano-ring Insulator-Metal-Insulator (IMI) plasmonic waveguides. This work can be achieved by manipulating the structure parameters, location of inputs and activation ports, the polarization angle of the input light field, and the geometrical dimensions of the proposed structure.

### 1.14 Literature Survey

Because of the importance of all-optical gates and its applications based on sub-wavelength structure (i.e. plasmonic structure) which give the advantage of overcoming the limitations of electronics and photonics devices, it has become a subject of enthusiasm for some specialists and papers as of late. Since the all-optical logic gates considered as the fundamental blocks in Nano-photonic integrated circuits and all-optical signal processing systems, many papers were published with different proposed structures to investigate and realize these devices. Some of these papers, which suggested performing this objective, are listed here:

**In 2007, Q. Xu and M. Lipson**, proposed “All-optical logic based on silicon micro-ring resonators”. AND and NAND all-optical logic gates in a micron-size silicon ring resonator based on the free-carrier dispersion effect in silicon were achieved as shown in Figure (1.20) [21]. The device used in the experiment consists of a silicon micro-ring resonator coupled to a straight waveguide. It is fabricated on SOI substrate using E-beam lithography, plasma dry etching, and plasma enhanced chemical vapor deposition (PECVD) for the SiO<sub>2</sub> cladding deposition. The silicon

waveguides forming the structure have a width of **450 nm** and a height of **250 nm**. The radius of the ring is  $R = 5 \mu\text{m}$ , and the spacing between the ring and the straight waveguide is 200 nm. The maximum contrast ratio of **10 dB** was achieved.

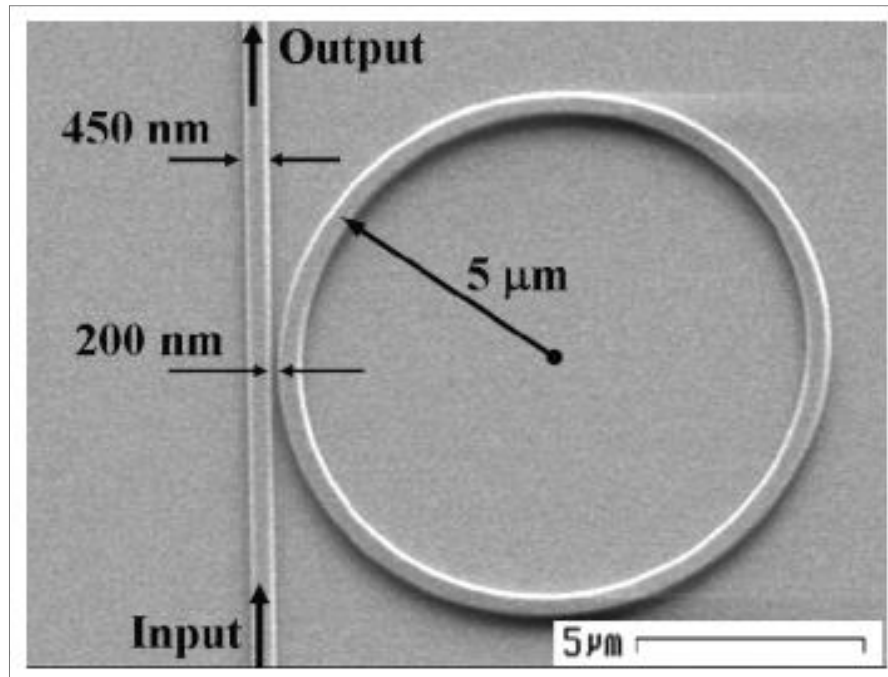


**Fig. 1.10** The proposed structure for [21]

**In 2011, J. Tao, et al.** proposed “All-Optical Plasmonic Switches Based on Coupled Nano disk Cavity Structures Containing Nonlinear Material”. All-optical plasmonic switches based on a novel coupled nano-disk cavity configuration containing nonlinear material are proposed and numerically investigated as shown in Figure (1.21) [12]. The metal material was silver and the insulator material was air. The geometrical parameters for the proposed structure the width of the bus waveguide is set to be **50 nm** while the length of  $L$  is fixed to **250 nm**. Atypical transmission and reflection spectra of the coupled disk cavity structure with  $R=210 \text{ nm}$  and gap  $G=10 \text{ nm}$ . The maximum contrast ratio of **18.4 dB** was achieved.

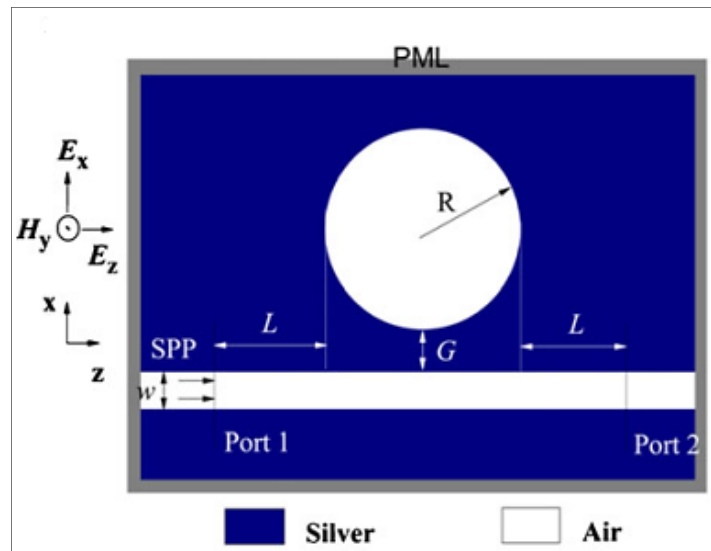


Fig. 1.11 The proposed structure for [12].

In 2012, A. Dolatabady, et al. proposed “All-Optical Logic Gates Based on Two Dimensional Plasmonic Waveguides with Nanodisk Resonators”. The proposed gates were; NAND, EX-OR, and EX-NOR based on Metal-Insulator-Metal (MIM) plasmonic waveguides and Nano-disk resonator as shown in Figure (1.22 a and b) [25]. The geometrical dimension for the proposed structure is  $(1220\text{nm} \times 1120\text{nm})$ . The maximum contrast ratio of **26 dB** was obtained at a wavelength of **525 nm**.

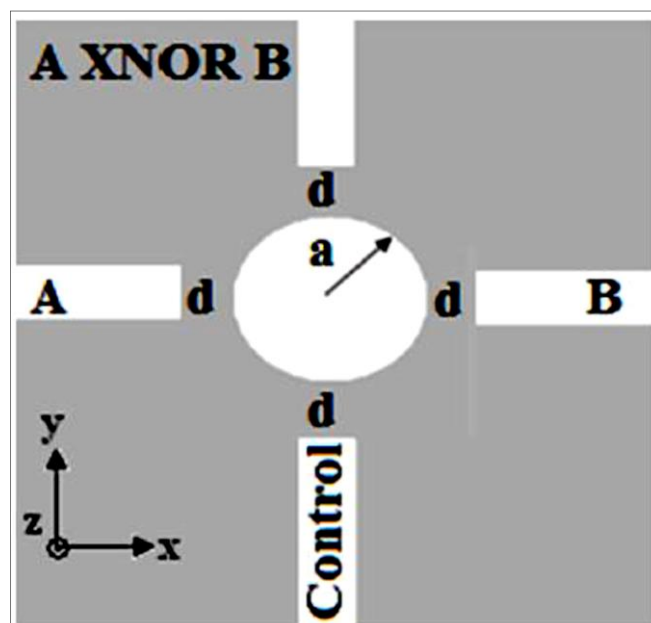
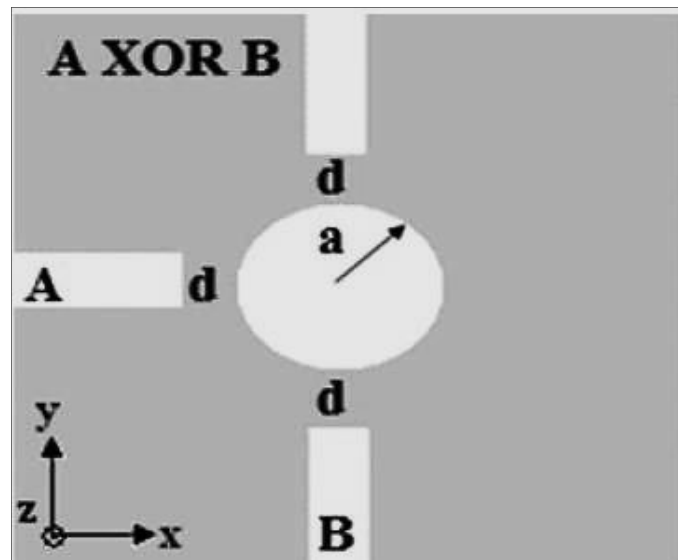


Fig. 1.12 The proposed structure for [25].

(a)



(b)

Fig.1.22 (Continued).

In 2014, N. Nozhat and N. Granpayeh, proposed “All-optical nonlinear plasmonic ring resonator switches”. All-optical nonlinear plasmonic ring resonator (PRR) switches containing  $90^\circ$  sharp and smooth bends have been proposed and numerically analyzed by the finite-difference time-domain method. It consists of a sharp corner square-shaped PRR between two parallel straight waveguides. The parameters of the structure are the width of the waveguides and resonator ( $d$ ), the gap between the waveguides and the resonator ( $g$ ), and the side length of the ring resonator in the  $x$  ( $L_x$ ) and  $z$  ( $L_z$ ) directions.

The metal is silver and the dielectric in the waveguides and the ring resonator is chosen to be  $\text{SiO}_2$  composite. The parameters of the square sharp corners PRR of is set to be  $d = 50$  nm, and  $g = 20$  nm, and  $L_x = L_z = 570$  nm. We have chosen these values to attain the ring resonant wavelength at **1535 nm** as shown in Figure (1.23) [11].

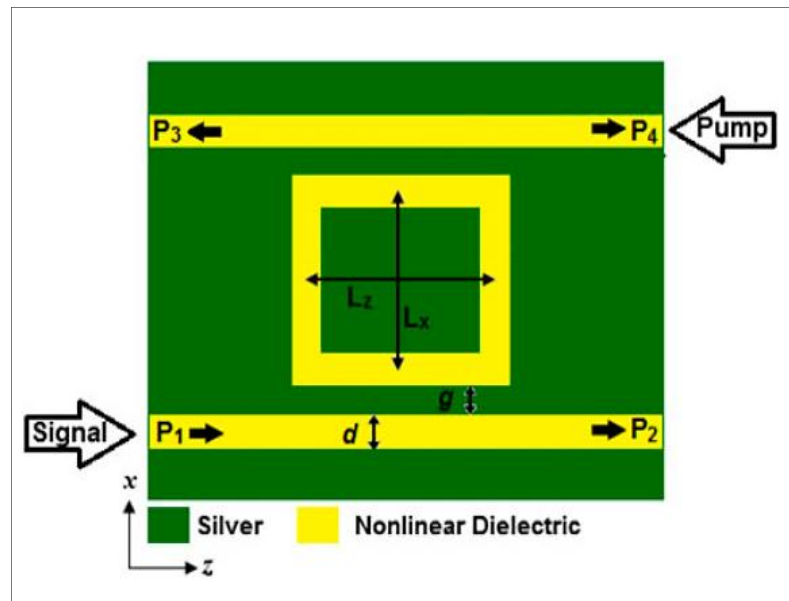


Fig. 1.13 The proposed structure for [11].

In 2015, they proposed “All-optical logic gates based on nonlinear plasmonic ring resonators”. Three all-optical logic gates NOT, AND, and NOR based on Metal -Insulator -Metal (MIM) plasmonic waveguides were proposed as shown in Figure (1.24) [27]. The parameters of the structure are chosen as: waveguide width  $w$  **50 nm**, waveguide and ring gap  $g$  **20 nm**, and side length of the square ring in the  $x$  and  $z$  directions  $L$  **570 nm**. The metal and dielectric materials are silver and  $\text{SiO}_2$  composite, respectively.

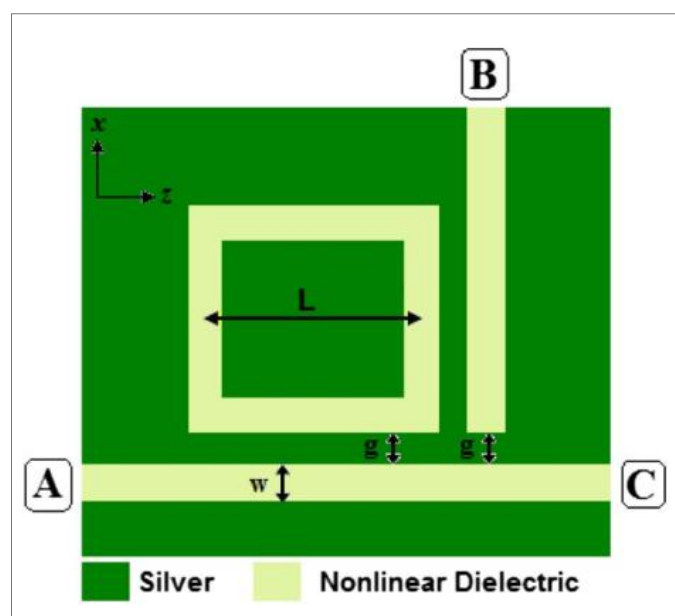


Fig. 1.14 The proposed structure for [27].

In 2018, Z. Liu, et al. proposed “Design of a multi-bits input optical logic device with high intensity contrast based on plasmonic waveguides structure”. The proposed gates were; AND and NOR gates based on MIM structure as shown in Figure (1.25) [29]. In the structure  $r = 340 \text{ nm}$  is the radii of ring resonators, and center distance  $L$  is set to be  $750 \text{ nm}$ . Other geometrical parameters of the structure are set as follows:  $w = 50 \text{ nm}$ ,  $d = 50 \text{ nm}$ , and  $g = 20 \text{ nm}$ . Due to stable optoelectronic properties at sub-wavelength, silver is chosen for metal medium.

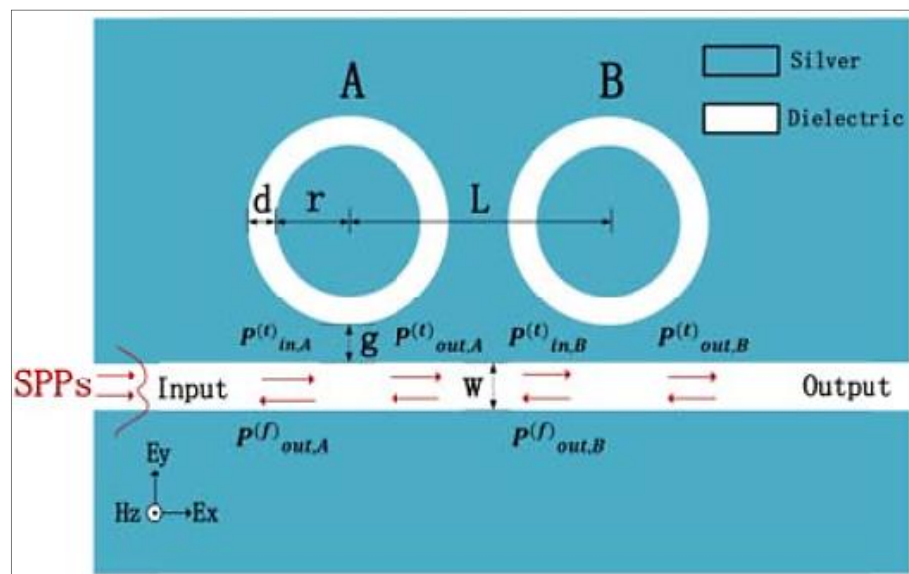


Fig. 1.15 The proposed structure for [29].

In 2019, S. H. Abdalnabi and M. N. Abbas, proposed “All-optical logic gates based on nanoring insulator–metal–insulator plasmonic waveguides at optical communications band”. The analyzed gates are NOT, OR, AND, NOR, NAND, XOR, and XNOR. The operation principle of these gates is based on the constructive and destructive interferences between the input signal(s) and the control signal. as shown in Figure (1.26) [99]. The proposed structure is designed with a very small area ( $400 \text{ nm} \times 400 \text{ nm}$ ). The maximum contrast ratio of **14 dB** was obtained.

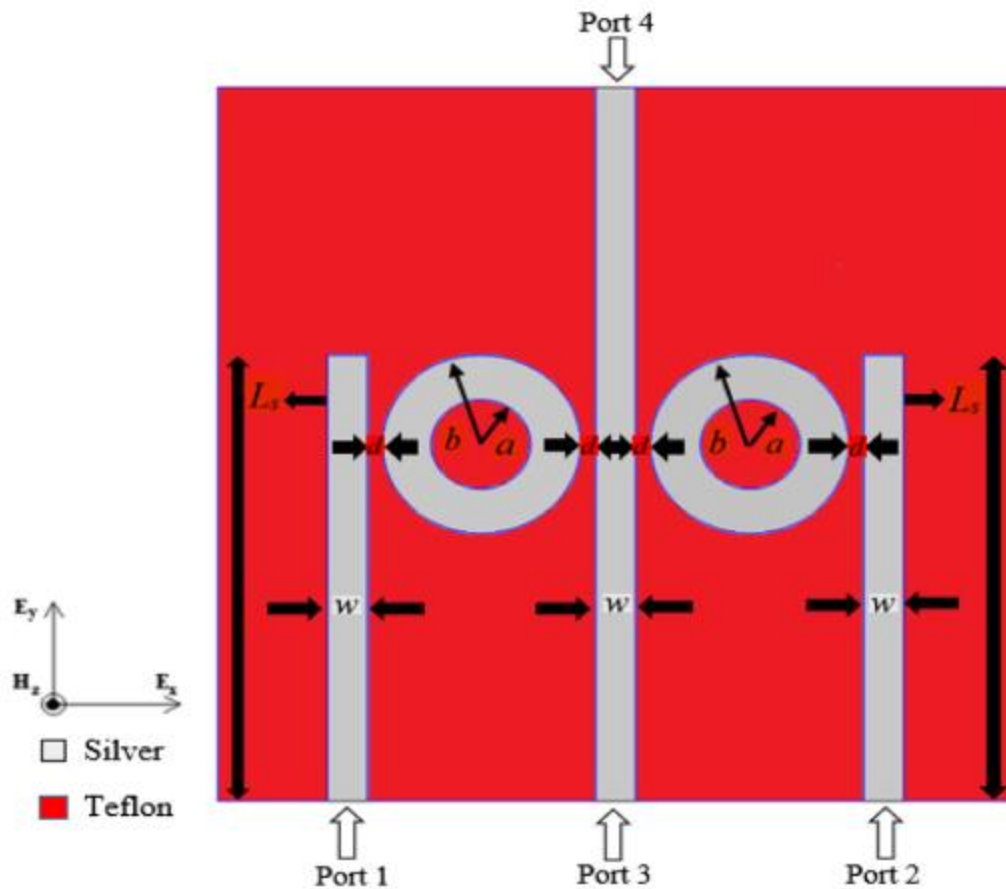


Fig. 1.16 The proposed structure for [99].

In 2019, S. H. Abdulnabi and M. N. Abbas, proposed “Design an all-optical combinational logic circuits based on nano-ring insulator-metal-insulator plasmonic waveguides”. The analyzed combinational logic functions are Half-Adder, Full-Adder, Half-Subtractor, and Comparator One-Bit. The operation principle of these combinational logic functions is based on the constructive and destructive interferences between the input signal(s) and control signal as shown in Figure (1.27) [100]. The structure that construct four combinational logic functions consists of two sub-structures of dimensions (400nm×400nm) separated by 50nm width of perfect mirror to do the isolation process between the two sub-structures.

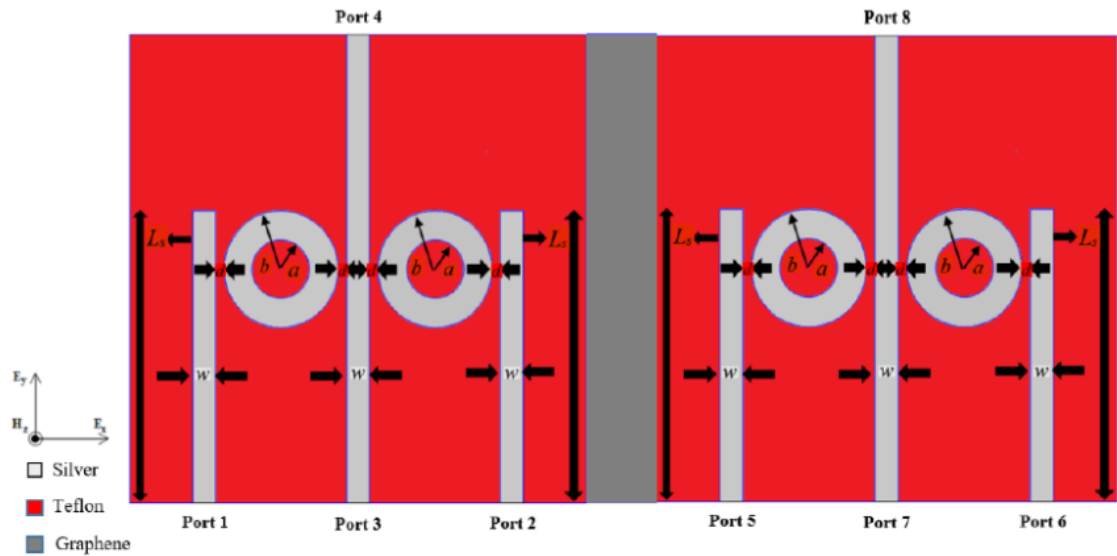


Fig. 1.17 The proposed structure for [100].

## 1.15 Thesis Organization

This thesis is structured as follows; Chapter One: Introduces the theoretical concepts of the main topics in the thesis. Chapter Two: Introduces the proposed design structures and validation parameters of the proposed plasmonic logic gates structure. In addition, the concept of constructive and destructive interferences will be presented. Chapter Three: Includes the simulation results and discussion for the proposed plasmonic logic gates based on its proposed structure in Chapter Two. Chapter Four: Presents the conclusions of the work and the suggestions for future work.

# **Chapter Two**

**Design of The Plasmonic Logic Gates**

The structures of all-optical logic gates will be presented in this chapter. The normalized transmission of the structures as a function of structure parameters are shown in this chapter. In this part of thesis, Section 2.2 introduces the structures of the all-optical NOT logic gate. Section 2.3 demonstrates the structure of the all-optical logic gates. Section 2.4 presents the ports distributions in the structure. Section 2.5 includes the structure to implement the multiple inputs all-optical logic gates. Section 2.6 presents the ports distributions in the structure of multiple inputs all-optical logic gates. The normalized transmission of the structures as a function of structure parameters are demonstrated in Section 2.7.

## 2.1 The Structures of all-optical NOT gate

The first structure to simulate the plasmonic NOT gate is shown in Figure (2.1).

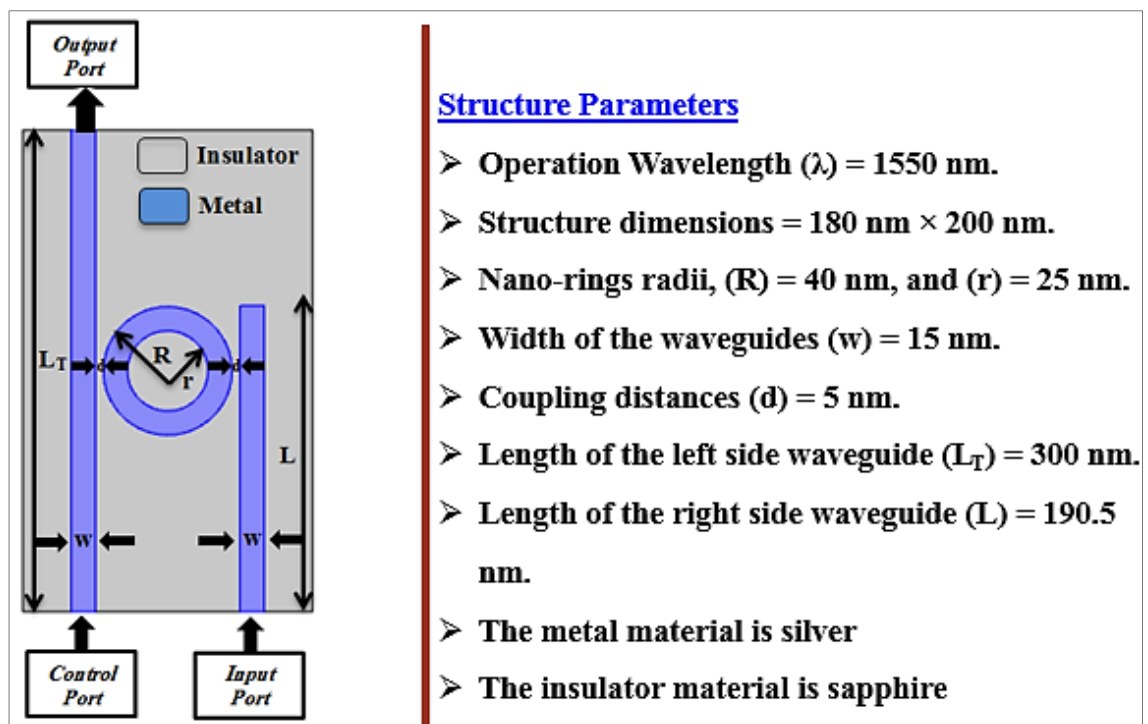
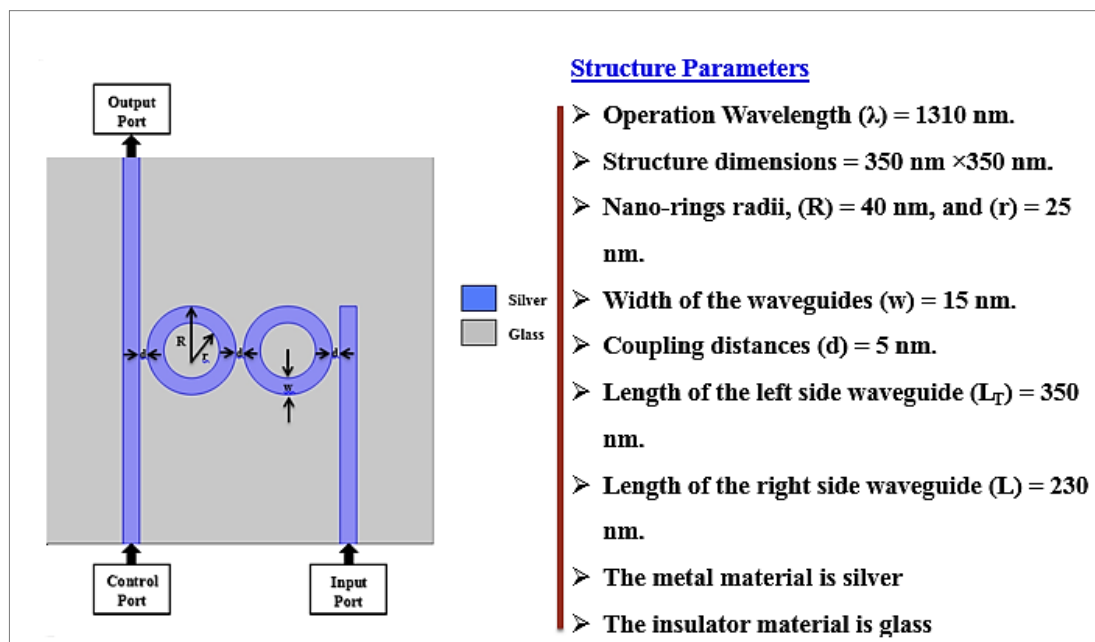


Fig.2. 1 All-optical NOT gate at C-band.

The operation wavelength ( $\lambda$ ) is 1550 nm, the structure dimensions are (width 180 nm × height 200 nm), the Nano-rings structure radii are (R) = 40

nm and  $(r) = 25$  nm, the width of the straight waveguide ( $w$ ) is (15 nm), and the coupling distances ( $d$ ) between the Nano-rings structure and straight waveguides is (5 nm). The length of the left side ( $L_T$ ), middle and the right side stripes ( $L$ ) are (300 and 190.5) nm, respectively. In the proposed NOT logic gate, there are three ports, input, output, and control ports, the control port is always in (ON) state. The metal material is silver, while the insulator material refractive index ( $n=1.78$ ) at room temperature. The straight waveguides are represented by the metal material (silver), the remaining part of the proposed structure is represented by the insulator material. The second proposed structure to simulate and realize the plasmonic NOT gate is shown in Figure (2.2).



**Fig.2. 2 All-optical NOT gate at L-band**

The operation wavelength ( $\lambda$ ) is 1310 nm, the structure dimensions are (350 nm  $\times$  350 nm), the nano-rings structure radii are (R) = 40 nm and (r) = 25 nm, the width of the straight waveguide ( $w$ ) is (15 nm), and the coupling distances ( $d$ ) between the nano-rings structures and straight waveguides is (5 nm). The length of the left side ( $L_T$ ), middle and the right side stripes ( $L$ ) are (350 and 230) nm, respectively. In the proposed NOT logic gate, there

are three ports, input, output, and control ports, the control port is always in (ON) state. The metal material is silver, while the insulator material refractive index ( $n=1.5$ ). The straight waveguides are represented by the metal material (silver); the remaining part of the proposed structure is represented by the insulator material.

## 2.2 The Structure of All-Optical Logics Gates

The structure realize the entire basic logic gate OR, AND, NOT, NOR, NAND, XNOR, and XOR, is shown in Figure (2.3).

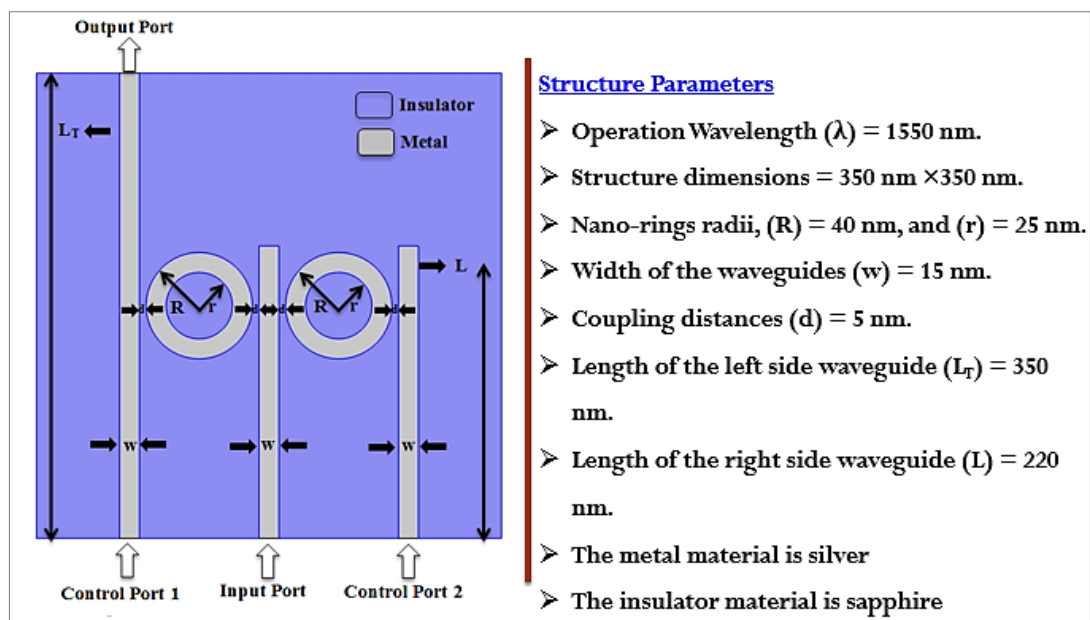


**Fig.2. 3** The structure all-optical logic gates

By employing the plasmonic IMI waveguides technology the insulating material is sapphire which is sandwiched on the silver substrate the proposed gates are simulated and realized. The structure consists of three straight stripes and two dual-ring resonator to implement the desired gates based on the insulator–metal–insulator (IMI) plasmonic waveguides. The dimensions of the proposed structure are (350  $\times$  350) nm, the length of the left side ( $L_T$ ), middle and the right side stripes ( $L$ ) are (350 and 220) nm, respectively. The width of all linear waveguides ( $W$ ) is taken as (15) nm, the radii of the inner ( $r$ ) and outer ring ( $R$ ) resonators are (25 and 40) nm,

respectively, and the spacing distance ( $d$ ) between the stripes and the ring resonators is (5) nm. The resonance wavelengths of the plasmonic systems are based on the structure dimensions and effective refractive index of the material. In the proposed design, the resonance wavelength is (1550) nm because this wavelength has a wide variety of applications in optical systems. This work centers around the wavelength of 1550 nm since this wavelength has a wide variety applications especially in optical communications. Maxwell conditions are settled numerically utilizing the two-dimensional Finite Element Method (FEM) by utilizing COMSOL Multiphysics bundle programming (Version 5.3) with a convolutional impeccably coordinated layer (CPML) as the engrossing limit state of the territory under recreation. The decision of this product program originated from the exactness of its outcomes contrasted and other programming programs utilized in a similar field, which relies upon the recurrence space as opposed to the time area. What's more, the structure is isolated into too little focuses to explain the conditions dependent on FEM right now. The structure is energized by a TM enraptured plane wave with electromagnetic field segments of  $E_x$ ,  $E_y$ , and  $H_z$ . The proposed structure has four ports which are the input port(s), control port(s), and the output port. These ports are concluded by the required plasmonic gate. The SPPs are energized by propelling a TM-polarized plane wave to the input port(s) and control port(s). The exhibition of the plasmonic logic gates is estimated by two criteria: the first is the optical transmission which is the ratio between optical output power to the optical applied power. This should be possible by picking an edge estimation of transmission between logic 1 (ON state) and logic 0 (OFF state) at the output so as to decide the status of output [92]. The estimation of the transmission threshold has been picked as (0.5) so as to realize all the plasmonic gates using the same structural parameters. The second parameter is the contrast or an extinction ratio between the minimum optical power of the ON state and the maximum optical power of the OFF

state of the output port. Whenever the variance between these output optical powers of these states is large, the performance of the plasmonic logic gate becomes better. These two criteria are described by Equations (2.1) and (2.2) [28], [93], respectively.

$$T = \frac{P_{\text{out}}}{P_{\text{in}}} \quad (\text{for both states ON and OFF of the output port}) \quad (2.1)$$

Where  $T$  represents the optical transmission,  $P_{\text{out}}$  represents the output power at the output port, and  $P_{\text{in}}$  represents the input power to the input port.

$$\text{Contrast Ratio (dB)} = 10 \log \left[ \frac{P_{\text{out}}(\text{ON State})}{P_{\text{in}}(\text{OFF State})} \right] \quad (2.2)$$

where  $P_{\text{out}}(\text{ON State})$  is the transmitted optical power in the case of ON state (logic 1), and  $P_{\text{in}}(\text{OFF State})$  is the transmitted optical power in case of OFF state (logic 0). The transmitted optical power can be maximized or minimized based on the structure design, dimensions, and other parameters such as material refractive index, the polarization of the applied field and its phase. The basic operations of the logic gates are achieved based on the principle of the constructive and destructive interferences between the signals which propagate in the linear waveguides and as a result of the interaction between the linear waveguides and the dual rings resonators new localized surface plasmon resonances (SPR) will be generated. The interference between the input light signals depends on the phase of the input light field and the position(s) of the active port(s) (input, control) where the (SPR) is strong in near field regime thus, as the spacing distance ( $d$ ) decreased, the constructive interference increased and as a result the transmitted power will be increased. According to our simulation results, the optimum spacing distance ( $d$ ) between the dual ring resonators and the linear waveguides is (5 nm). To realize the constructive interference the phase of the applied signals to the ports (input ports + activation port) as well as the propagation directions are the same, whereas the destructive

interference can be activated by making either the phase of the propagation directions of the applied waves to the ports are different.

### 2.3 Distribution of Structure Ports

To realize the behavior of NOT gate in the proposed design only one input port (port 2) is used, with two control ports (port 1 and port 3). Figure (2.4) shows the ports distribution of the proposed structure to realize the function of NOT logic gate. In order to perform the functions of the OR, AND, and EX-OR logic gates in the proposed design, two input ports are used (port 1 and port 2), with one control port (port 3), and output port (port 4). Figure (2.5) shows the ports distribution of the proposed structure to realize the function of these logic gates. In order to perform the functions of the NOR, NAND, and EX-NOR logic gates in the proposed design, two input ports are used (port 2 and port 3), with one control port (port 1), and output port (port 4). Figure (2.6) shows the ports distribution of the proposed structure to realize the function of these logic gates.

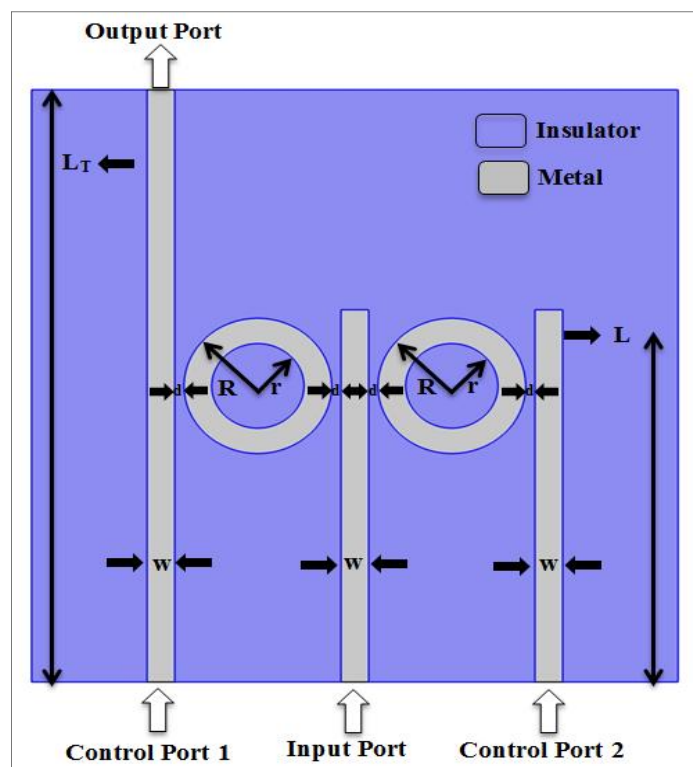


**Fig.2. 4 NOT logic gate ports distribution**

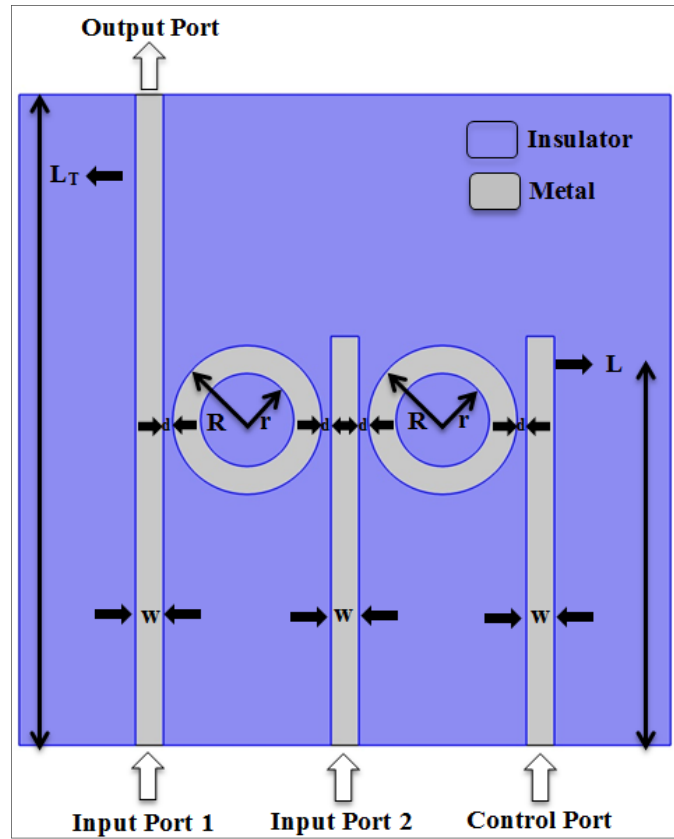


Fig.2.5 OR, AND, and EX-OR logic gates ports distribution.

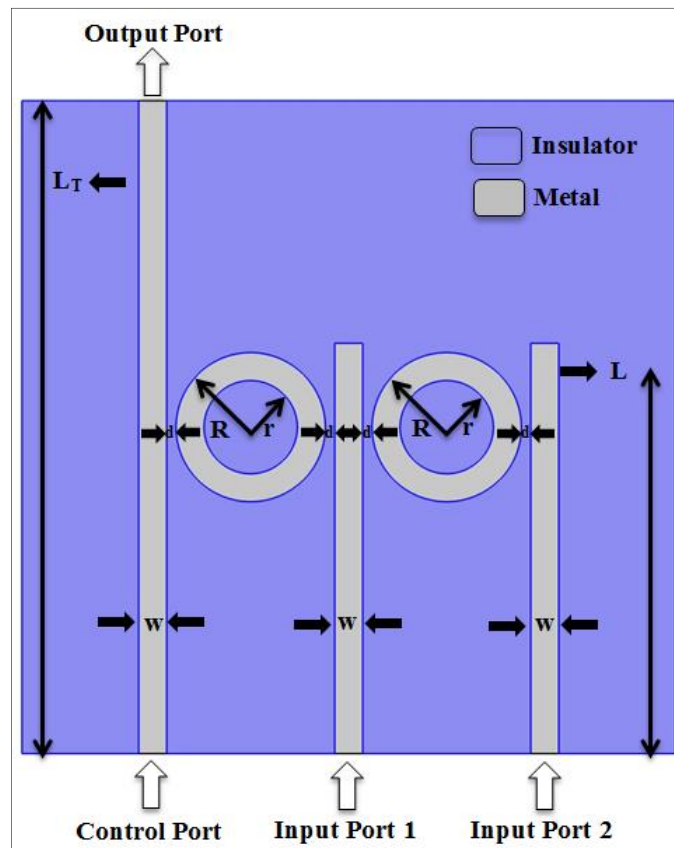
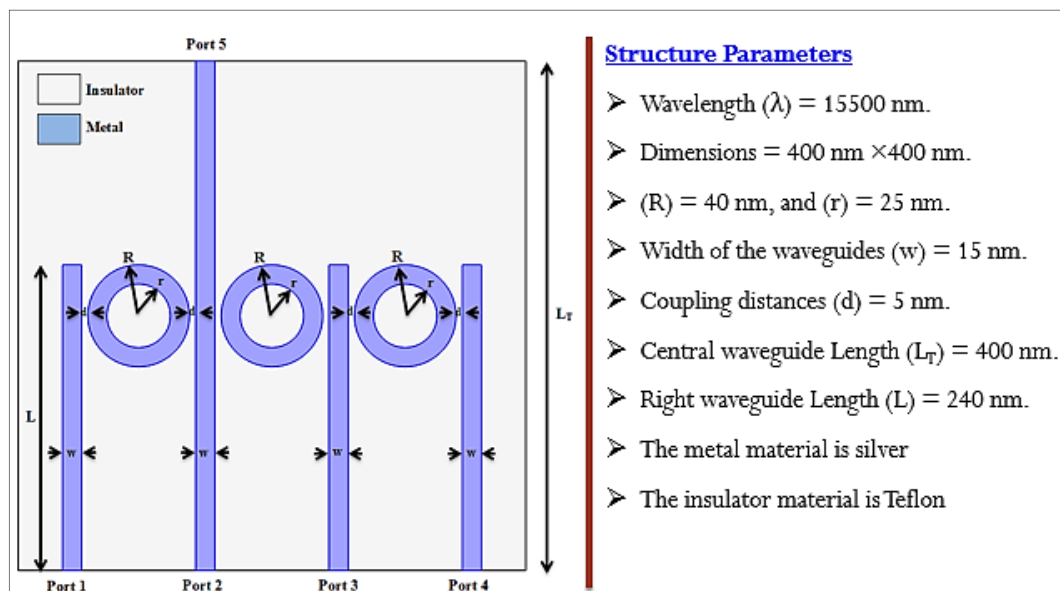


Fig.2.6 NOR, NAND, and EX-NOR logic gates ports distribution.

## 2.4 The Structure of Multiple Inputs All-Optical Logic Gates

The proposed structure to simulate three inputs all-optical logic gates is shown in Figure (2.7). NOT, AND, NAND, NOR, and EX-NOR all-optical logic gates were suitably designed and investigated based on the linear interface between the propagated waves through the waveguides. The dimensions of the proposed structure are  $(400 \times 400)$  nm. The structure has four linear waveguides (straight waveguides) and three nano-rings resonators based on plasmonic IMI technology. The length of the second straight waveguide ( $L_T$ ) is (400 nm), while the length of the other straight waveguides ( $L$ ) is (240 nm); the width ( $w$ ) of the waveguides is (15 nm). The radii of the outer ( $R$ ) and inner ( $r$ ) ring resonators are (40 nm) and (25 nm) respectively. The spacing distance ( $d$ ) between the straight waveguides and ring resonators is (5 nm). The metal material was silver, and the refractive index ( $n$ ) of the insulator material was (1.292). Due to its wide applications in optical communications, the operation wavelength of (1550 nm) is selected to be used in the proposed design.



**Fig. 2.7** The proposed structure of multiple inputs all-optical logic gates.

## 2.5 Ports Distribution of Multiple Inputs Logic Gates Proposed Structure

In order to realize the behavior of all-optical multiple inputs AND logic gate in our design, (port 2) is considered as control (activation) port, ports (1, 3, and 4) are the input ports, and port 5 is the output port. Figure (2.8) shows the ports distribution of the proposed structure to realize the function of multiple inputs AND logic gate. The output status of the NAND logic gate is (OFF) only in case of all inputs states are (ON); otherwise, the output status of the NAND gate is (ON). In the proposed design, in order to realize the behavior of the NAND logic gate, the constructive and destructive phenomena between the inputs and control ports are employed. The selected input ports are; (2, 3, and 4), and the control port is (port 1) while (port 5) is the output port. Figure (2.9) shows the ports distribution of the proposed structure to realize the function of multiple inputs NAND logic gate. In our proposed structure, the realization of NOR logic gate behavior was done by using ports (2, 3, and 4) as inputs ports, (port 1) as a control (activation) port, and (port 5) as an output port. Figure (2.9) shows the ports distribution of the proposed structure to realize the function of multiple inputs NOR logic gate. The output state of the EX-NOR gate is (ON) only when; even number of inputs is in (ON) state or all the inputs are in (OFF) state otherwise, the output state is OFF. In our EX-NOR gate proposed structure, the input ports are (2, 3, and 4); the control port is (port 1), (port 5) is the output port. Figure (2.9) shows the ports distribution of the proposed structure to realize the function of multiple inputs EX-NOR logic gate. To realize the behavior of all-optical NOT gate in our proposed structure, only three ports are used, and the remaining two ports are not used. (Port 2) is the input port, the control port is (port 1), and (port 5) is the output port. Figure (2.10) shows the ports distribution of the proposed structure to realize the function of NOT logic gate.

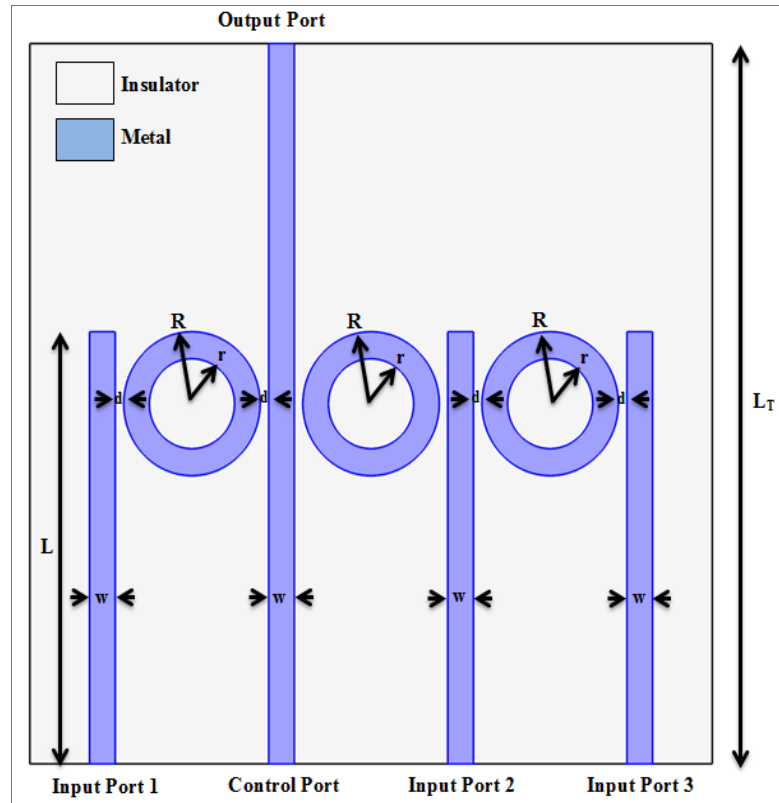


Fig. 2.8 The proposed structure of multiple inputs all-optical AND logics gates.

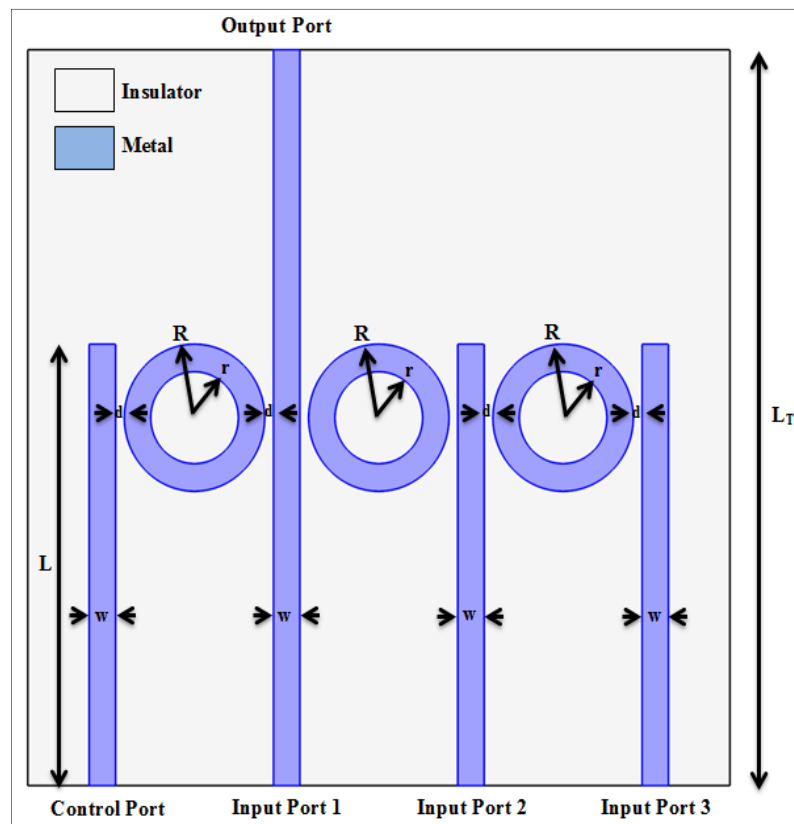
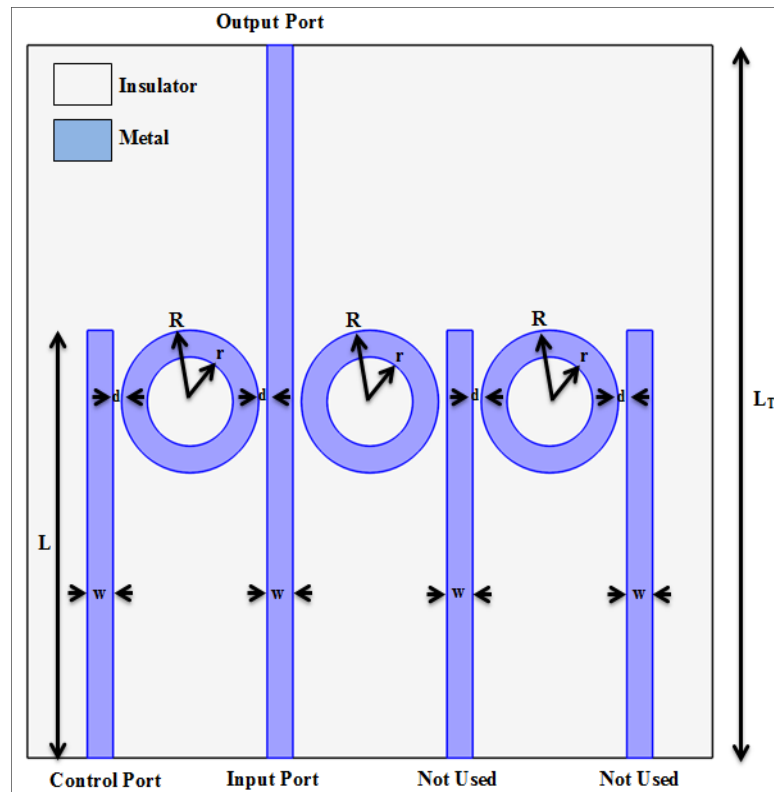


Fig. 2.9 The proposed structures of multiple inputs all-optical NAND, NOR, and EX-NOR logic gates.



**Fig. 2.10** The proposed structure all-optical NOT logic gate.

## 2.6 Optical Transmission Based on Structure Parameters

The normalized optical transmission of the proposed structure to realize all-optical logic gates is changed according to the structure parameters such as the geometrical parameters which are; waveguides length ( $L$ ), nano-rings radii ( $R$  and  $r$ ), width of the waveguides ( $w$ ), and the spacing distance between the waveguides ( $d$ ) as presented in Figures; (2.2), (2.3), and (2.6). Also, the normalized transmission depends on the materials that used to construct the structure; metals and insulators because each material has own refractive index which effect on the transmission of the structure. In this section the effect of geometrical structure parameters and type of used metal on the normalized optical transmission will be presented as a function of wavelength.

### 2.6.1 Optical Transmission as a Function of Spacing Distance

The interaction between the straight waveguides and Nano-rings leads to create new localized surface plasmon Resonance (LSPR) resulted from the coupling between the rings and straight waveguides [96]. Since the plasmon resonances is strongly coupled at near-field regime, which occurs at very short distance, thus; the coupling distance ( $d$ ) between the waveguides and Nano-rings should be decreased as much as possible to increase the value of the plasmonic field. In the proposed structure the coupling distance ( $d$ ) is assumed to be (5 nm), it's not possible to make the coupling distance less than this value due to the problems of fabrication limitations and interferences when this structure is practically implemented. Figure (2.11) shows that when the coupling distance ( $d$ ) between the straight waveguides and Nano-rings is increased, the normalized optical transmission is decreased at the resonance wavelength (1550 nm) of the proposed structure. The simulation results shows that the spacing distance ( $d$ ) of (5 nm) is the optimum value to reach the best transmission at the resonance wavelength in the proposed structure.

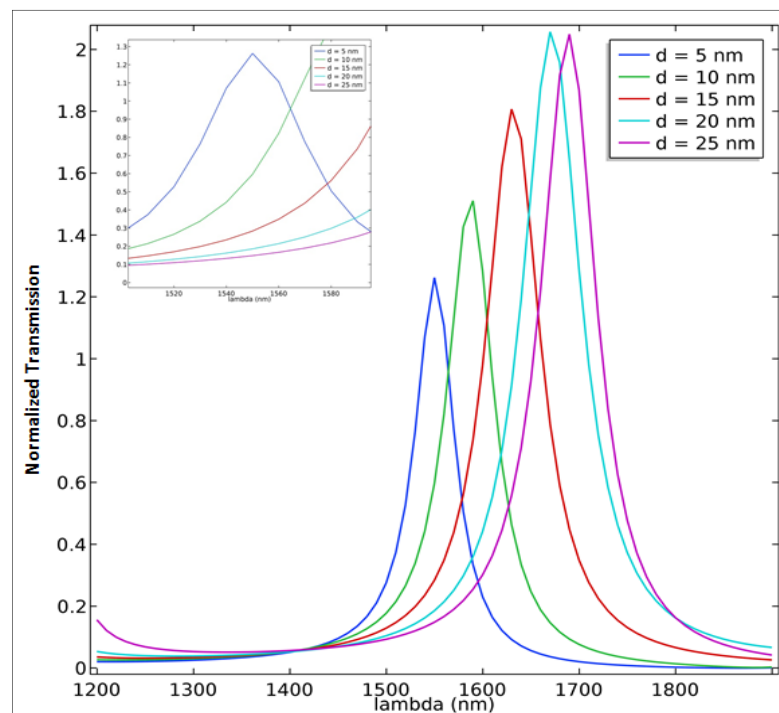


**Fig. 2.11** The optical transmission as a function of coupling distance ( $d$ ).

## 2.6.2 Optical Transmission as a Function of Waveguide Length

In the designed structures; Figures; (2.1), (2.2), (2.3) and (2.6), when the waveguide length ( $L$ ) is changed with fixing all other structure parameters, the transmitted power is slightly changed. When the waveguide length ( $L$ ) is increased from (210 to 250) nm, the normalized optical transmitted is slightly reduced and shifted from (130 to 113) %. As shown from the simulation results in Figure (2.12), the optimum waveguide length ( $L$ ) is (220 nm) which gives the maximum peak at the center of resonance wavelength (1550 nm).

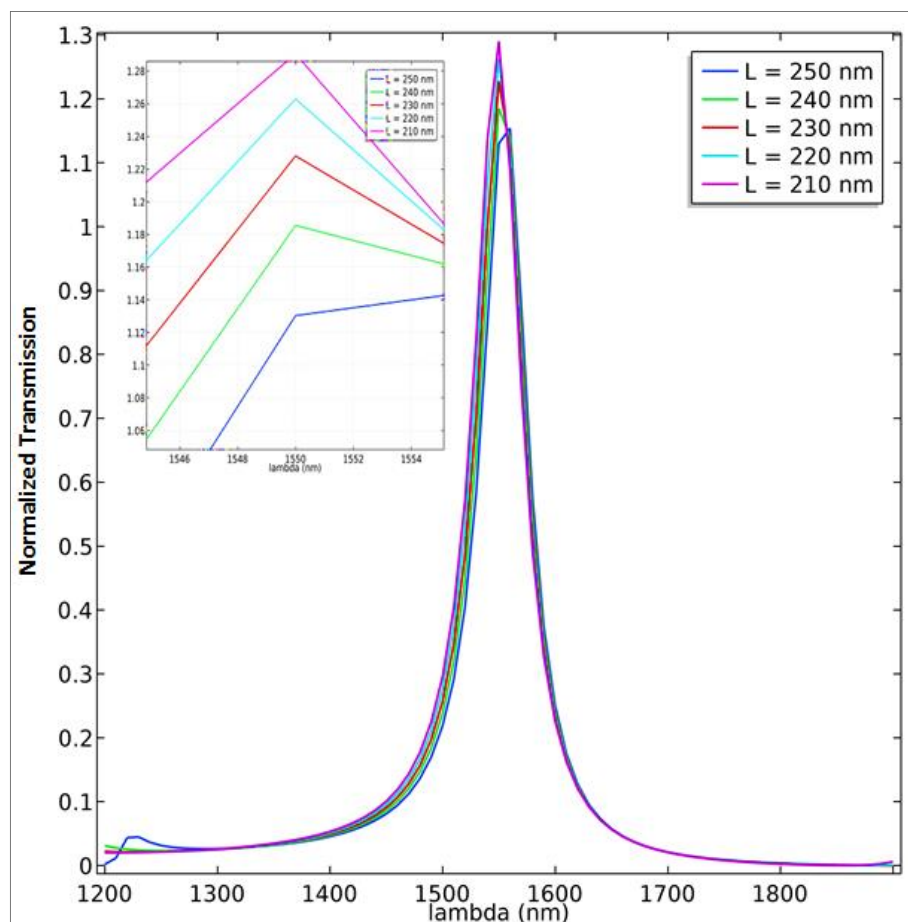


Fig. 2.12 The optical transmission as a function of waveguide length ( $L$ ).

### 2.6.3 Optical Transmission as a Function of Outer Ring Radius

In the proposed structures which are shown in Figures; (2.1), (2.2), (2.3) and (2.6), changing the bigger ring diameter ( $R$ ) with fixing all other parameters results in variation in normalized transmission with slightly blue or red shifting. If the diameter ( $R$ ) of the outer ring is above (40 nm), the transmission of the proposed structure will decrease and the resonance wavelength will have slight blue shifting. If the diameter ( $R$ ) of the outer ring is below (40 nm), the transmission increased with red shifting, till specific value which is (30 nm) the transmission again will be decreased. As shown from the simulation results in Figure (2.13), the optimum radius ( $R$ ) of the bigger ring is (40 nm) which gives the maximum transmission peak at the center of resonance wavelength (1550 nm).

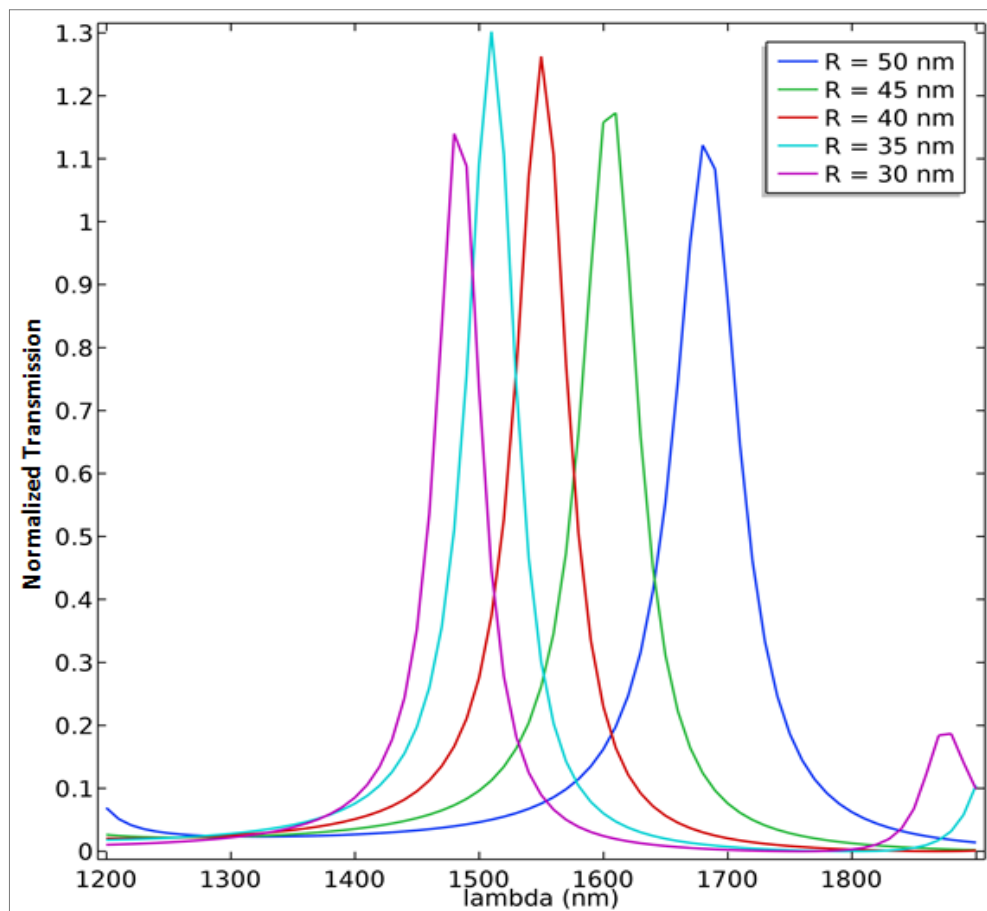
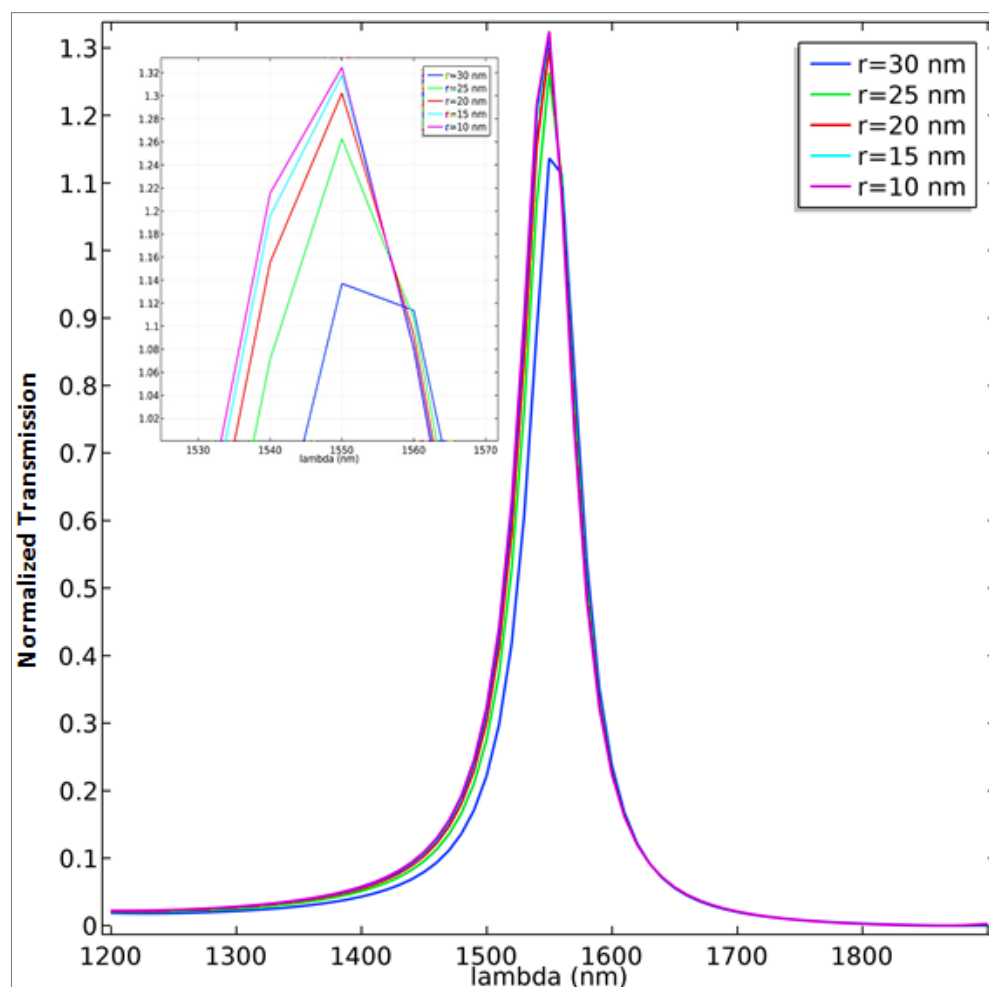


Fig. 2.13 The optical transmission as a function of bigger ring radius ( $R$ ).

### 2.6.4 Optical Transmission as a Function of Inner Ring Radius

In the proposed structures which are shown in Figures; (2.1), (2.2), (2.3) and (2.6), changing the smaller ring diameter ( $r$ ) with fixing all other parameters leads to slightly variation in transmission and shifting in resonance wavelength. As shown from the simulation results in Figure (2.14), when radius ( $r$ ) of the smaller ring is (25 nm), this gives a maximum transmission peak at the center of resonance wavelength (1550 nm).



**Fig. 2.14** The optical transmission as a function of smaller ring radius ( $r$ ).

### 2.6.5 Optical Transmission as a Function of Structure Metal

In the proposed structures which are shown in Figures; (2.1), (2.2), (2.3) and (2.6), changing the structure metal which is used in the structure gives different transmissions at different resonance wavelengths. Based on the proposed structure aims of design, and as appeared from the simulation results in Figure (2.15) only (Ag) metal gives the desired transmission at the desired resonance wavelength which is (1550 nm) due to its applications in optical communications domain as a result of low attenuation of this band.

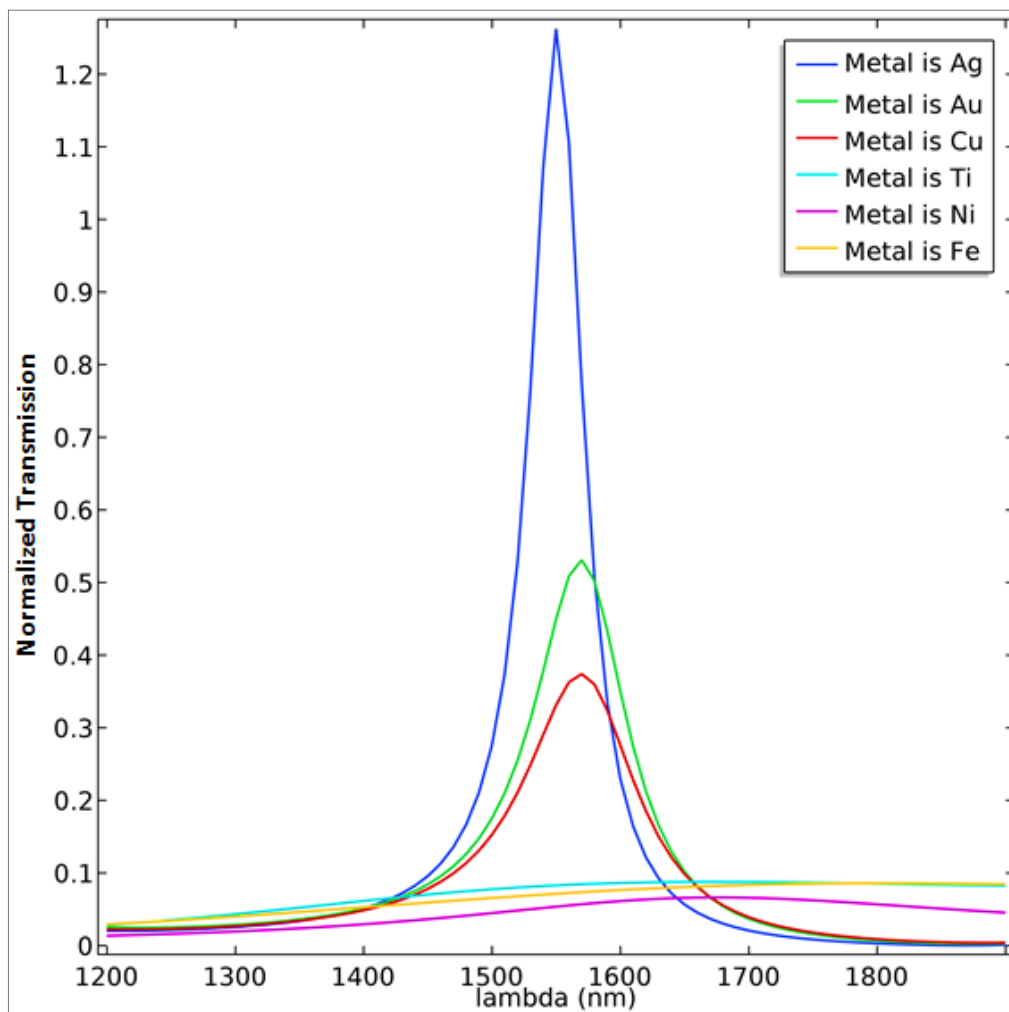


**Fig. 2.15** The optical transmission as a function of structure metal.

# **Chapter Three**

## **Simulation Results and Discussions**

## Chapter Three

This chapter gives the simulated results to evaluate the performance of the proposed plasmonic logic gates. The proposed structures have been simulated by using COMSOL Multiphysics package software (version 5.3) in order to perform the functions of the proposed plasmonic logic gates optically based on Nano-ring IMI plasmonic waveguide. The transmission of optical power and contrast ratio depend on the two criteria which determine the performance of the desired logic gate. The two criteria will be explained and discussed in this chapter. In this part of thesis, Section 3.2 introduces the simulation results and their discussions of the proposed plasmonic NOT logic gate. Section 3.3 presents simulation results and discussions for the proposed all-optical plasmonic logic gates, in addition to explaining the operation of each proposed plasmonic logic gate and calculating the constant ratio of each one. A comparison between the proposed plasmonic logic gates and previous works is presented in section 3.4. Section 3.5 presents the simulation results and the discussions of the proposed multiple inputs all-optical logic gates.

### 3.1 The All-Optical NOT Logic Gate

In the case of the input port was in OFF state, the transmission value which described in Equation (2.1) is calculated by dividing the output power which is the power of the light signal in the output port to the input power which is the power of the light signal in the control port. In the first proposed structure shown in Figure (2.1), the transmission value was (0.718) which exceeds the transmission threshold which was (0.5). In case of the input port was in (ON) state, the light signal is applied to the input port at the wavelength of (1550 nm) and phase angle of ( $180^\circ$ ), while the light signal which is applied to the control port at the same wavelength (1550 nm) and phase angle of ( $45^\circ$ ), due to the phase difference between the two light

signals in the input and control ports the destructive interference between them will occur which makes the output state is in (OFF) state because the transmission, in this case, is (0.258) which is below the transmission threshold of (0.5). In the second proposed structure shown in Figure (2.2), the transmission value was (0.725) which exceeds the transmission threshold which was (0.5). In case of the input port was in (ON) state, the light signal is applied to the input port at the wavelength of (1310 nm) and phase angle of ( $180^\circ$ ), while the light signal which is applied to the control port at the same wavelength (1310 nm) and phase angle of ( $45^\circ$ ), due to the phase difference between the two light signals in the input and control ports the destructive interference between them will occur which makes the output state is in (OFF) state because the transmission, in this case, is (0.35) which is below the transmission threshold of (0.5).

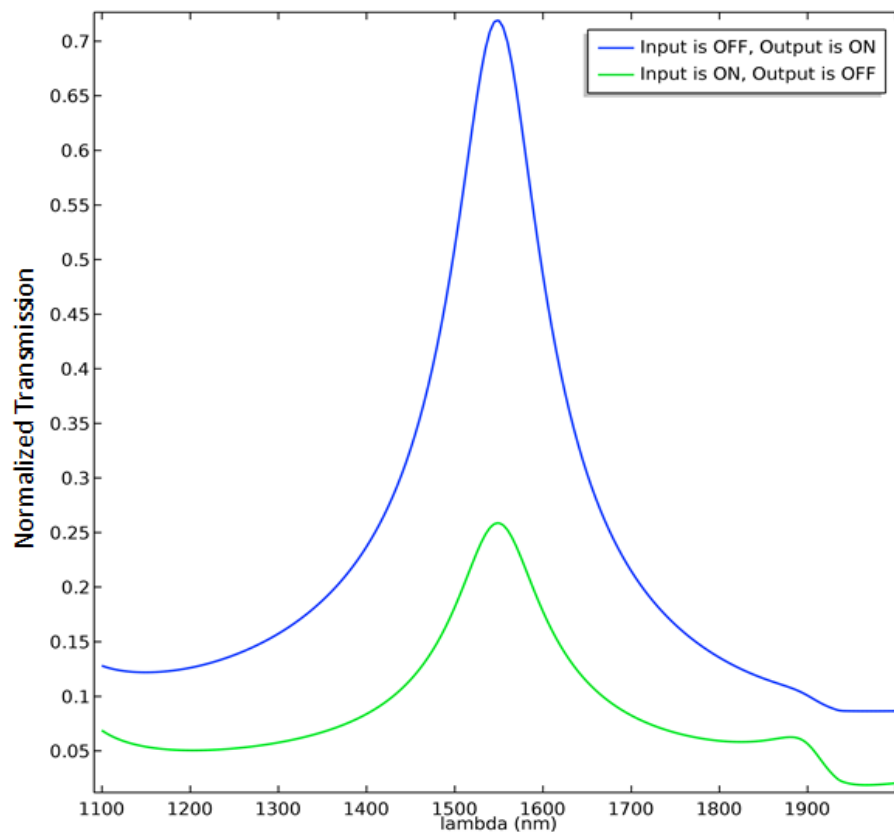
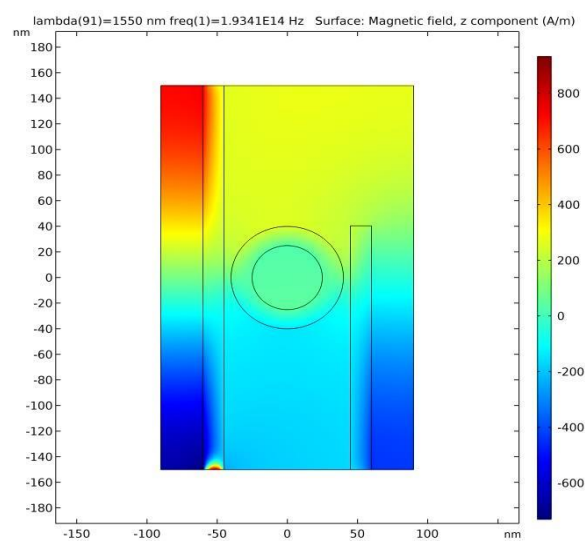
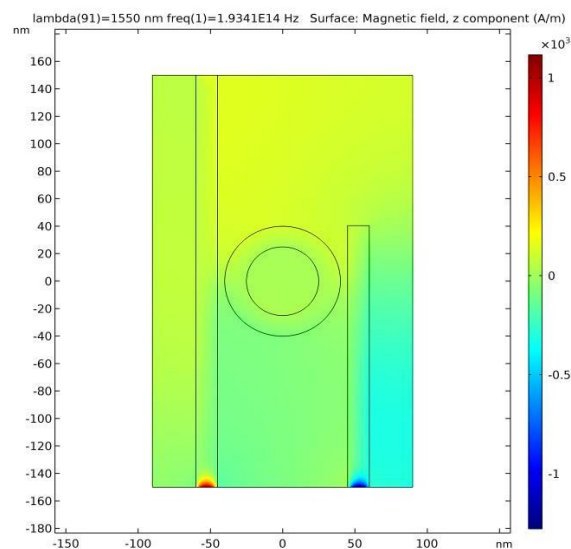


**Fig.3.1 Normalized transmission of the first proposed all-optical NOT logic gate as a function of wavelength for different input states**

The normalized transmission of the first proposed NOT logic gate, and the magnetic field distributions of the proposed gate at different input states are shown in Figure (3.1) and (3.2), respectively. The operation details of the proposed all-optical NOT logic gate are presented in Table (3.1). The normalized transmission of the second proposed NOT logic gate, and the magnetic field distributions of the proposed gate at different input states are shown in Figure (3.3) and (3.4), respectively. The operation details of the proposed all-optical NOT logic gate are presented in Table (3.2).



(a)

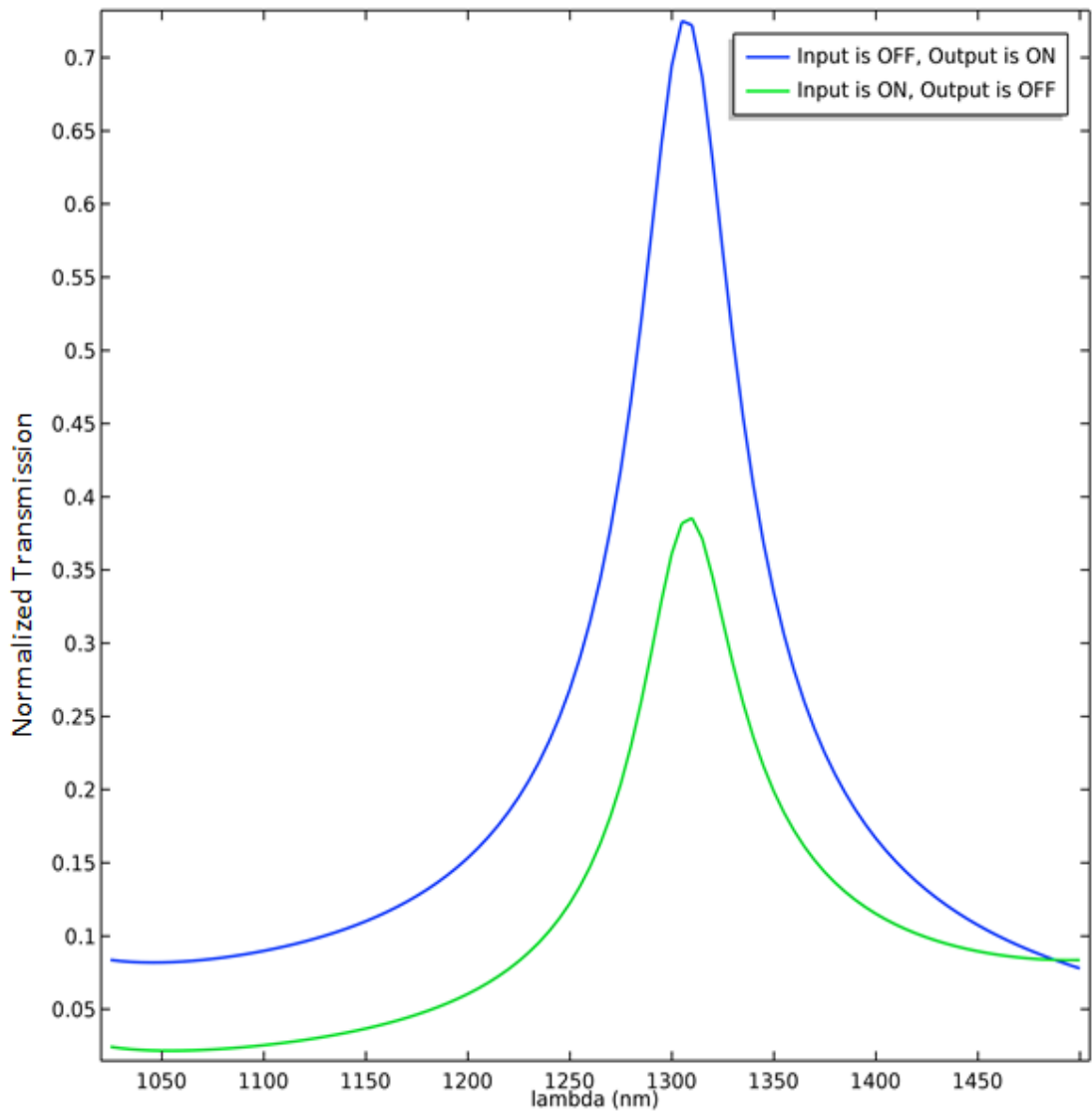


(b)

**Fig.3. 2 The magnetic field distribution of the first proposed all-optical NOT logic gate at the different input states; (a) off input state, and (b) on input state.**

**Table 3. 1** The operation details of the first proposed all-optical NOT logic gate.

Input Port State	Phase Angle Degree	Control Port State	Phase Angle Degree	Optical Transmission	Transmission Threshold	Output Port State
OFF	0	ON	0	0.718	0.5	ON
ON	180	ON	45	0.258	0.5	OFF
<b>Contrast Ratio (CR) = 4.44 (dB)</b>						

**Fig.3. 3** Normalized transmission of the proposed all-optical not logic gate as a function of wavelength for different input states.

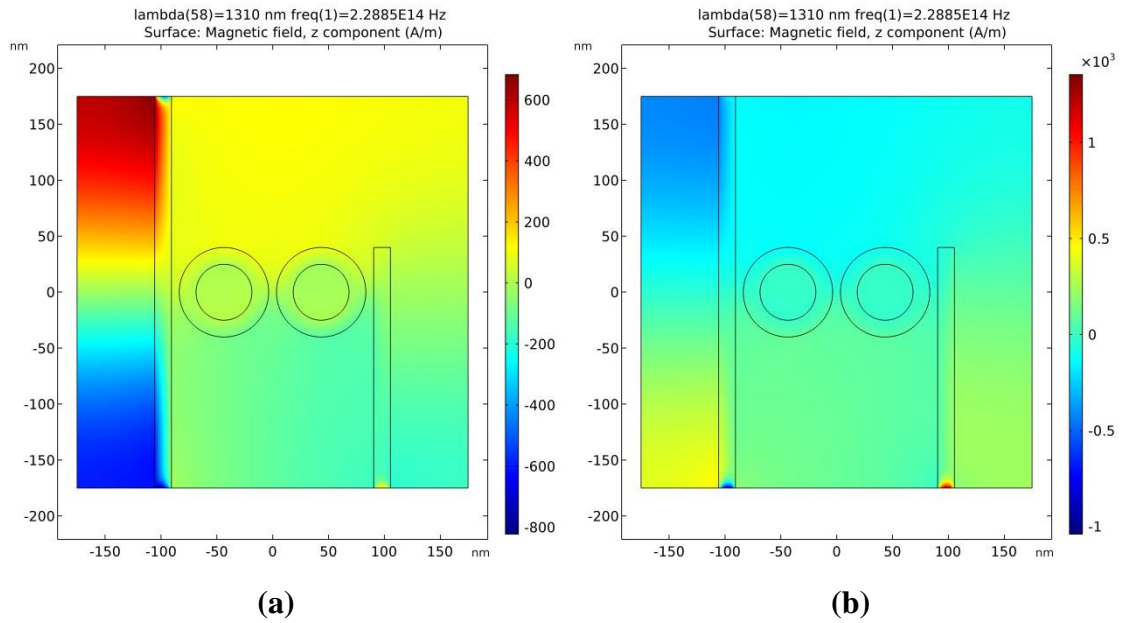


**Fig. 3. 4** The magnetic field distribution of the proposed all-optical NOT logic gate at the different input states; (a) off input state, and (b) on input state.

**Table 3. 2** The Operation Details of the Proposed All-Optical NOT Logic Gate

Input Port State	Phase Angle Degree	Control Port State	Phase Angle Degree	Optical Transmission	Transmission Threshold	Output Port State
OFF	0	ON	0	0.725	0.5	ON
ON	180	ON	45	0.35	0.5	OFF
<b>Contrast Ratio (CR) = 3.16 (dB)</b>						

### 3.2 All-Optical Logic Gates

In this section, the simulated results of all-optical logic gates are presented and discussed. The simulated gates are; NOT, OR, AND, NOR, NAND, EX-OR, and EX-NOR. The normalized transmission of each simulated logic gate, the magnetic field distribution at different input states, and the operation information tables are presented and discussed.

### 3.2.1 All-Optical NOT Logic Gate

In the proposed design of all-optical NOT gate shown in Figure (2.3), two control ports are used (port 1 and 3), one input port (port 2), and one output port (port 4) is presented in Figure (2.4). As mentioned earlier, in this chapter, the control ports are always in (ON) state to provide the necessary power to the proposed structure and to employ the interference phenomena between the propagated signals in (input and control) ports. In case of the input, port state is in (OFF) state, the light signals which are lurching to the control ports at the wavelength of (1550 nm) will propagate through the ports in the same directions and in the same phase, as a result, the constructive interference between these signals occurs and that leads to amplify the propagated signals which make the transmission at the output port, in this case, is (0.882), the transmission value at the input state is in (OFF) state exceeds the transmission threshold which is (0.5). Thus, in the case of the input state is (OFF), the output state is (ON). In case of the input port is in (ON) state, the light signal is applied to input port at the wavelength of (1550 nm) with phase angle of ( $180^\circ$ ), while the light signal which is lurching to the control port 1 is at the wavelength of (1550 nm) with phase angle of ( $45^\circ$ ), and the light signal that propagates through the control port 2 is at the wavelength of (1550 nm) with phase angle of ( $180^\circ$ ). The constructive interference between the three signals due to different propagation directions and different phase angles plays a big role to make the transmission, in this case, is (0.09) which is below the transmission threshold of the proposed structure. Thus, in the case of the input state is (ON), the output state is (OFF). The normalized transmission of the proposed NOT logic gate, and the magnetic field distributions of the proposed gate at different input states is shown in Figures (3.5) and (3.6), respectively. The operation details of the proposed all-optical NOT logic gate are presented in Table (3.3).

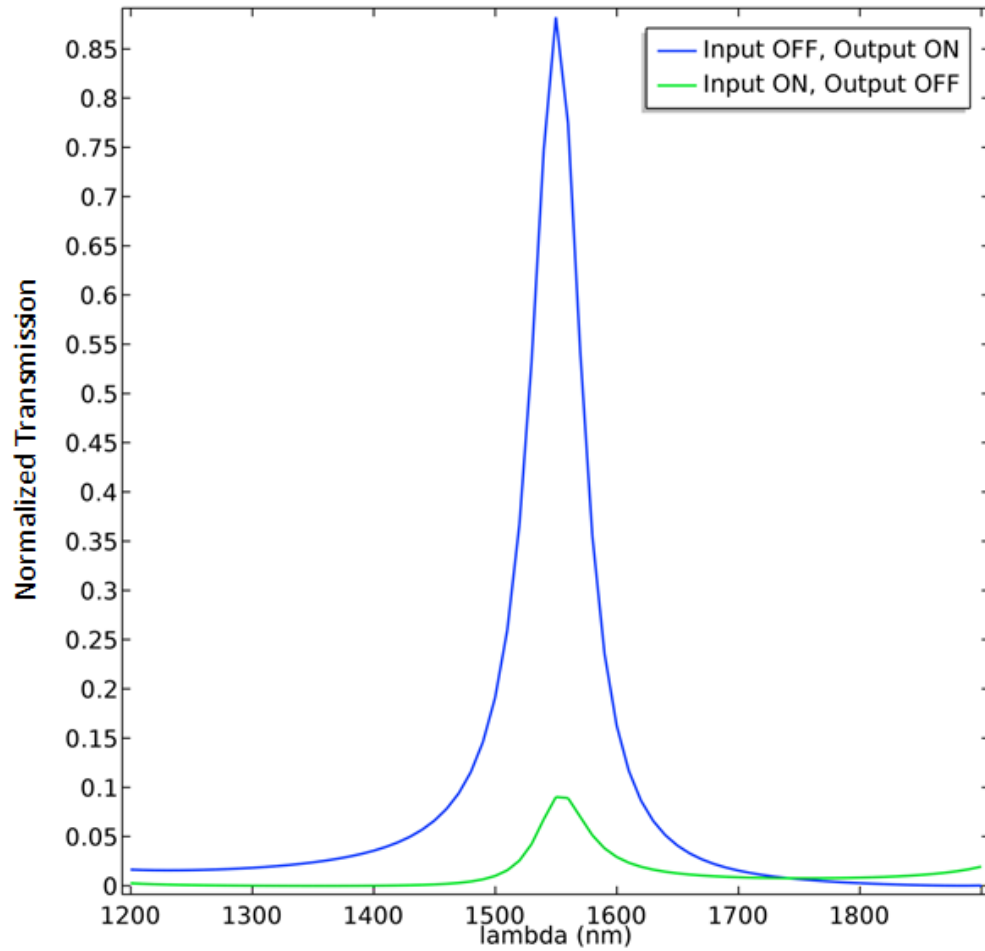


**Fig.3. 5 Normalized transmission of the proposed all-optical NOT logic gate as a function of wavelength for different input states.**

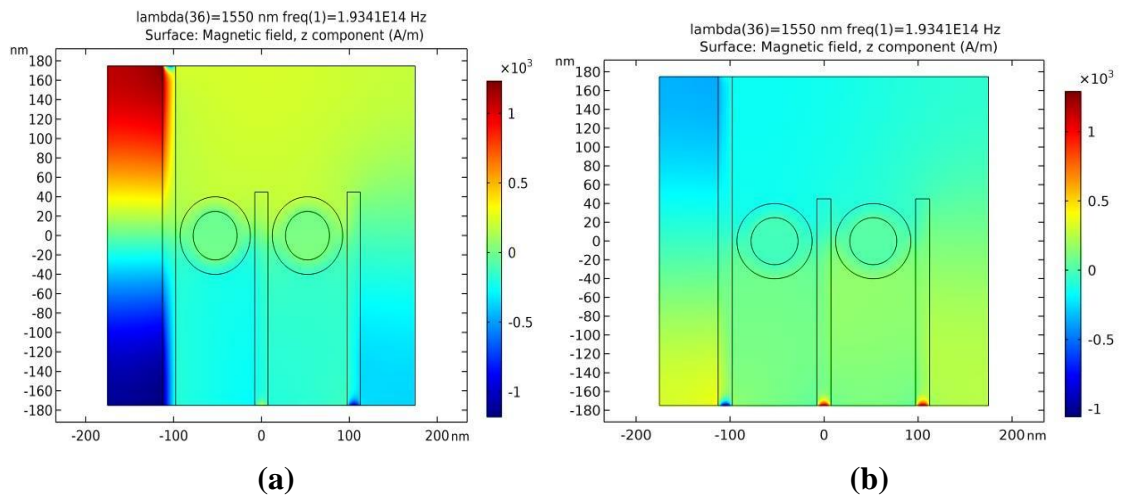


**Fig.3. 6 The magnetic field distribution of the proposed all-optical NOT logic gate at the different input states; (a) off input state, and (b) on input state.**

**Table 3. 3 The Operation Details of the Proposed All-Optical NOT Logic Gate**

Input port status	Phase degree	Control port 1 status	Phase degree of control 1	Control port 2 status	Phase degree of control 2	(T)	T Threshold	Output port status
OFF	0	ON	0	ON	0	0.882	0.5	ON
ON	180	ON	45	ON	180	0.09	0.5	OFF
<b>Contrast Ratio (CR) of The Proposed Gate = 9.91 (dB)</b>								

Equation (2.3) is used to calculate the contrast ratio (CR) where the minimum transmission at the output port in case of the output state is (ON) is (0.882), and the maximum transmission at the output in case of the output state is (OFF) is (0.09), and thus the contrast ratio (CR) is (9.91 dB). The value of the contrast ratio for the proposed NOT logic gate is relatively high value due to the large variance between the transmissions, and thus the performance of this gate is very good and efficient where whenever the contrast ratio is high, the performance is better and vice versa.

### 3.2.2 All-Optical OR Logic Gate

In the proposed design of all-optical OR gate shown in Figure (2.3), two input ports are used (port 1 and 2), one control port (port 3), and one output port (port4) as presented in Figure (2.5). In the first case of this gate, when the two input ports are in (OFF) state, only the control port is (ON). According to OR logic gate truth table, in case of all inputs are in (OFF) state, the output should be in (OFF) state also, thus the ports distribution of this gate (Figure 2.5) are selected to realize the truth table of this gate and this is the reason of considering (port 3) as the control port which is always (ON) to give low transmission of (0.053) in the case of both inputs are in (OFF) state which is below the transmission threshold which is (0.5), this distribution leads to realizing the first case of OR gate truth table. The second case of OR logic gate, when only one input of the two inputs is in (ON) state and the other input is in (OFF) state; (OFF-ON) or (ON-OFF). In the second case the light fields at the wavelength of (1550 nm) that are

inserted to the input and control ports are in phase and propagate in the same direction to employ the constructive interference between these fields to actualize the function of OR gate which state that if any input of the inputs is in (ON) state, the output has to be in (ON) state. According to the simulation results, the transmission of the cases; (OFF-ON) and (ON-OFF) are (0.88) and (0.8) respectively, and they are above the transmission threshold of (0.5). In the last case, when all the inputs are in (ON) state; (ON-ON) the light fields at (1550 nm) are launched to the inputs and control ports without any phase difference and in the same propagation direction. The constructive interference between the three light fields leads to great amplification of the output transmission exceeds (100%) and thus the transmission, in this case, is (1.26). The normalized transmission of the proposed OR logic gate and the magnetic field distributions of the proposed gate at different input states is shown in Figure (3.7) and (3.8) respectively. The operation details of the proposed all-optical OR logic gate are presented in Table (3.4).

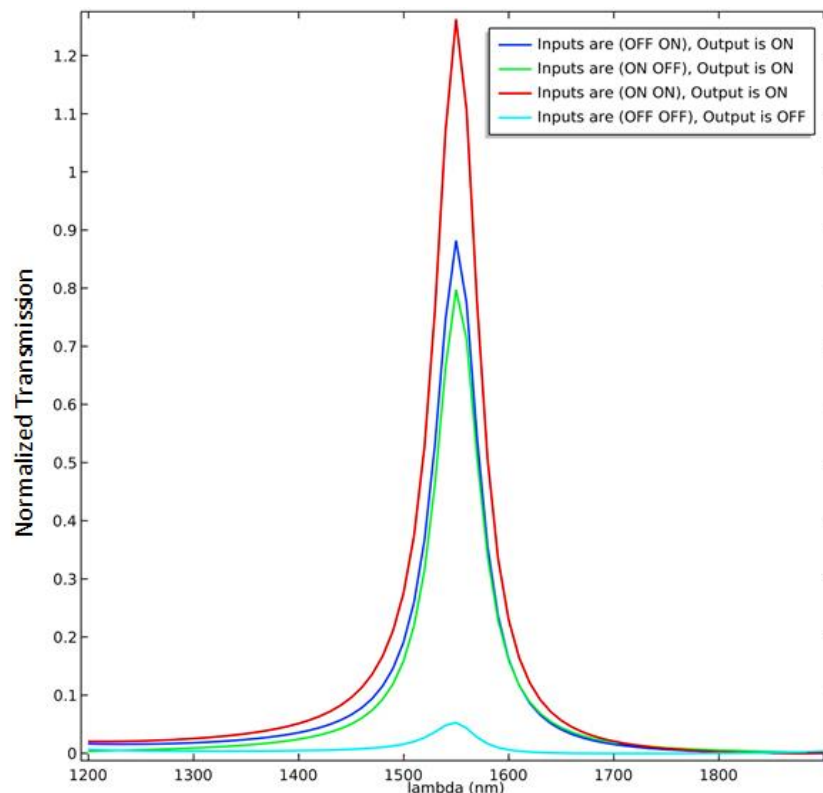


**Fig.3. 7 Normalized transmission of the proposed all-optical OR logic gate as a function of wavelength for different input states.**

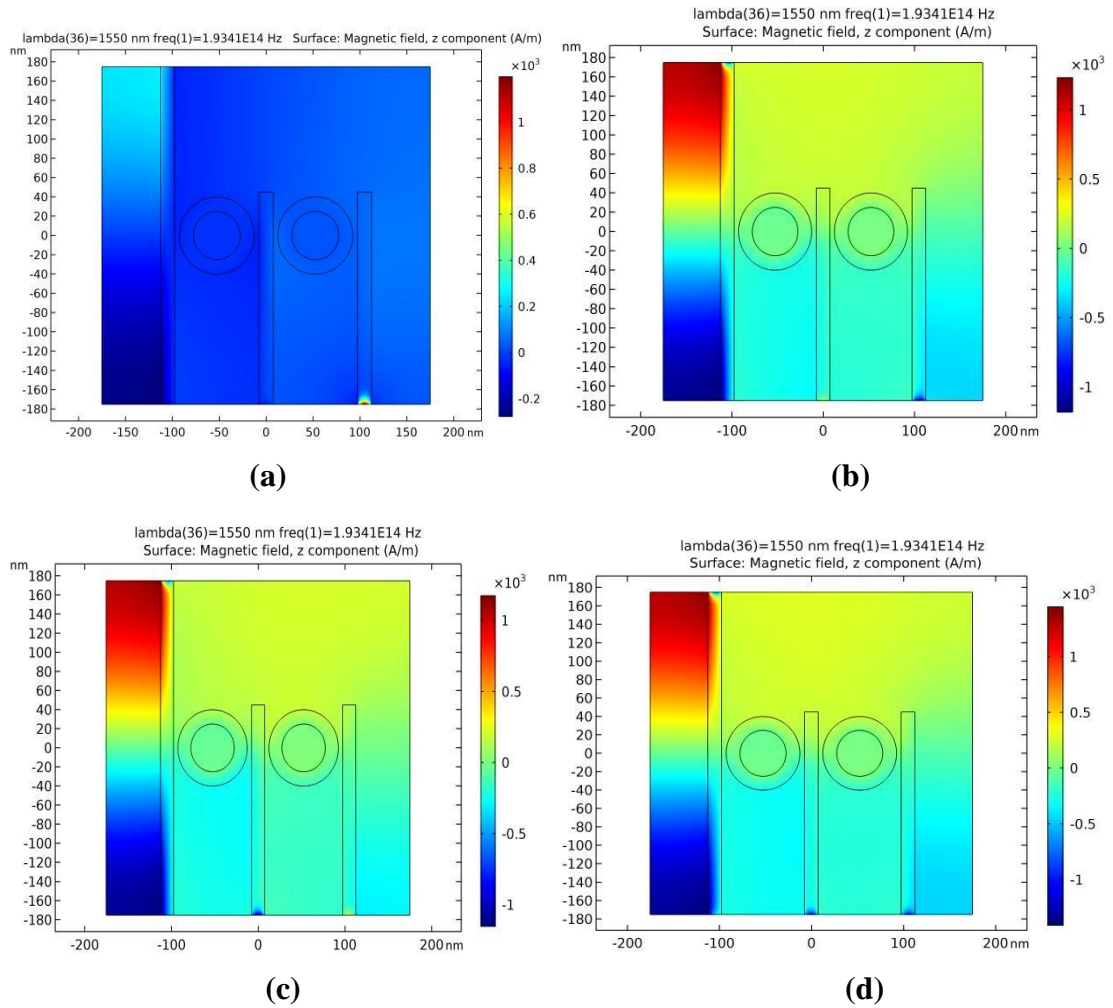


**Fig.3. 8** The magnetic field distribution of the proposed all-optical OR logic gate at the different input states; (a) (off-off) input states, (b) (off-on) input states, (c) (on-off) input states, and (d) (on-on) input states.

**Table 3. 4** The operation details of the proposed all-optical OR logic gate

Input Port 1 Status	Phase Degree	Input Port 2 Status	Phase Degree	Control Port Status	Phase Degree	(T)	T Threshold	Output Port Status
OFF	0	OFF	0	ON	0	0.053	0.5	OFF
OFF	0	ON	0	ON	0	0.88	0.5	ON
ON	0	OFF	0	ON	0	0.8	0.5	ON
ON	0	ON	0	ON	0	1.26	0.5	ON
<b>Contrast Ratio (CR) of The Proposed Gate = 11.78 (dB)</b>								

The minimum transmission at the output port in case of the output state is (ON) is (0.8), and the maximum transmission at the output in case of the output state is (OFF) is (0.053), according to Equation (2.3) the contrast

ratio (CR) is equal to (11.78 dB). The performance of the proposed OR logic gate is very good and efficient due to the high contrast ratio between the (ON) and (OFF) states.

### 3.2.3 All-Optical AND Logic Gate

In the proposed design of all-optical AND gate shown in Figure (2.3), ports distribution of proposed AND gate is similar to that of OR gate which is; input ports (port 1 and 2), control port (port 3), and output port (port4) as presented in Figure (2.5). To realize the function of the AND logic gate according to its truth table the ports are selected and distributed to exploit the interference between the signals of these ports. The outputs of AND gate are (OFF) in all cases, except in case of all inputs are in (ON) state. In the first case of AND gate cases where the inputs are in (OFF) state, only the control port is (ON) as usual. The position of the control port is selected to give low transmission below the transmission threshold (0.5) to actualize the function of the AND gate. In the first case, only the light signal in the control port is propagated and thus the transmission of this case is (0.053) and the output state is (OFF). The second case of AND gate is one of the inputs is (ON), and the other one is (OFF), in such condition in order to realize the AND gate behavior the phase difference between the light signals in the input and control ports is inserted. In (OFF-ON) input state, the light signal in the input port is lunched with a phase difference of ( $45^\circ$ ), and the light signal in the control port is lunched with ( $180^\circ$ ) phase difference. The destructive interference between these signals due to different phase angles and different propagation direction makes the transmission of this state is (0.003), the output state is (OFF). In (ON-OFF) state, the light field in the input port is lunched with ( $45^\circ$ ) phase difference angle while the control ports signal with ( $180^\circ$ ) phase difference the same as the (OFF-ON) setup. The transmission, in this case, is (0.231), higher than

the transmission of the previous case due to the position of the port with respect to the output port.

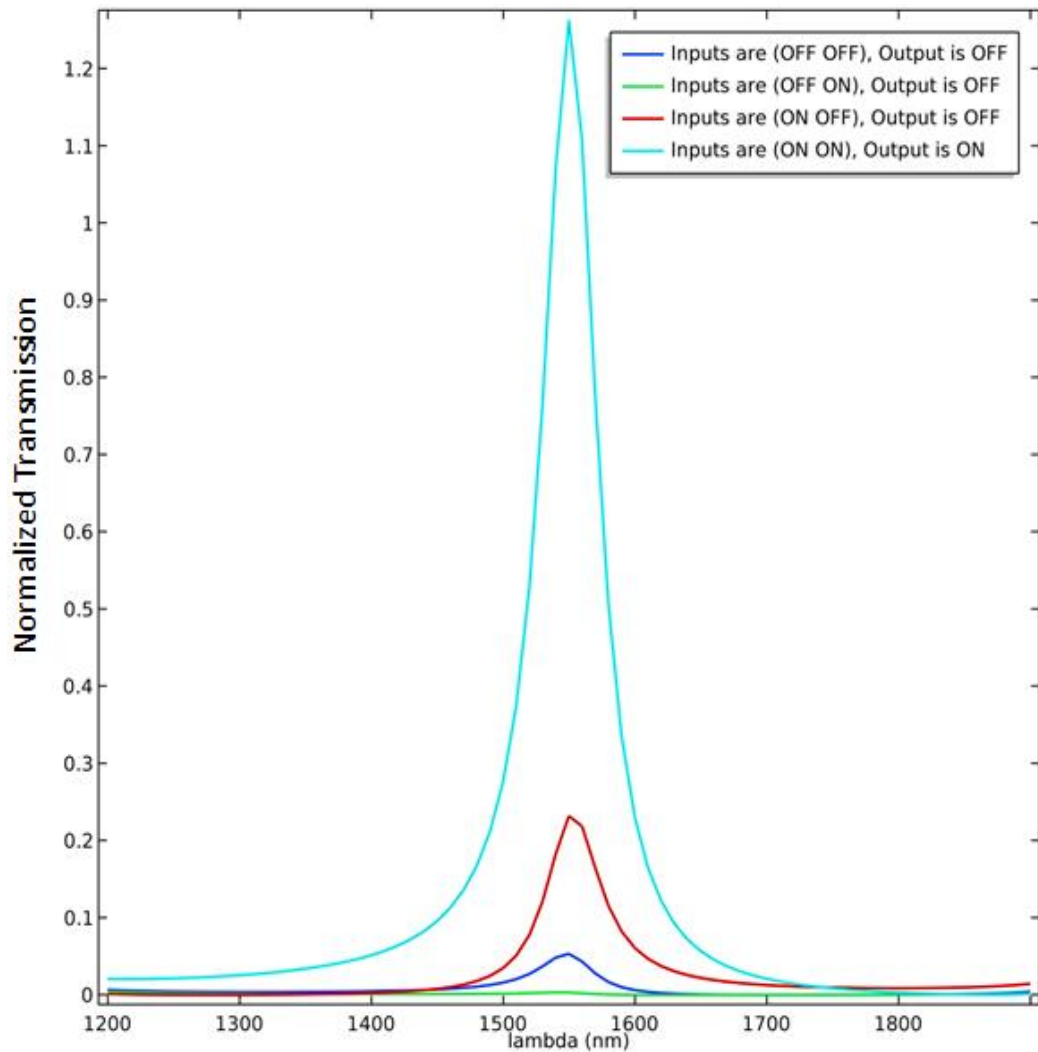


**Fig.3. 9 Normalized transmission of the proposed all-optical AND logic gate as a function of wavelength for different input states.**

The last case is (ON-ON) state, where all the inputs and control ports are in (ON) state, the light fields propagate in the waveguides in phase and in the same propagation direction to exploit the constructive interference between these fields which realize the function of AND gate of this case. Again, the high constructive interference between the three light signals propagating in phase and in the same propagation direction leads to make the transmission of this case more than (100%) where the transmission is equal to (1.26).

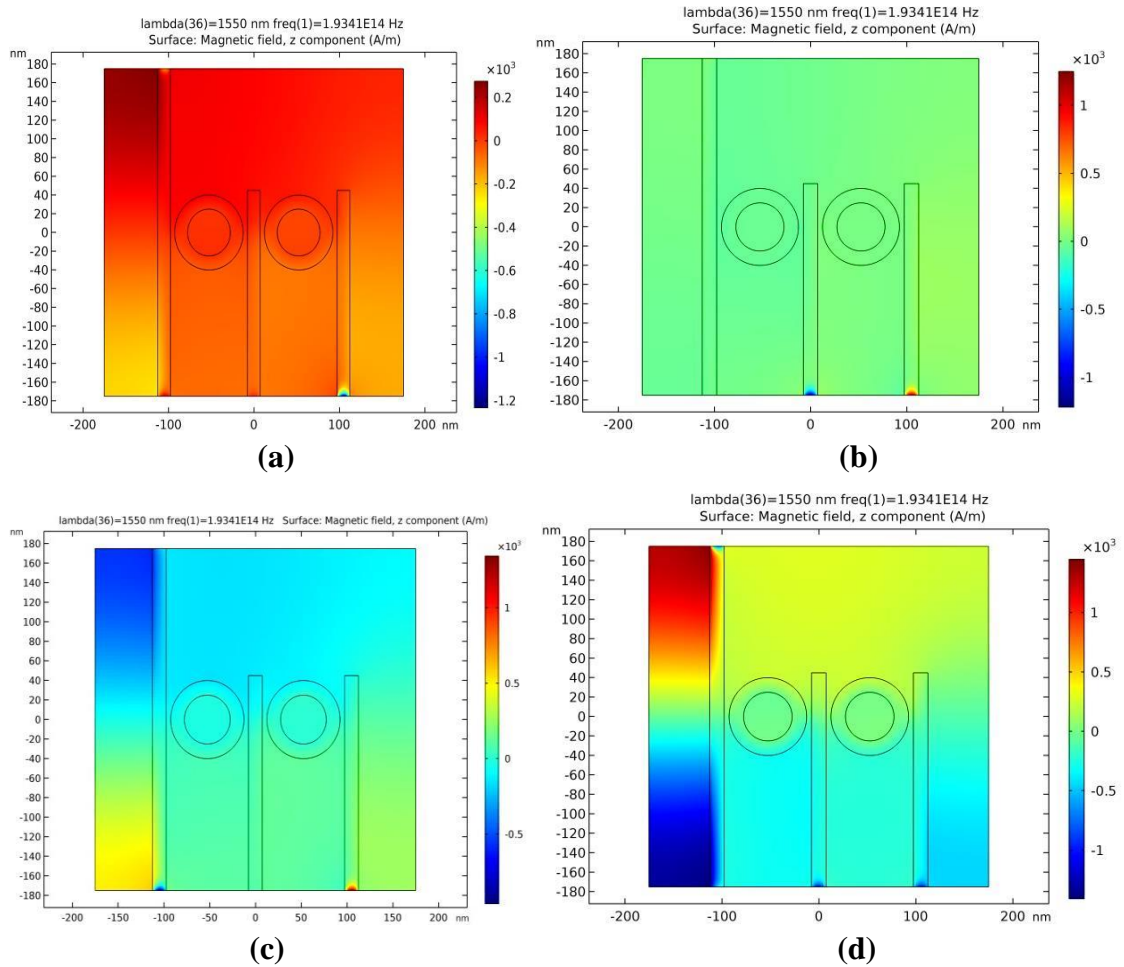


**Fig.3. 10** The magnetic field distribution of the proposed all-optical AND logic gate at different input states; (a) (off-off) input states, (b) (off-on) input states, (c) (on-off) input states, and (d) (on-on) input states.

The normalized transmission of the proposed AND logic gate and the magnetic field distributions of the proposed gate at different input states is shown in Figure (3.9) and (3.10) respectively. The operation details of the proposed all-optical AND logic gate are presented in Table (3.5).

**Table 3. 5** The operation details of the proposed all-optical AND logic gate

Input Port 1 Status	Phase Degree	Input Port 2 Status	Phase Degree	Control Port Status	Phase Degree	(T)	T Threshold	Output Port Status
OFF	0	OFF	0	ON	0	0.053	0.5	OFF
OFF	0	ON	45	ON	180	0.003	0.5	OFF
ON	45	OFF	0	ON	180	0.231	0.5	OFF
ON	0	ON	0	ON	0	1.26	0.5	ON
<b>Contrast Ratio (CR) of The Proposed Gate = 7.36 (dB)</b>								

The minimum transmission at the output port in case of the output state is (ON) is (1.26), and the maximum transmission at the output in case of the output state is (OFF) is (0.231), according to Equation (2.3) the contrast ratio (CR) is equal to (7.36 dB). The performance of the proposed NOT logic gate is good.

### 3.2.4 All-Optical NOR Logic Gate

In the proposed design of all-optical NOR gate shown in Figure (2.3), ports distribution of proposed NOR gate is; input ports (port 2 and 3), control port (port 1), and output port (port4) as presented in Figure (2.6). The function of the NOR logic gate states that; the output of this gate is (ON) only when all inputs are in (OFF) state, otherwise, the output of the gate is (OFF). To realize the behavior of this gate (port 1) is selected as the control port according to its location with respect to the output port, to give a transmission value above the threshold (0.5) especially at the first case when the inputs are (OFF) to actualize the function of NOR logic gate. In the first case, when all the inputs are in (OFF) state, only the light field of control port is propagating towards the output port, the transmission of this case is (0.502) which is above the threshold (0.5) and thus the output state of this case is (ON) state. The second case of NOR gate is when only one input port is (ON) and the other input port is (OFF), in the case in order to realize the function of NOR gate the destructive interference between the light fields in the inputs and control ports is employed by tuning the phase difference to achieve the desired output state based on the truth table of the NOR gate. In the case of the input states are; (OFF-ON) or (ON-OFF), the light field is lunched to the input port with a phase difference of ( $180^\circ$ ), and the phase difference of the control port light field is ( $45^\circ$ ). The destructive interference between the fields will take place and thus the transmissions of both cases (OFF-ON) and (ON-OFF) are; (0,233) and (0.275) respectively, and thus the output states of these cases are (OFF). In the last case; when the two inputs

are in (ON) state, the light fields in the input ports is lunched to the input ports with a phase angle of ( $180^\circ$ ), while the light phase angle of the control port is ( $45^\circ$ ). The effect of destructive interference is higher than the previous case because the number of light fields which are propagating with different phase and direction is increased. The transmission of the last case is (0.09) and thus the output state of this case is (OFF). The normalized transmission of the proposed NOR logic gate and the magnetic field distributions of the proposed gate at different input states is shown in Figure (3.11) and (3.12) respectively. The operation details of the proposed all-optical NOR logic gate are presented in Table (3.6).

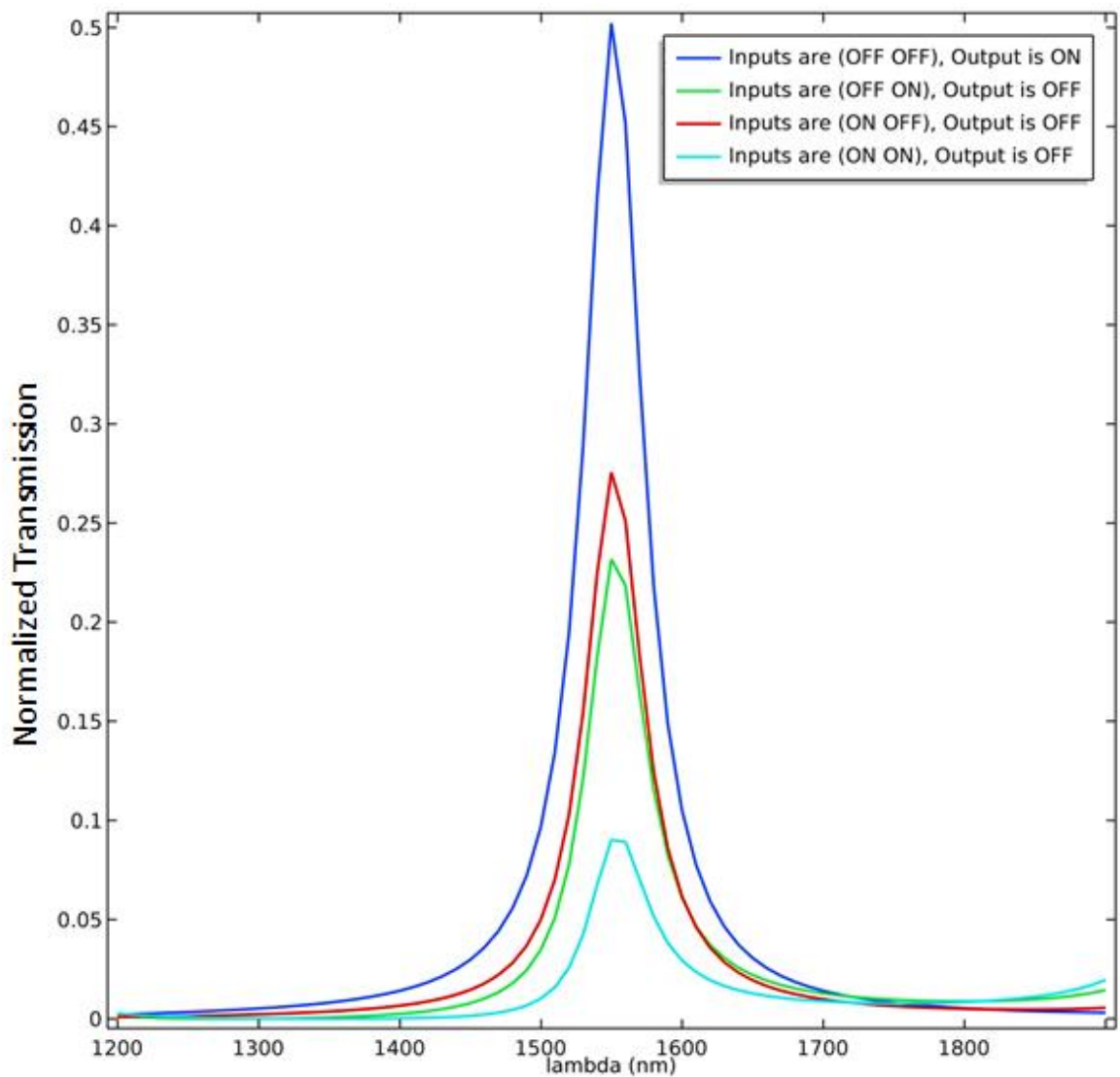


**Fig.3. 11 Normalized transmission of the proposed all-optical NOR logic gate as a function of wavelength for different input states.**

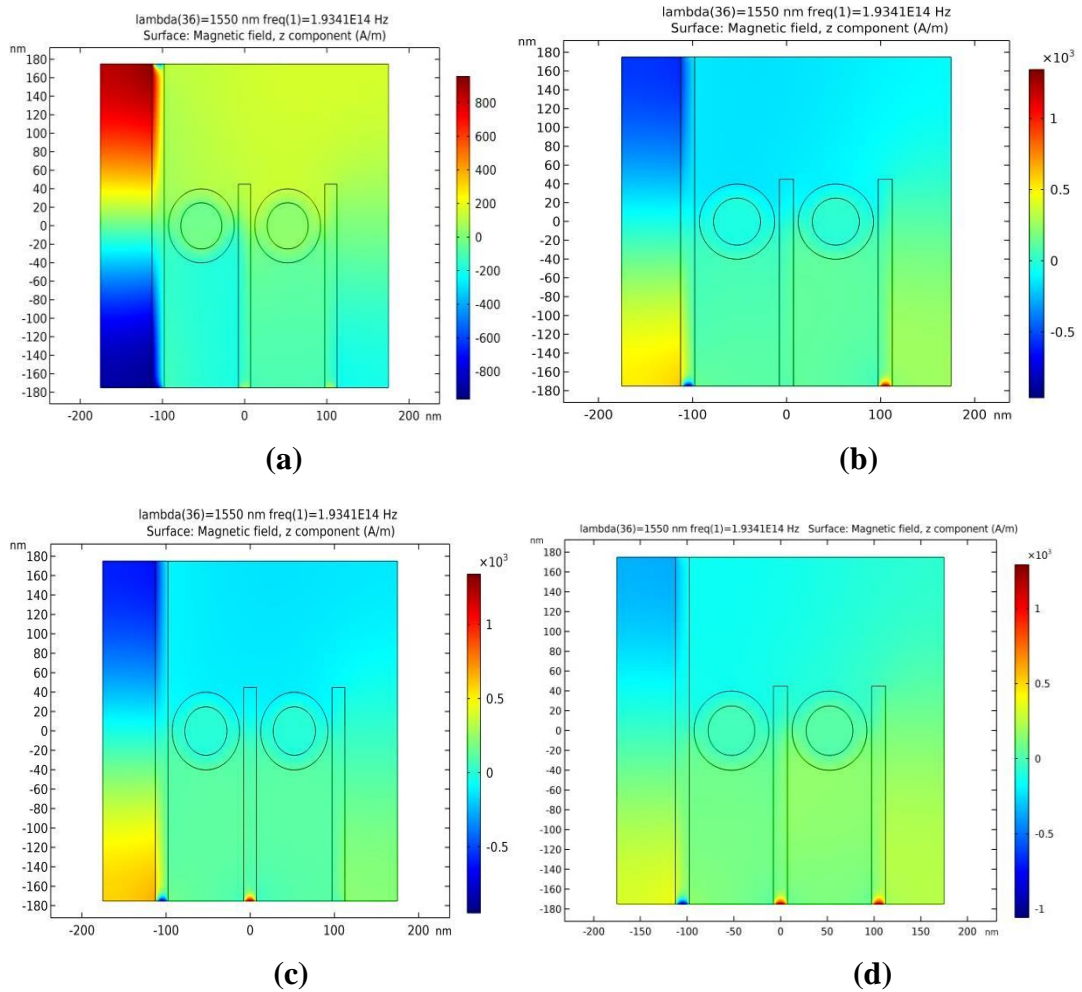


**Fig.3. 12** The magnetic field distribution of the proposed all-optical NOR logic gate at different input states; (a) (off-off) input states, (b) (off-on) input states, (c) (on-off) input states, and (d) (on-on) input states.

**Table 3. 6** The Operation Details of the Proposed All-Optical NOR Logic Gate

Input Port 1 Status	Phase Degree	Input Port 2 Status	Phase Degree	Control Port Status	Phase Degree	(T)	T Threshold	Output Port Status
OFF	0	OFF	0	ON	0	0.502	0.5	ON
OFF	0	ON	180	ON	45	0.233	0.5	OFF
ON	180	OFF	0	ON	45	0.275	0.5	OFF
ON	180	ON	180	ON	45	0.09	0.5	OFF

**Contrast Ratio (CR) of The Proposed Gate = 2.6 (dB)**

### 3.2.5 All-Optical NAND Logic Gate

In the proposed design of all-optical NAND gate shown in Figure (2.3), ports distribution of the proposed NAND gate is; input ports (port 2 and 3), control port (port 1), and output port (port4) as presented in Figure (2.6). The function of NAND gate states that; the output state of the NAND in all cases is (ON) except in the case of both inputs are (OFF), the output state in this case is (OFF).

In order to realize the function of NAND gate in the cases of; (OFF-OFF), (OFF-ON), and (ON-OFF) the light fields is lunched to the inputs and control ports without any phase difference angle and in the same propagation direction to activate the constructive interference and thus the output will be (ON). In the first three input states which are; (OFF-OFF), (OFF-ON), and (ON-OFF), the output state is (ON) and the transmissions are (0.502, 0.88, and 0.798) respectively, all these transmissions are above the transmission threshold of (0.5). The fourth input state is (ON-ON), in this case the light signals are lunched to the inputs and control ports with phase angle difference to activate the destructive interference and make the output state of this case is (OFF).

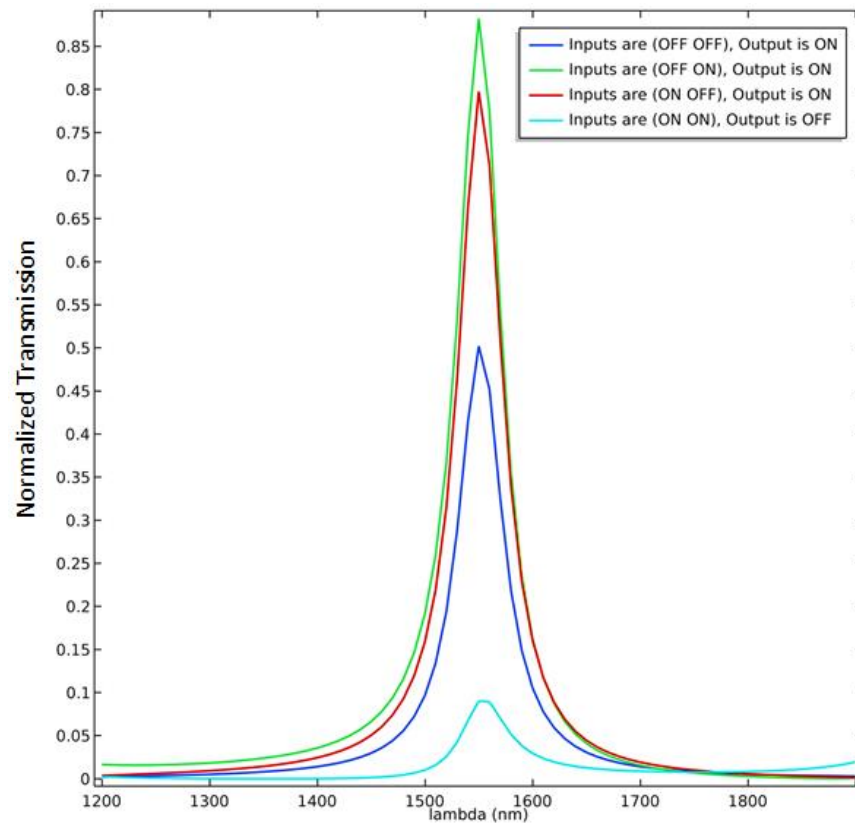


**Fig.3. 13 Normalized transmission of the proposed all-optical NAND logic gate as a function of wavelength for different input states.**

The phase angles associated with the three ports (input port 1, input port 2, and control port) are ( $180^\circ$ ,  $180^\circ$ , and  $45^\circ$ ) respectively. The transmission of the last case is (0.09) which is below the transmission threshold of (0.5) and thus the output state of this case is (OFF). The normalized transmission of the proposed NAND logic gate and the magnetic field distributions of the proposed gate at different input states is shown in Figure (3.13) and (3.14) respectively. The operation details of the proposed all-optical NAND logic gate are presented in Table (3.7).

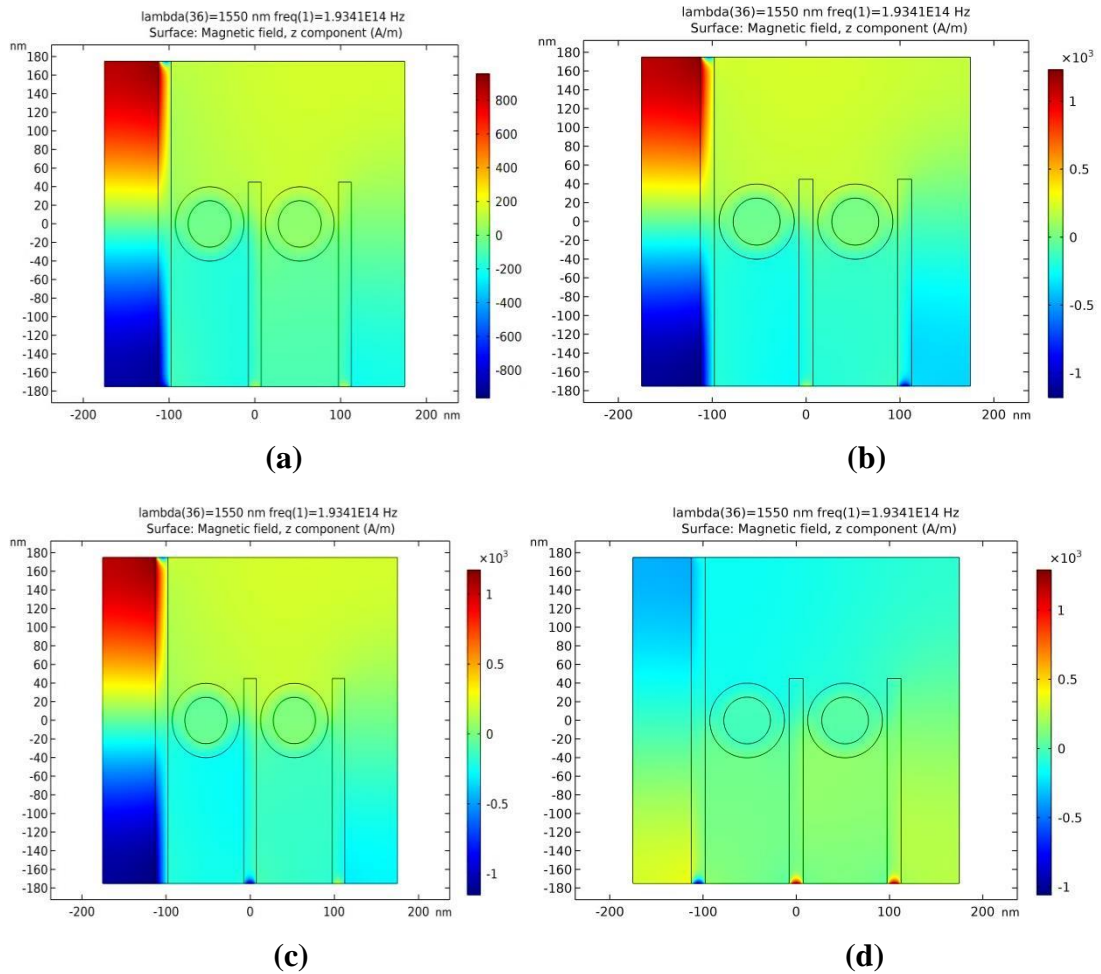


**Fig.3. 14** The magnetic field distribution of the proposed all-optical NAND logic gate at different input states; (a) (off-off) input states, (b) (off-on) input states, (c) (on-off) input states, and (d) (on-on) input states.

**Table 3. 7** The operation details of the proposed all-optical NAND logic gate

Input Port 1 Status	Phase Degree	Input Port 2 Status	Phase Degree	Control Port Status	Phase Degree	(T)	T Threshold	Output Port Status
OFF	0	OFF	0	ON	0	0.502	0.5	ON
OFF	0	ON	0	ON	0	0.88	0.5	ON
ON	0	OFF	0	ON	0	0.798	0.5	ON
ON	180	ON	180	ON	45	0.09	0.5	OFF

**Contrast Ratio (CR) of The Proposed Gate = 7.46 (dB)**

The minimum transmission at the output port in case of the output state is (ON) is (0.502), and the maximum transmission at the output in case of the output state is (OFF) is (0.09), according to Equation (2.3) the contrast ratio (CR) is equal to (7.46 dB).

### 3.2.6 All-Optical EX-OR Logic Gate

The output state of the EX-OR logic gate is ON only when the two input states are in opposite input logic states (OFF-ON) or (ON-OFF) otherwise, the output state is OFF. In the proposed design of all-optical EX-OR gate shown in Figure (2.3), ports distribution of proposed EX-OR gate is similar to that of OR, and AND gates which is; input ports (port 1 and 2), control port (port 3), and output port (port4) as presented in Figure (2.5). Only in the cases of the input states are similar (OFF-OFF), and (ON-ON) the phase angle difference is inserted when the light signals are launched to the inputs and control ports to take the advantage of destructive interference between the light signals and thus the function of EX-OR logic gate is realized. In the case of opposite input states; (OFF-ON) and (ON-OFF), the light fields are propagates in phase and in the same propagation direction and thus the transmissions of these two states are above the transmission threshold of (0.5), the transmissions were (0.883 and 0.8) respectively. In the other input states; (OFF-OFF) and (ON-ON) the phase angle difference between the light fields in the input and control ports are inserted to employ the destructive interference between them. In (ON-ON) input state the phase angle difference was ( $180^\circ$ ,  $180^\circ$ , and  $45^\circ$ ) respectively. The transmission of the (OFF-OFF) and (ON-ON) input states are (0.053 and 0.09), respectively.

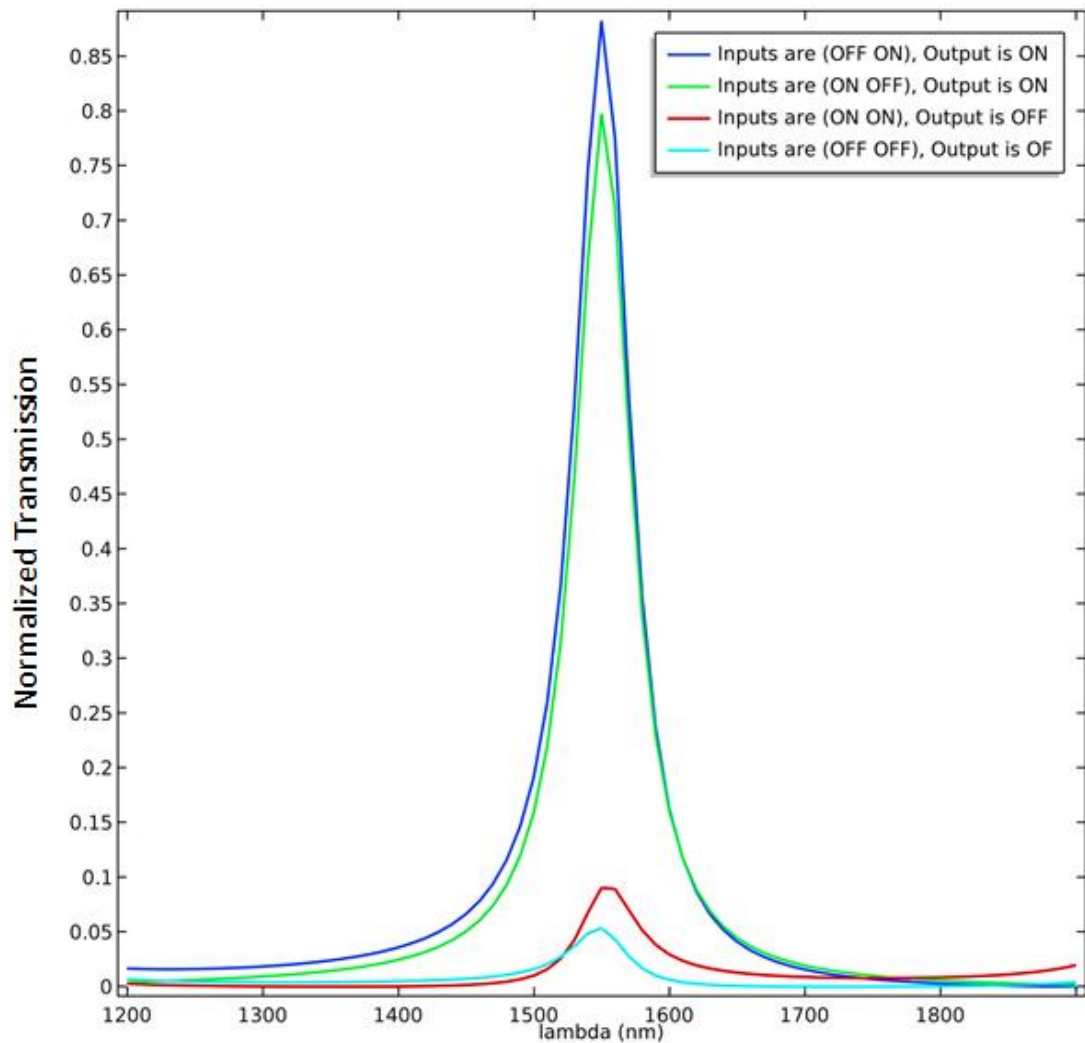


**Fig.3. 15 Normalized transmission of the proposed all-optical EX-OR logic gate as a function of wavelength for different input states.**

The normalized transmission of the proposed EX-OR logic gate and the magnetic field distributions of the proposed gate at different input states is shown in Figure (3.15) and (3.16) respectively. The operation details of the proposed all-optical EX-OR logic gate are presented in Table (3.8). The minimum transmission at the output port in case of the output state is (ON) is (0.8), and the maximum transmission at the output in case of the output state is (OFF) is (0.09), according to Equation (2.3) the contrast ratio (CR) is equal to (11.78 dB).

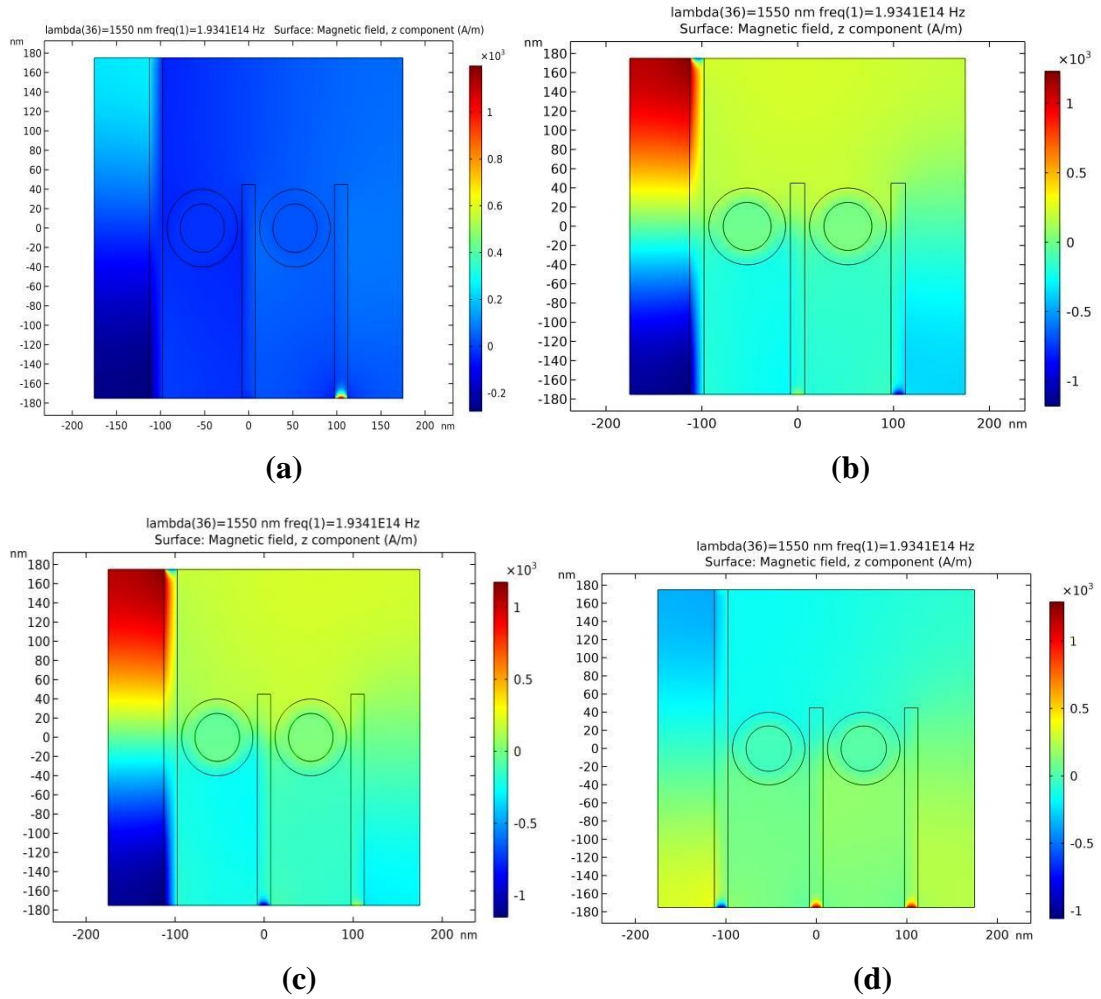


**Fig.3. 16** The magnetic field distribution of the proposed all-optical EX-OR logic gate at different input states; (a) (off-off) input states, (b) (off-on) input states, (c) (on-off) input states, and (d) (on-on) input states.

**Table 3. 8** The operation details of the proposed all-optical EX-OR logic gate

Input Port 1 Status	Phase Degree	Input Port 2 Status	Phase Degree	Control Port Status	Phase Degree	(T)	T Threshold	Output Port Status
OFF	0	OFF	0	ON	180	0.053	0.5	OFF
OFF	0	ON	0	ON	0	0.883	0.5	ON
ON	0	OFF	0	ON	0	0.80	0.5	ON
ON	180	ON	180	ON	45	0.09	0.5	OFF

**Contrast Ratio (CR) of The Proposed Gate = 11.78 (dB)**

### 3.2.7 All-Optical EX-NOR Logic Gate

The output state of EX-NOR logic gate is (ON) only when the two input states are the same (OFF-OFF) or (ON-ON); otherwise, the output state is (OFF). In the proposed EX-NOR logic gate structure shown in Figure (2.3), the two input ports are (port 2 and port 3), the control port is (port 1), and the output port is (port 4) as presented in Figure (2.6). The function of the EX-NOR gate can be realized by employing the phenomena of the constructive and destructive interference between the propagating signals in input and control ports. In the similar input states; (OFF-OFF) and (ON-ON), the light signals are launched to the inputs and control ports without phase difference between them and in the same propagation direction in order to accomplish (ON) output state. In (OFF-ON) and (ON-OFF) input states, the light signals are launched with phase difference angle between them in order to activate the destructive interference between the signals and thus the output state will be (OFF). The normalized transmission of the proposed EX-NOR logic gate and the magnetic field distributions of the proposed gate at different input states is shown in Figures (3.17) and (3.18), respectively. The operation details of the proposed all-optical EX-NOR logic gate are presented in Table (3.9).

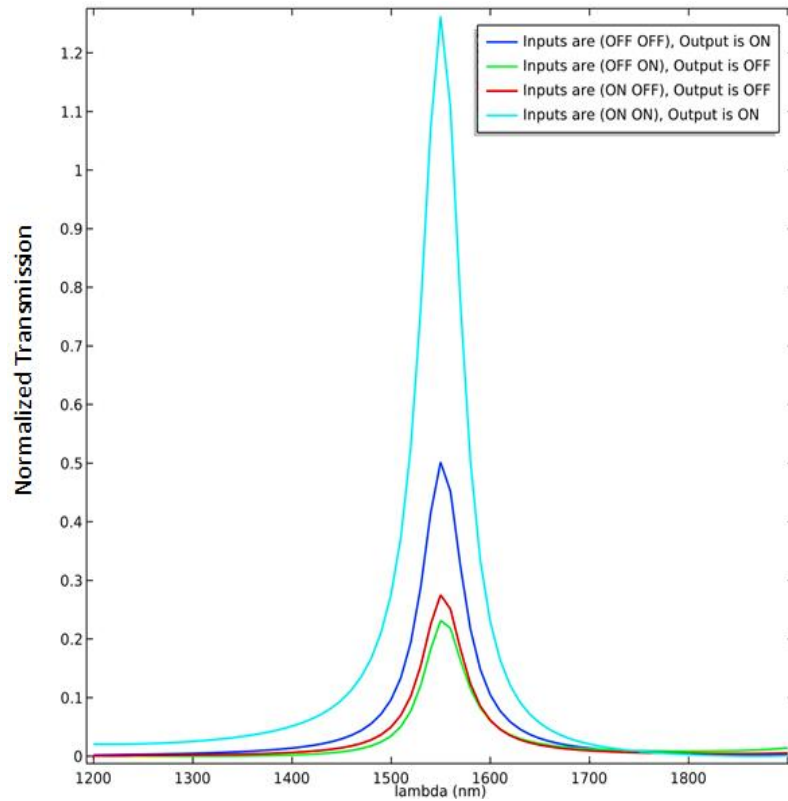


**Fig.3. 17 Normalized transmission of the proposed all-optical EX-NOR logic gate as a function of wavelength for different input states.**

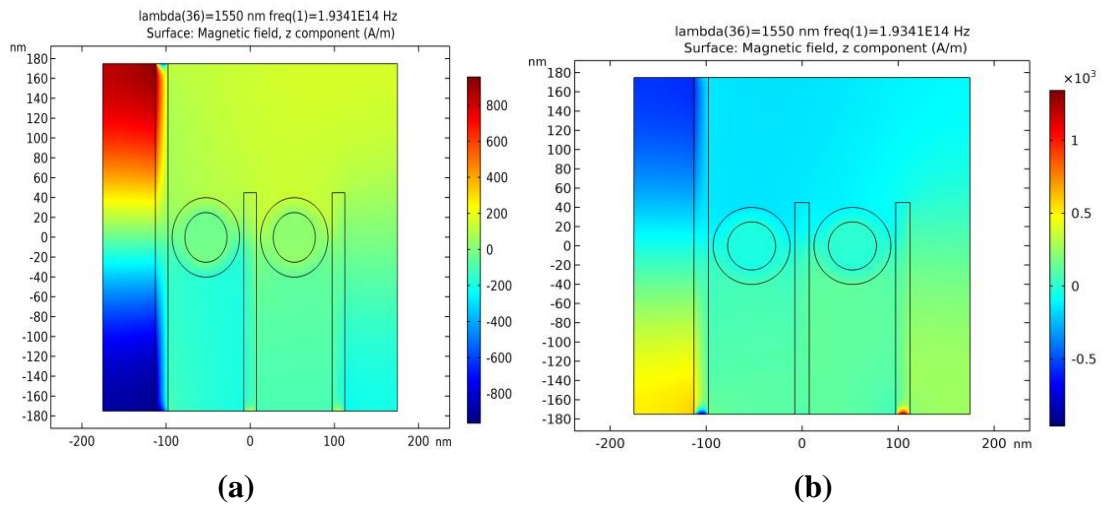


**Fig.3. 18 The magnetic field distribution of the proposed all-optical EX-NOR logic gate at different input states; (a) (off-off) input states, (b) (off-on) input states, (c) (on-off) input states, and (d) (on-on) input states.**

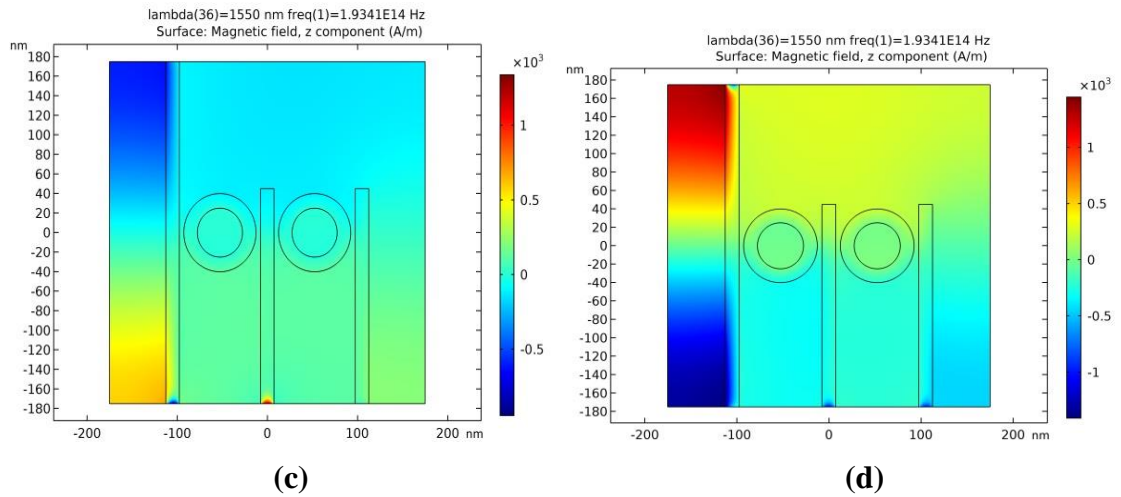


**Fig. 3. 18 (Continued).**

**Table 3. 9 The operation details of the proposed all-optical EX-NOR logic gate**

Input Port 1 Status	Phase Degree	Input Port 2 Status	Phase Degree	Control Port Status	Phase Degree	(T)	T Threshold	Output Port Status
OFF	0	OFF	0	ON	0	0.505	0.5	ON
OFF	0	ON	180	ON	45	0.228	0.5	OFF
ON	180	OFF	0	ON	45	0.26	0.5	OFF
ON	0	ON	0	ON	0	1.26	0.5	ON
<b>Contrast Ratio (CR) of The Proposed Gate = 2.88 (dB)</b>								

### 3.3. Comparison between the Proposed Structure and the Previous Related Works.

Table (3.10) shows brief comparison between the proposed structure of two inputs all-optical logic gates with the previous related works in terms of; No. of the Proposed Logic Gates, Dimensions, Operation Wavelength, The Proposed Logic Gates, Insulator-Metal Materials, Max. Optical Transmission, and Transmission Threshold.

**Table 3. 10 Comparison between the proposed structure and related works**

<b>Comparison Element</b>	<b>Proposed Structure</b>	<b>Reference No. [99]</b>	<b>Reference No. [27]</b>	<b>Reference No. [29]</b>	<b>Reference No. [69]</b>
<b>No. of the Proposed Logic Gates</b>	7 logic gates	7 logic gates	3 logic gates	2 logic gates	2 logic gates
<b>Dimensions</b>	350 nm × 350 nm	400 nm × 400 nm	750 nm × 900 nm, and 1.5 μm × 1.8 μm	3 μm × 2 μm	1075 nm × 1000 nm for OR gate 1625 nm × 1000 nm for NOR gate
<b>Operation Wavelength</b>	1550 nm	1550	1535 nm	944 nm	1360 nm
<b>The Proposed Logic Gates</b>	All gates NOT, AND, OR, NOR, NAND, EX-OR, and EX-NOR gates	All gates NOT, AND, OR, NOR, NAND, EX-OR, and EX-NOR gates	NOT, AND, and NOR gates	AND and NOR gates	OR, and NOR gates
<b>Insulator-Metal Materials</b>	Sapphire – silver	Teflon – silver	Sio <sub>2</sub> – silver	Air – silver	Air – silver
<b>Max. Optical Transmission</b>	88.2% for NOT gate, 126% for OR gate, 126 for AND gate, 88% for NAND gate, 50% for NOR gate, 88.3% for EX-OR gate, and 126% for EX-NOR gate	28 % for NOT gate, 175% for OR gate, 72 for AND gate, 112% for NAND gate, 28% for NOR gate, 63% for EX-OR gate, and 175% for EX-NOR gate	70% for NOT gate, 70% for NOR gate, and 90% for AND gate	84.06% for AND gate, 80.07 for NOR gate	62 % for OR gate 69% for NOR gate
<b>Transmission Threshold</b>	50 %	25 %	35 %	50% or less	30 %

### 3.4. The Multiple Inputs All-Optical Logic Gates

In this section, all the simulation results of three inputs all-optical logic gates were presented and well discussed. The simulated gates are; NOT, AND, NAND, NOR, and EX-NOR all-optical logic gates. The operation wavelength was 1550 nm. The simulation results show that the optical transmission threshold of (0.26) which performs the operation of

planned logic gates to be accomplished. Moreover, simulation results show that the proposed compact structure of all-optical logic gates may have potential applications in all-optical integrated networks. The normalized transmission of each simulated logic gate, the magnetic field distribution at different input states, and the operation information tables will be presented and discussed.

### 3.4.1 Three Inputs All-Optical NOT Logic Gate

To perform the function of all-optical NOT gate in the proposed multiple inputs logic gates structure shown in Figure (2.7), only three ports are used, and the remaining two ports are not used. (Port 2) is the input port, the control port is (port 1), and (port 5) is the output port as presented in Figure (2.10). The NOT logic gate have only two input states either (OFF) or (ON), this the reason of using only one input port to present the two input states. In the case of the input port state is in (OFF) state, the light field in the control port is propagating towards the output port directly without any interference between the light fields. The transmission of this case is (0.289) which is above the transmission threshold of (0.26), and thus the output state of this case in (ON) state. In case of input port is in (ON) state, phase difference angle of ( $180^\circ$ ) is inserted with the light signal in the input port and phase angle of ( $45^\circ$ ) is inserted with the light angle in the control port. Due to the phase angle difference between the light signals and different propagation direction, the destructive interference takes place between them which makes the transmission of this case is (0.113) below the transmission threshold of (0.26) and thus the output state is (OFF). The normalized transmission of the proposed three inputs NOT logic gate and the magnetic field distributions of the proposed gate at different input states are shown in Figure (3.19) and (3.20) respectively. The operation details of the proposed all-optical three inputs NOT gate are presented in Table (3.11).

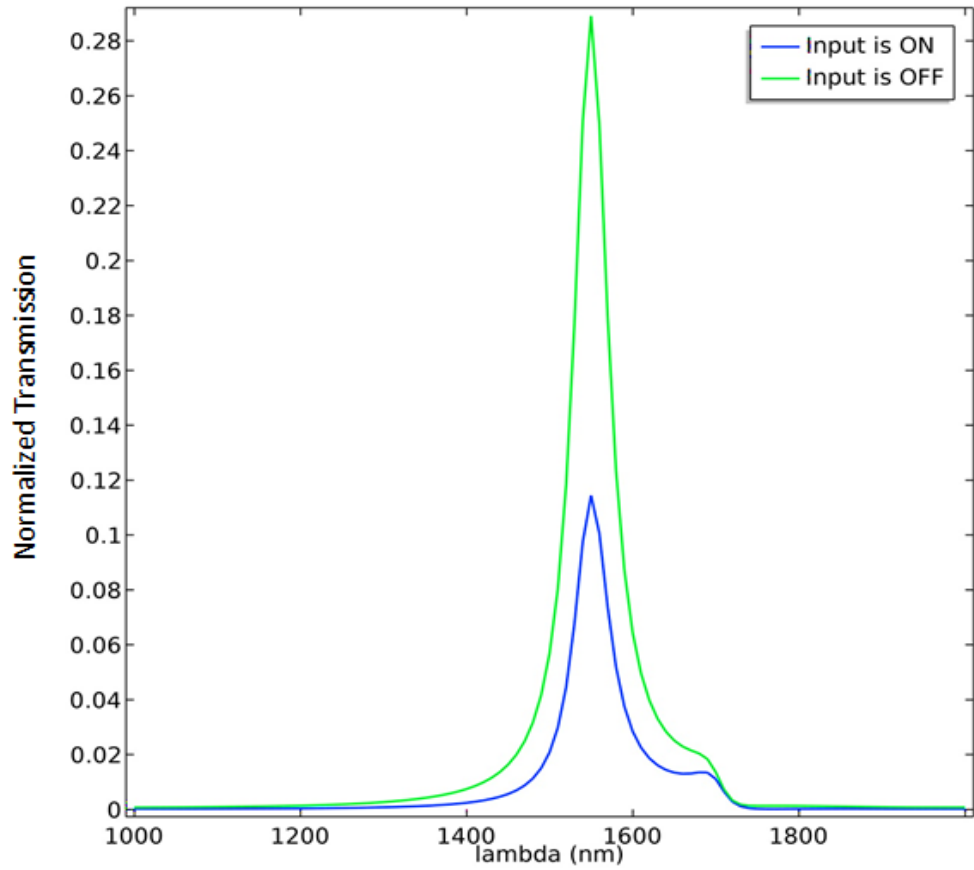


**Fig.3. 19 Normalized transmission of the proposed all-optical three inputs NOT logic gate as a function of wavelength for different input states.**

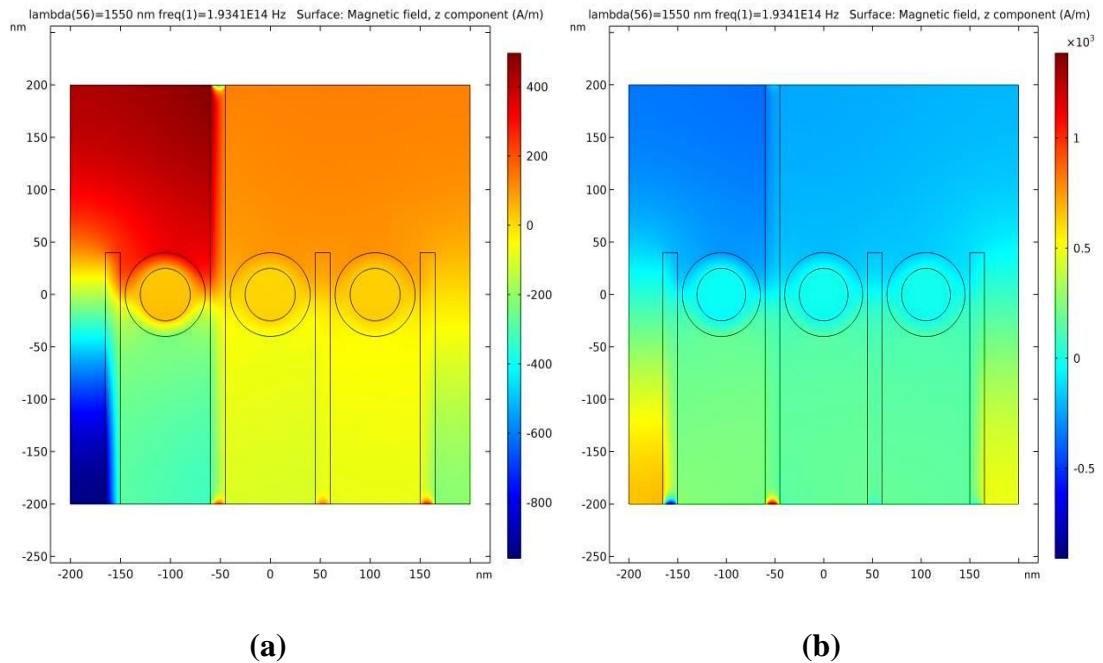


**Fig.3. 20 The magnetic field distribution of the proposed all-optical three inputs NOT logic gate at the different input states; (a) off input state, and (b) on input state.**

**Table 3. 11 The operation details of the proposed all-optical three inputs NOT logic gate**

Input Port 1 Status and (Phase°)	Input Port 2 Status and (Phase°)	Input Port 3 Status and (Phase°)	Control Port Status and (Phase°)	Output Port Status	Transmission Threshold $T_{Threshold}$	Normalized Transmission $T$
OFF (0°)	Not Used	Not Used	ON (0°)	ON	0.26	0.289
ON (180°)			ON (45°)	OFF	0.26	0.113
<b>Contrast Ratio (CR) of The Proposed Gate = 4.07 (dB)</b>						

### 3.4.2 Three Inputs All-Optical AND Logic Gate

In order to realize the function of the all-optical three inputs AND logic gate in the proposed design shown in Figure (2.6), (port 2) is considered as control port, (ports 1, 3, and 4) are the input ports, and (port 5) is the output port as presented in Figure (2.8). According to the truth table of multiple inputs AND logic gate, the output state of multiple inputs AND logic gate is (ON) only in the case of all the inputs states are in (ON). As mentioned in the previous sections, as a result of the desired destructive interference between the light signals which propagate in inputs and control port due to the inserted phase angle difference between the light signals to actualize the function of the proposed multiple inputs AND gate, the output states of this gate are (OFF) in all cases except in the first case of all inputs were in (ON) state. In the case of all inputs states are (ON), the constructive interference between the four propagated light signals which is propagating in phase with each other and in the same propagation direction, leads to make the normalized transmission as high as possible (exceeds 100%), in this case the transmission is (1.271).

The lowest transmission of the proposed structure transmissions was in the case of input states of (OFF-OFF-ON), where the transmission of this case is only (0.004) because of the phase difference and the ports distribution positions. The remaining transmission is varied between (0.004

to 1.271) according to the inserted phase angle difference and ports distribution to accomplish the function of all-optical three inputs AND logic gate. The transmission threshold of the proposed AND gate is (0.26). The normalized transmission of the proposed three inputs AND logic gate and the magnetic field distributions of the proposed gate at different input states are shown in Figure (3.21) and (3.22) respectively. The operation details of the proposed all-optical three inputs AND logic gate are presented in Table (3.12). The minimum transmission at the output port in case of the output state is (ON) is (1.271), and the maximum transmission at the output in case of the output state is (OFF) is (0.11), according to Equation (2.3) the contrast ratio (CR) is equal to (10.62 dB).

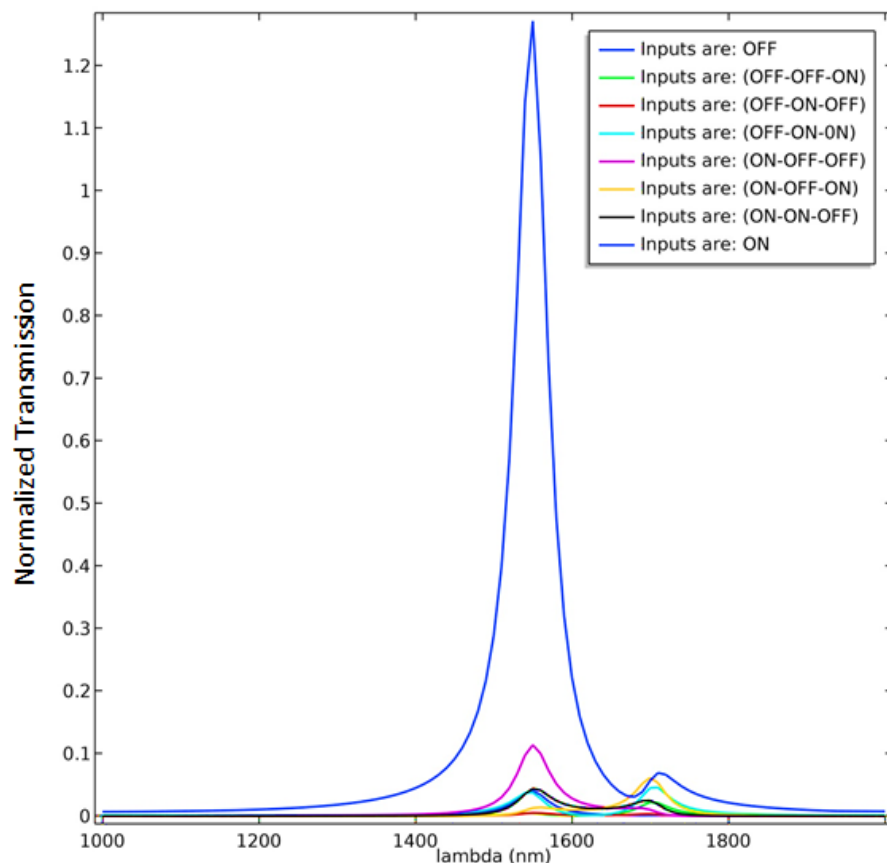


**Fig.3. 21 Normalized Transmission of The Proposed All-Optical Three Inputs AND Logic Gate as a Function of Wavelength for Different Input States.**

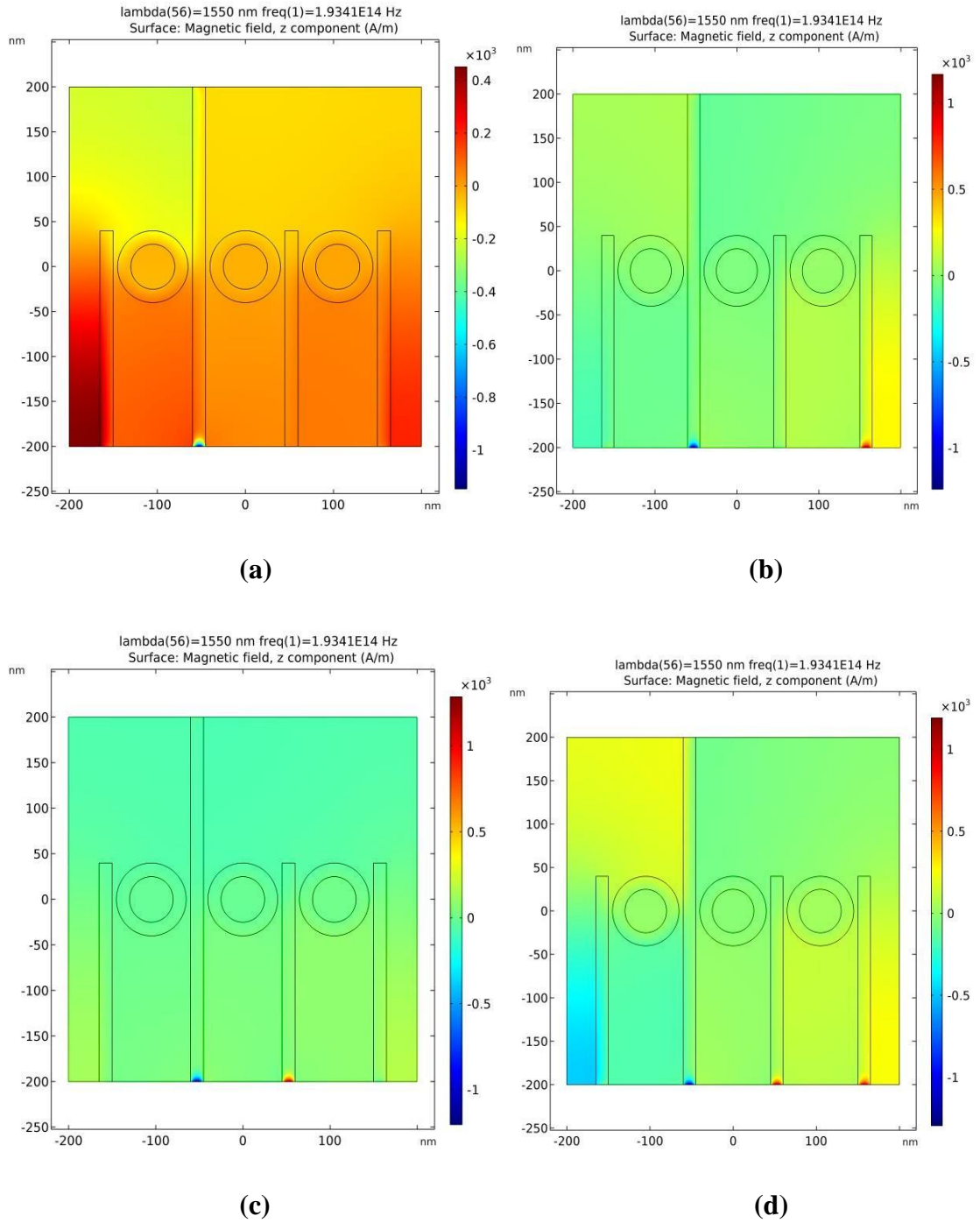


**Fig.3. 22 The magnetic field distribution of the proposed all-optical three inputs AND logic gate at the different inputs states; (a) (off-off-off), (b) (off-off-on), (c) (off-on-off), (d) (off-on-on), (e) (on-off-off), (f) (on-off-on), (g) (on-on-off), and (h) (on-on-on) inputs states.**

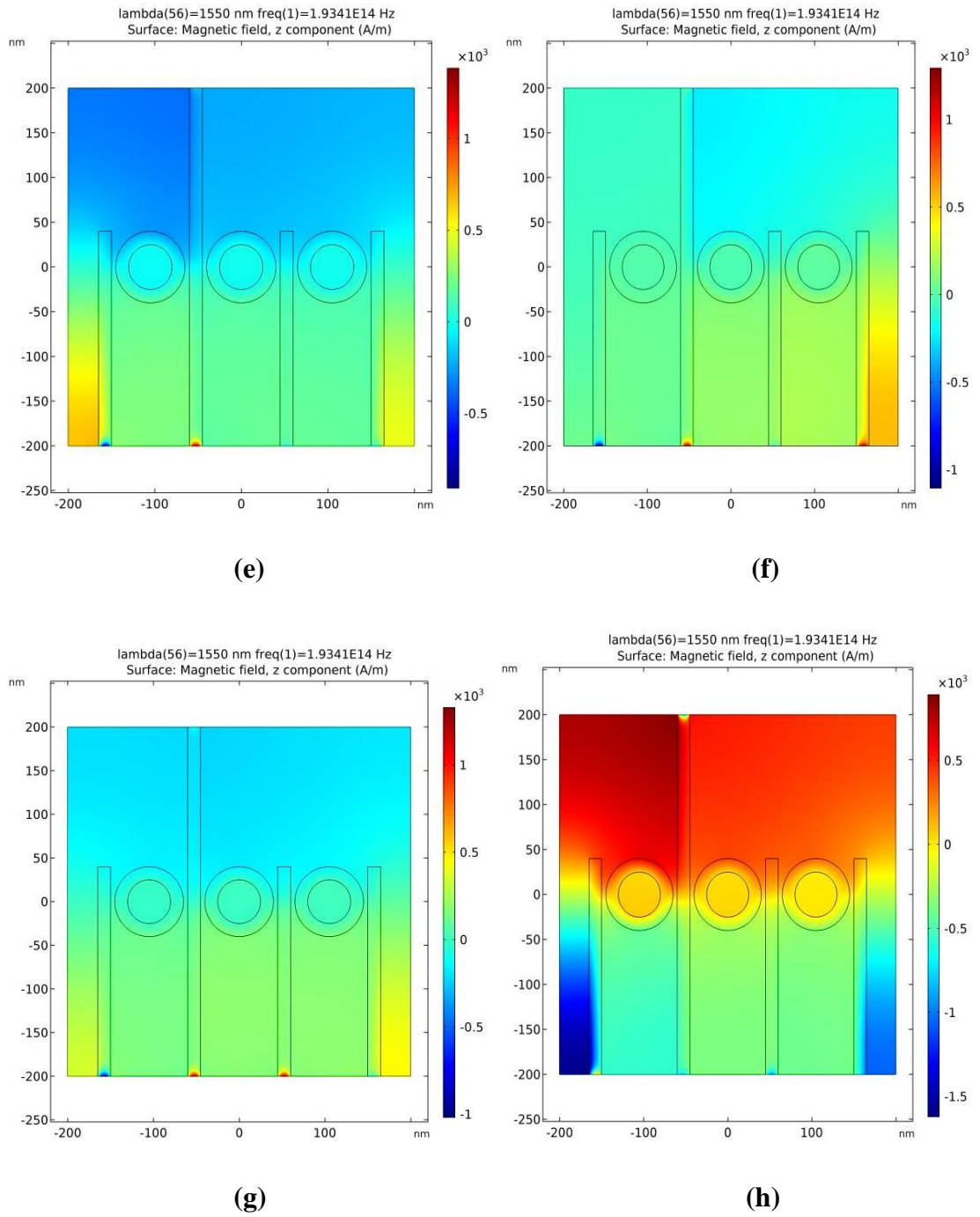


Fig.3. 22 (Continued).

**Table 3. 12 The operation details of the proposed all-optical three inputs AND logic gate**

Input Port 1 Status and (Phase°)	Input Port 2 Status and (Phase°)	Input Port 3 Status and (Phase°)	Control Port Status and (Phase°)	Output Port Status	Transmission Threshold $T_{Threshold}$	Normalized Transmission $T$
OFF (0°)	OFF (0°)	OFF (0°)	ON (0°)	OFF	0.26	0.04
OFF (0°)	OFF (0°)	ON (180°)	ON (45°)	OFF	0.26	0.004
OFF (0°)	ON (180°)	OFF (0°)	ON (45°)	OFF	0.26	0.005
OFF (0°)	ON (180°)	ON (180°)	ON (45°)	OFF	0.26	0.037
ON (45°)	OFF (0°)	OFF (0°)	ON (180°)	OFF	0.26	0.11
ON (45°)	OFF (0°)	ON (180°)	ON (180°)	OFF	0.26	0.012
ON (45°)	ON (180°)	OFF (0°)	ON (180°)	OFF	0.26	0.043
ON (0°)	ON (0°)	ON (0°)	ON (0°)	ON	0.26	1.271
<b>Contrast Ratio (CR) of The Proposed Gate = 10.62 (dB)</b>						

### 3.4.3 Three Inputs All-Optical NAND Logic Gate

The output status of the NAND logic gate is (OFF) only in the case of all the inputs states are in (ON) state, otherwise, the output status of the NAND gate is (ON). In order to realize the function of the proposed structure design of the NAND logic gate shown in Figure (2.7), the destructive interference between the inputs and control ports is employed in the case of all the inputs are in (ON) states by inserting phase angle difference between the propagating light signals in the inputs and control ports. The selected input ports are; (2, 3, and 4), and the control port is (port 1) while (port 5) is the output port as presented in Figure (2.9). The constructive interference between the light signals in the remaining input states takes place to accomplish the function of the three inputs all-optical NAND logic gate, the constructive interference occurs because all the propagated light signals are in the same phase and propagation direction. The maximum transmission of

the proposed structure occurs in the input states of (ON-OFF-ON), where the transmission in this case is (0.985) which is above the transmission threshold of (0.26). The output state of the proposed structure is (OFF) only in the case of the inputs states are; (ON-ON-ON), where the transmission of this case is (0.01) below the transmission threshold of (0.26).

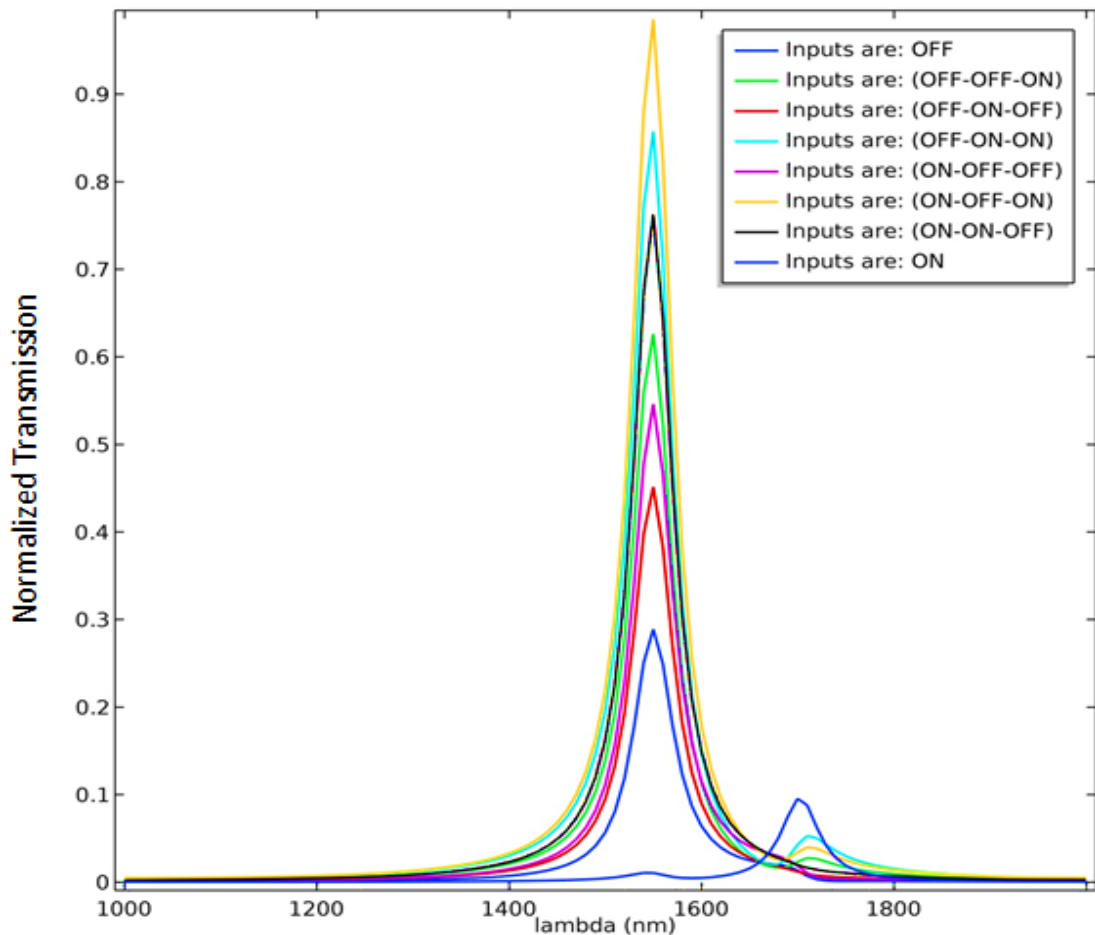
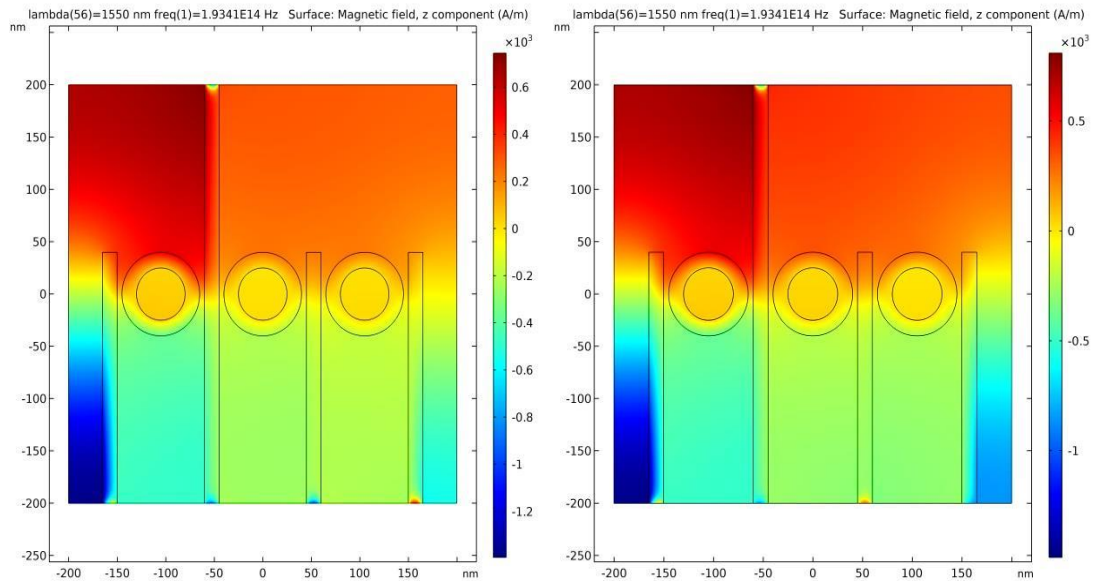


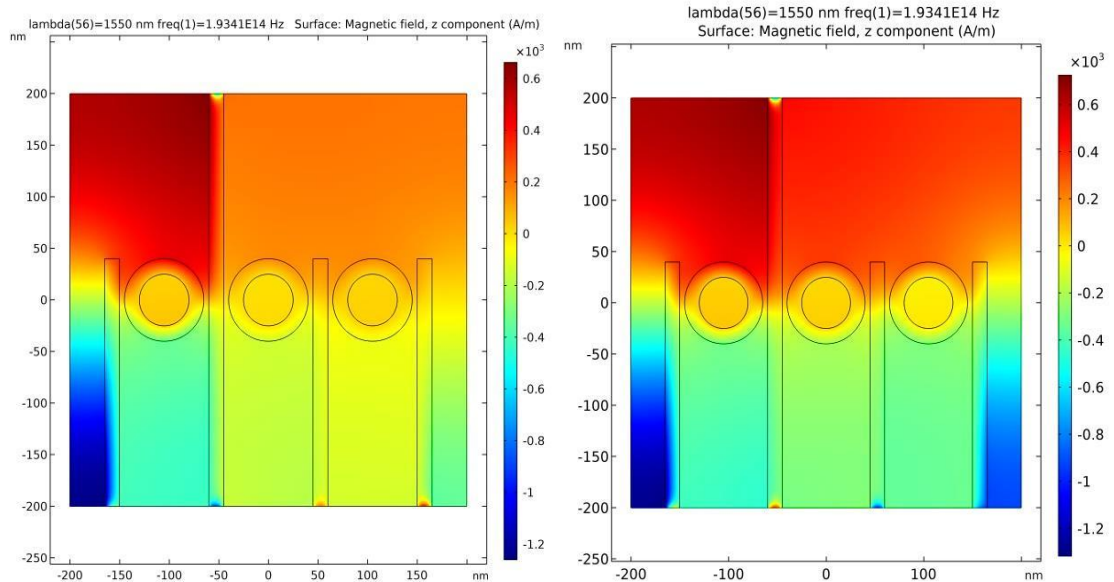
**Fig.3. 23 Normalized transmission of the proposed all-optical three inputs NAND logic gate as a function of wavelength for different input states**

The normalized transmission of the proposed three inputs NAND logic gate and the magnetic field distributions of the proposed gate at different input states are shown in Figure (3.23) and (3.24) respectively. The operation details of the proposed all-optical three inputs NAND logic gate are presented in Table (3.13).



(a)

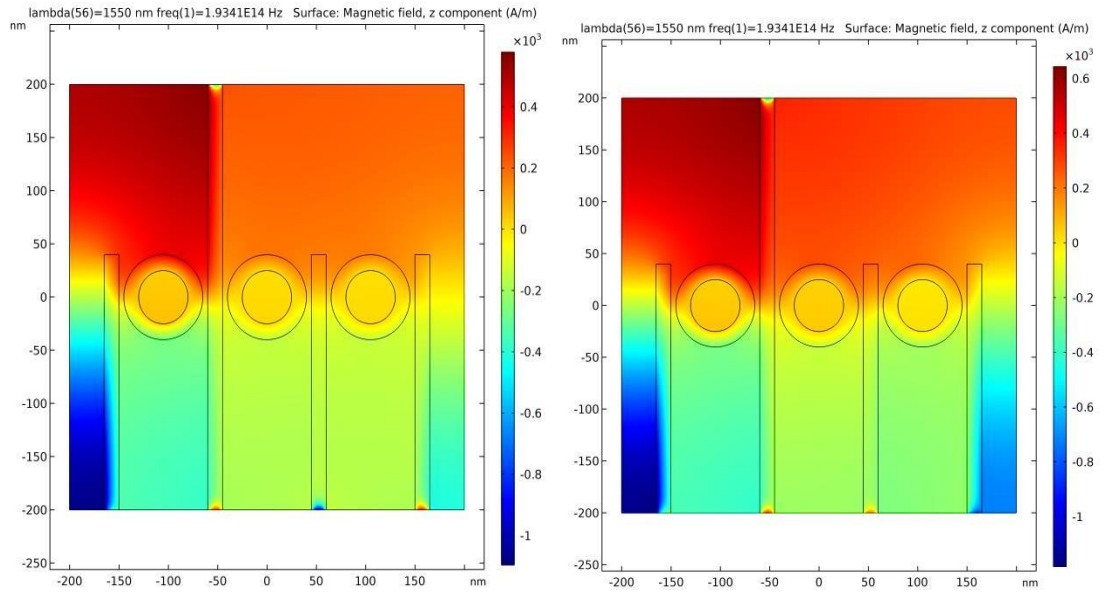
(b)



(a)

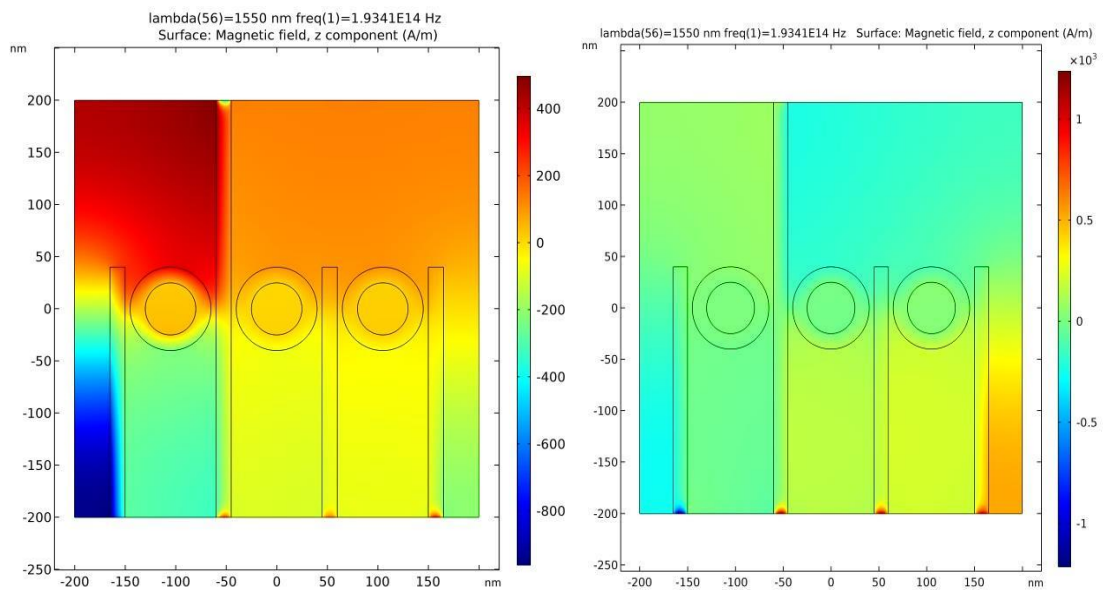
(d)

**Fig.3. 24** The magnetic field distribution of the proposed all-optical three inputs NAND logic gate at the different inputs states; (a) (off-off-off), (b) (off-off-on), (c) (off-on-off), (d) (off-on-on), (e) (on-off-off), (f) (on-off-on), (g) (on-on-off), and (h) (on-on-on) inputs states.



(e)

(f)



(g)

(h)

Fig.3. 24 (Continued).

**Table 3. 13 The operation details of the proposed all-optical three inputs NAND logic gate**

Input Port 1 Status and (Phase°)	Input Port 2 Status and (Phase°)	Input Port 3 Status and (Phase°)	Control Port Status and (Phase°)	Output Port Status	Transmission Threshold $T_{Threshold}$	Normalized Transmission $T$
OFF (0°)	OFF (0°)	OFF (0°)	ON (0°)	ON	0.26	0.289
OFF (0°)	OFF (0°)	ON (0°)	ON (0°)	ON	0.26	0.626
OFF (0°)	ON (0°)	OFF (0°)	ON (0°)	ON	0.26	0.451
OFF (0°)	ON (0°)	ON (0°)	ON (0°)	ON	0.26	0.857
ON (0°)	OFF (0°)	OFF (0°)	ON (0°)	ON	0.26	0.546
ON (0°)	OFF (0°)	ON (0°)	ON (0°)	ON	0.26	0.985
ON (0°)	ON (0°)	OFF (0°)	ON (0°)	ON	0.26	0.762
ON (45°)	ON (180°)	ON (180°)	ON (180°)	OFF	0.26	0.01
<b>Contrast Ratio (CR) of The Proposed Gate = 14.6 (dB)</b>						

The minimum transmission at the output port in case of the output state is (ON) is (0.289), and the maximum transmission at the output in case of the output state is (OFF) is (0.01), according to Equation (2.3) the contrast ratio (CR) is equal to (14.6 dB). The performance of the proposed three inputs all-optical NAND logic gate is very good and efficient.

### 3.4.4 Three Inputs All-Optical NOR Logic Gate

In the proposed structure of three inputs all-optical logic gates shown in Figure (2.7), the realization of NOR logic gate function is done by considering the (ports 2, 3, and 4) as inputs ports, (port 1) as a control port, and (port 5) as an output port as presented in Figure (2.9). According to the truth table of three inputs NOR logic gate, only in case of all the three inputs states are in (OFF) state, the output state at the output port is (ON). In all other inputs states, the phase angle difference between the propagating light

signals in the inputs and control ports is employed to generate the destructive interference which makes the output state at these inputs states is (OFF). The transmission threshold of the proposed NOR gate is (0.26). In the first input state, when the three inputs are in (OFF) state, only the light signal in the control port propagates in the waveguide and thus the transmission of this input state is low (0.289). Although the transmission of this input state is low, it's the only input state which gives the output state is (ON) state where the transmission of (0.289) is above the threshold of (0.26). The contrast ratio (CR) of the proposed NOR gate is relatively low (2.46 dB), because there is only one (ON) output state with low transmission (0.289) which gives low (CR) according to Equation (2.3). In all remaining input states, the destructive interference is generated by inserting a phase angle difference between the light signals.

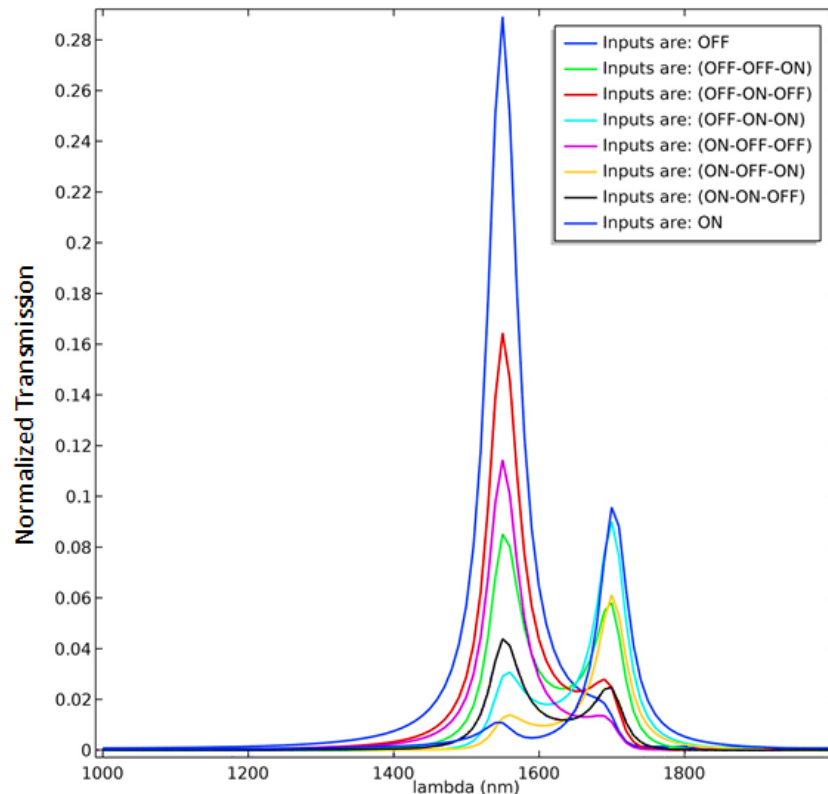


**Fig.3. 25 Normalized transmission of the proposed all-optical three inputs NOR logic gate as a function of wavelength for different input states**

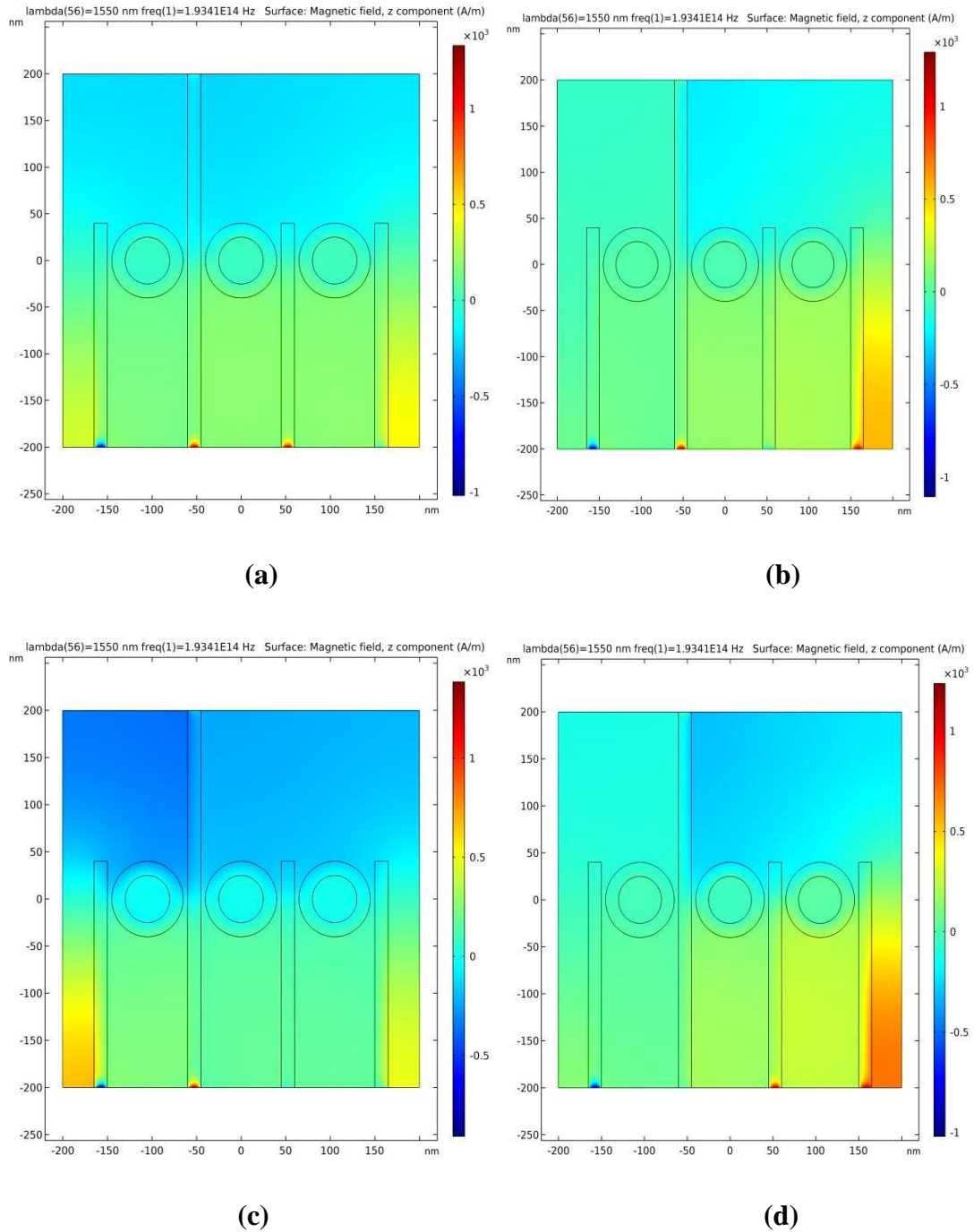


**Fig.3. 26 The Magnetic Field Distribution of The Proposed All-Optical Three Inputs NOR Logic Gate at the Different Inputs States; (a) (OFF-OFF-OFF), (b) (OFF-OFF-ON), (c) (OFF-ON-OFF), (d) (OFF-ON-ON), (e) (ON-OFF-OFF), (f) (ON-OFF-ON), (g) (ON-ON-OFF), and (h) (ON-ON-ON) Inputs States.**

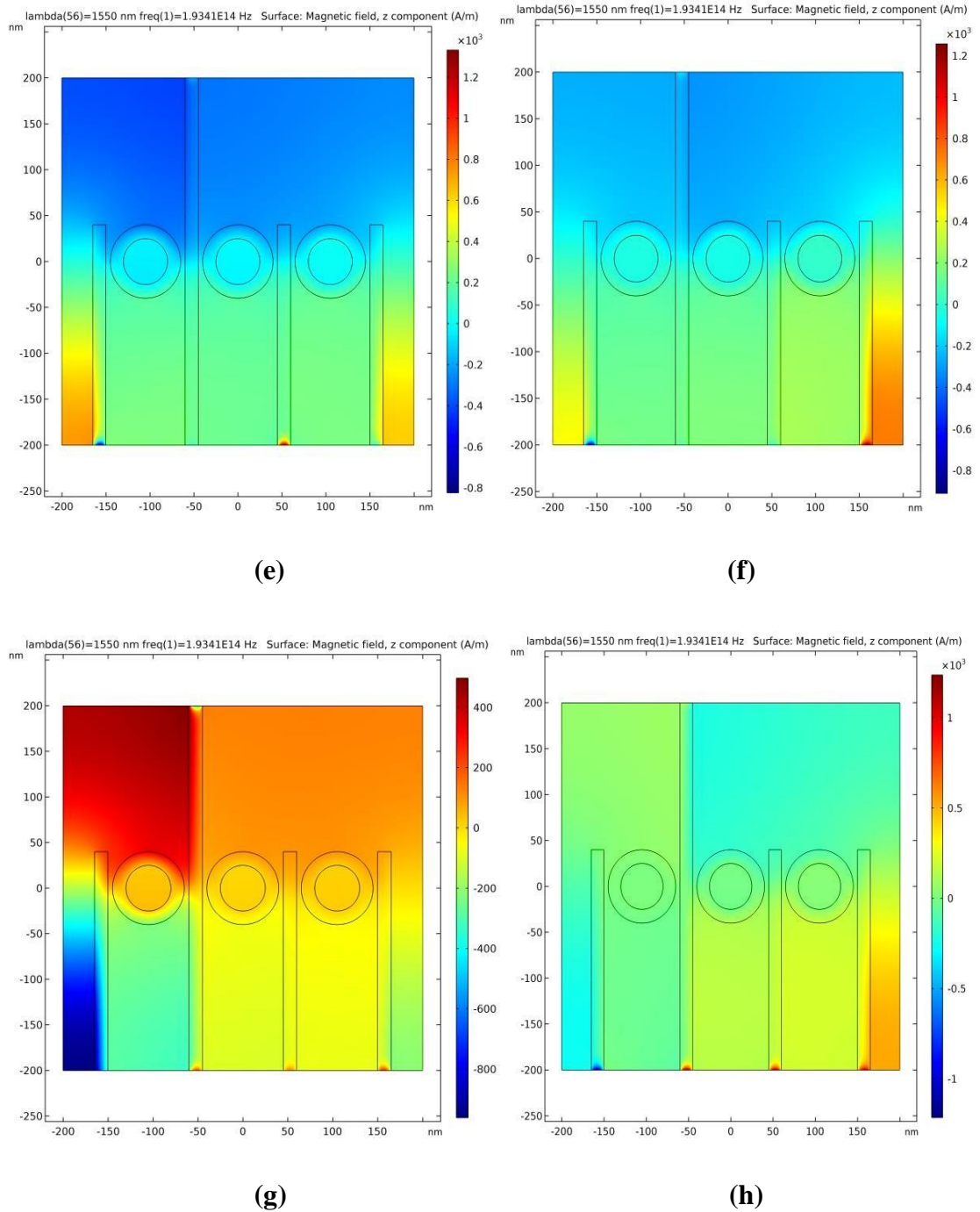


**Fig.3. 26 (Continued).**

The normalized transmission of the proposed three inputs NOR are logic gate and the magnetic field distributions of the proposed gate at different input states shown in Figure (3.25) and (3.26) respectively. The operation details of the proposed all-optical three inputs NOR logic gate are presented in Table (3.14). The minimum transmission at the output port in case of the output state is (ON) is (0.289), and the maximum transmission at

the output in case of the output state is (OFF) is (0.164), according to Equation (2.3) the contrast ratio (CR) is equal to (2.46 dB).

**Table 3. 14 The operation details of the proposed all-optical three inputs NOR logic gate**

Input Port 1 Status and (Phase°)	Input Port 2 Status and (Phase°)	Input Port 3 Status and (Phase°)	Control Port Status and (Phase°)	Output Port Status	Transmission Threshold $T_{Threshold}$	Normalized Transmission $T$
OFF (0°)	OFF (0°)	OFF (0°)	ON (0°)	ON	0.26	0.289
OFF (0°)	OFF (0°)	ON (180°)	ON (45°)	OFF	0.26	0.085
OFF (0°)	ON (180°)	OFF (0°)	ON (45°)	OFF	0.26	0.164
OFF (0°)	ON (180°)	ON (180°)	ON (45°)	OFF	0.26	0.029
ON (180°)	OFF (0°)	OFF (0°)	ON (45°)	OFF	0.26	0.114
ON (180°)	OFF (0°)	ON (180°)	ON (45°)	OFF	0.26	0.012
ON (180°)	ON (180°)	OFF (0°)	ON (45°)	OFF	0.26	0.043
ON (180°)	ON (180°)	ON (180°)	ON (45°)	OFF	0.26	0.01
<b>Contrast Ratio (CR) of The Proposed Gate = 2.46 (dB)</b>						

### 3.4.5 Three Inputs All-Optical EX-NOR Logic Gate

The output state of the EX-NOR gate is (ON) only when; even number of inputs is in (ON) state or all the inputs are in (OFF) state otherwise, the output state is (OFF). In the proposed EX-NOR gate structure shown in Figure (2.6), the input ports are (port 2, 3, and 4); the control port is (port 1), (port 5) is the output port as presented in Figure (2.8). The function of the EX-NOR gate can be realized by employing the phenomena of the constructive and destructive interference between the propagating light signals between the inputs and control ports. The transmission threshold of the proposed EX-NOR gate is (0.26). Similar to NOR gate, the proposed EX-NOR gate have relatively low contrast ratio (CR) of (2.46 dB)

and thus, the performance of this gate is moderate. The normalized transmission of the proposed three inputs EX-NOR logic gate and the magnetic field distributions of the proposed gate at different input states are shown in Figure (3.27) and (3.28) respectively. The operation details of the proposed all-optical three inputs EX-NOR logic gate are presented in Table (3.15).

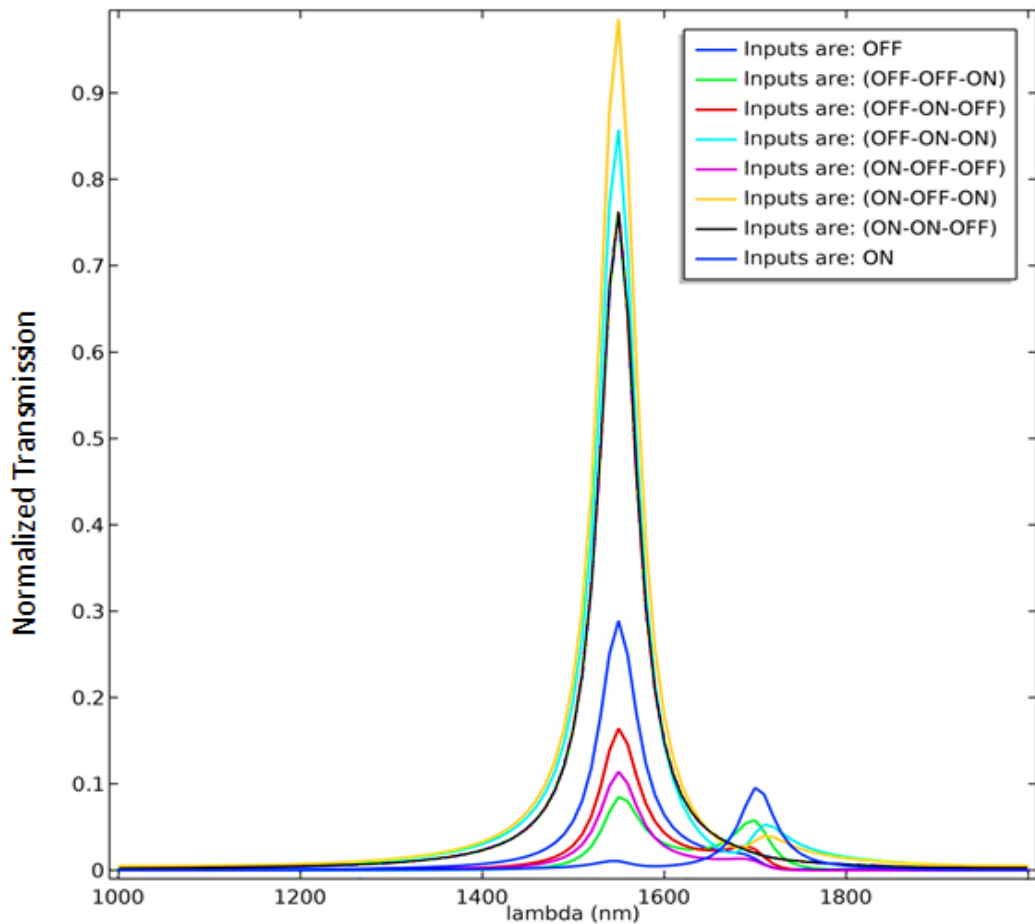


**Fig.3. 27 Normalized transmission of the proposed all-optical three inputs EX-NOR logic gate as a function of wavelength for different input states.**

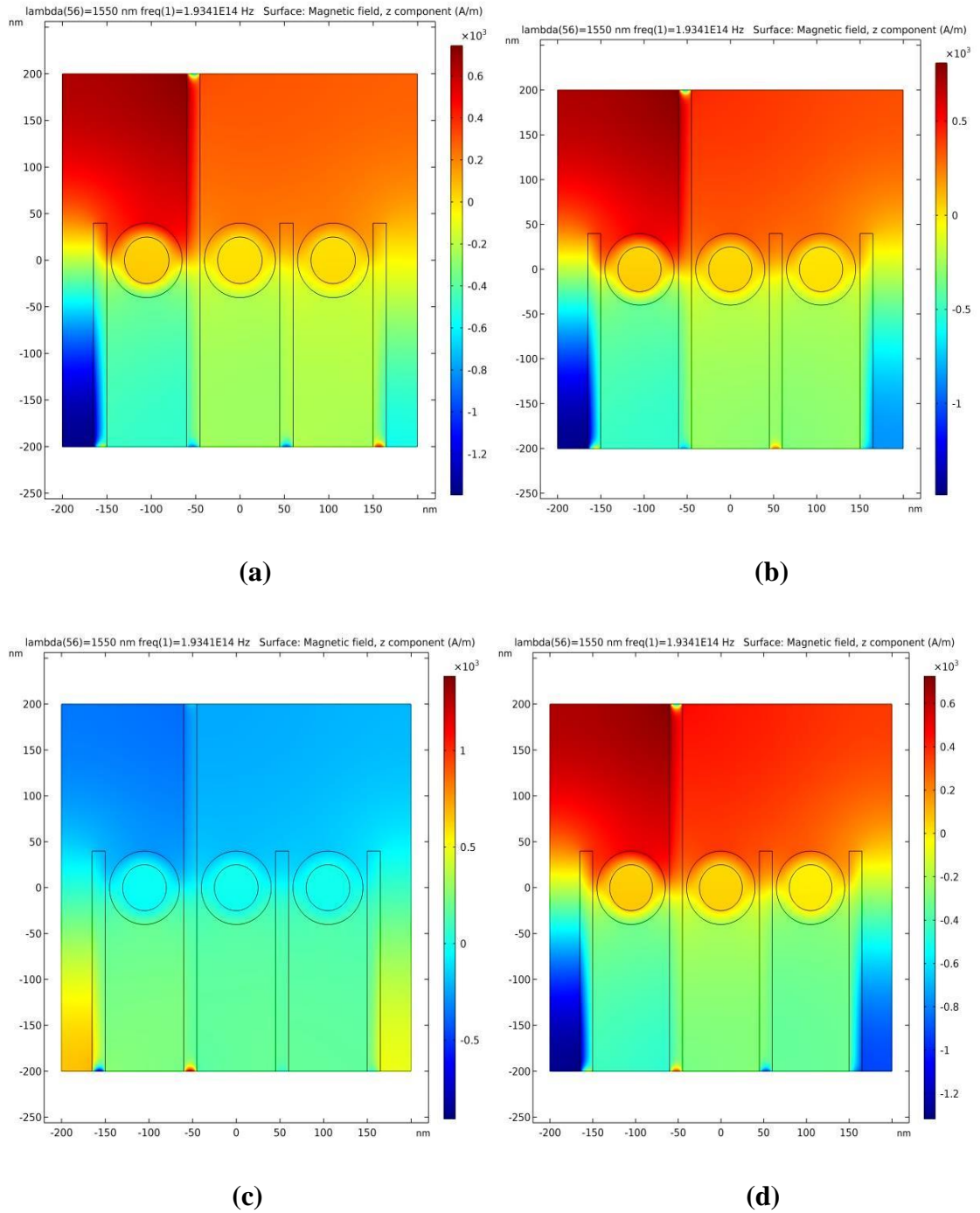
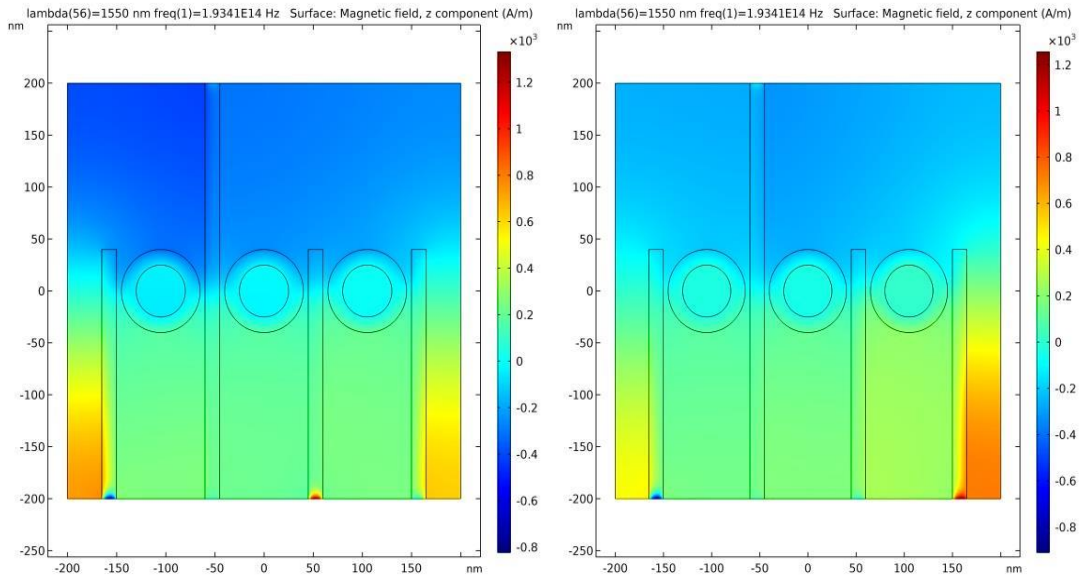
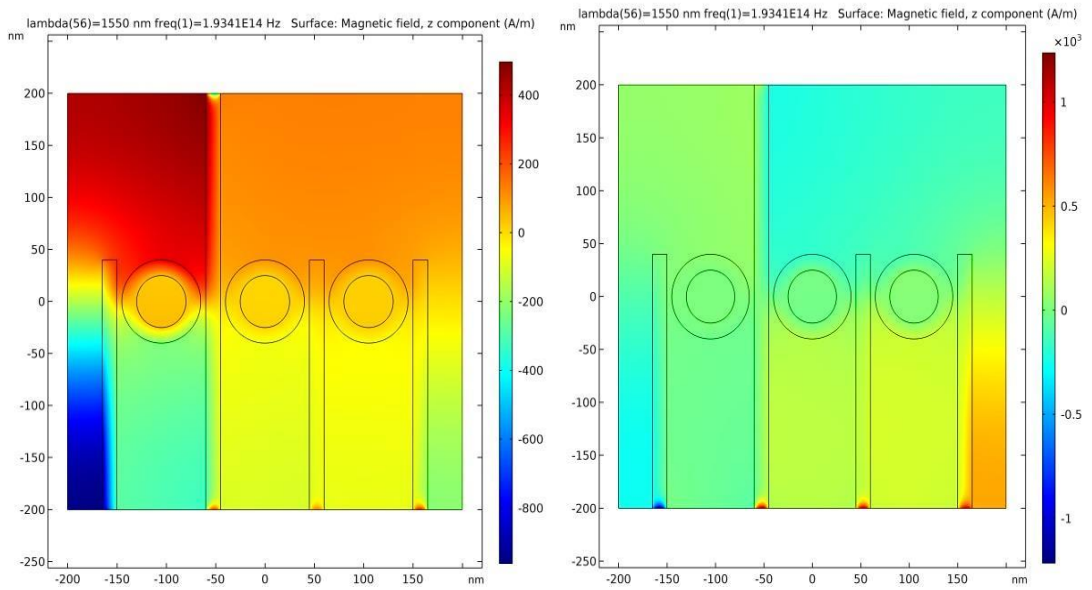


**Fig.3. 28** The magnetic field distribution of the proposed all-optical three inputs EX-NOR logic gate at the different inputs states; (a) (off-off-off), (b) (off-off-on), (c) (off-on-off), (d) (off-on-on), (e) (on-off-off), (f) (on-off-on), (g) (on-on-off), and (h) (on-on-on) inputs states.



(e)

(f)



(g)

(h)

Fig.3. 28 (Continued).

**Table 3. 15 The Operation Details of the Proposed All-Optical Three Inputs EX-NOR Logic Gate**

<b>Input Port 1 Status and (Phase°)</b>	<b>Input Port 2 Status and (Phase°)</b>	<b>Input Port 3 Status and (Phase°)</b>	<b>Control Port Status and (Phase°)</b>	<b>Output Port Status</b>	<b>Transmission Threshold <math>T_{Threshold}</math></b>	<b>Normalized Transmission <math>T</math></b>
<b>OFF (0°)</b>	<b>OFF (0°)</b>	<b>OFF (0°)</b>	<b>ON (0°)</b>	<b>ON</b>	<b>0.26</b>	<b>0.289</b>
<b>OFF (0°)</b>	<b>OFF (0°)</b>	<b>ON (180°)</b>	<b>ON (45°)</b>	<b>OFF</b>	<b>0.26</b>	<b>0.085</b>
<b>OFF (0°)</b>	<b>ON (180°)</b>	<b>OFF (0°)</b>	<b>ON (45°)</b>	<b>OFF</b>	<b>0.26</b>	<b>0.164</b>
<b>OFF (0°)</b>	<b>ON (0°)</b>	<b>ON (0°)</b>	<b>ON (0°)</b>	<b>ON</b>	<b>0.26</b>	<b>0.857</b>
<b>ON (180°)</b>	<b>OFF (0°)</b>	<b>OFF (0°)</b>	<b>ON (45°)</b>	<b>OFF</b>	<b>0.26</b>	<b>0.114</b>
<b>ON (0°)</b>	<b>OFF (0°)</b>	<b>ON (0°)</b>	<b>ON (0°)</b>	<b>ON</b>	<b>0.26</b>	<b>0.985</b>
<b>ON (0°)</b>	<b>ON (0°)</b>	<b>OFF (0°)</b>	<b>ON (0°)</b>	<b>ON</b>	<b>0.26</b>	<b>0.762</b>
<b>ON (180°)</b>	<b>ON (180°)</b>	<b>ON (180°)</b>	<b>ON (45°)</b>	<b>OFF</b>	<b>0.26</b>	<b>0.01</b>

# **Chapter Four**

## **Conclusions and Future Works**

## 4.1 Conclusion

After designing all optical plasmonic gates many design parameters could effect on the performance of the plasmonic gates (CR and transmission) that are dimensions, no of the nano rings (transmission threshold and shapes of the designed plasomnic gates. The concluded points from this work are summarized below:

1. The dimensions of the structure such as; the ring radii, the width and length of the straight waveguides, the coupling distance between the waveguides, number of Nano-rings structures, and number of straight waveguides are strongly affect the output results.
2. The distribution of the structure ports (control and inputs) ports plays important role in determining in the performance of the designed plasmonic gates.
3. In the case of symmetrical structure the output normalized transmission has no ripples.
4. In some cases, the output transmission may exceeds the (100%) as a results of high constructive interference between the propagated light signals which are all in the same phase and direction.
5. The designed universal plasmonics gates have compact size which is (350 nm×350 nm) which make it useful for ultra-compact all-optical systems.
6. Maximum (CR) of 14.6 dB is achieved in multiple inputs logic gates with dimensions of (400 nm × 400 nm) which is related to plasmonic NAND gate.

## 4.2 Future Works

This work can be expanded in the future as follow:

1. Trying to implement the designed structures practically via the accurate fabrication methods using lithography techniques and femtosecond lasers.
2. Using different materials either metals or dielectric with that effect on  $n_{eff}$  to perform all-optical logic gates.
3. Modifying the structure and materials to increase the contrast ratio (CR) as much as possible.
4. Design, realize, and investigate the combinational and sequential all-optical logic circuits.
5. Design tunable plasmonic filter by varying the outer ring radius and spacing distance between the waveguides.
6. Design plasmonic Bragg Grating Waveguide.

# REFERENCES

## References

- [1] H. J. Lezec, A. Degiron, E. Devaux, R. Linke, L. Martin-Moreno, F. Garcia-Vidal, *et al.*, "Beaming light from a subwavelength aperture," *science*, vol. 297, pp. 820-822, 2002.
- [2] X. Mei, X. G. Huang, and T. Jin, "A sub-wavelength electro-optic switch based on plasmonic T-shaped waveguide," *Plasmonics*, vol. 6, pp. 613-618, 2011.
- [3] X. Peng, H. Li, C. Wu, G. Cao, and Z. Liu, "Research on transmission characteristics of aperture-coupled square-ring resonator based filter," *Optics Communications*, vol. 294, pp. 368-371, 2013.
- [4] Y. Guo, L. Yan, W. Pan, B. Luo, K. Wen, Z. Guo, *et al.*, "Transmission characteristics of the aperture-coupled rectangular resonators based on metal–insulator–metal waveguides," *Optics Communications*, vol. 300, pp. 277-281, 2013.
- [5] B. Wang and G. P. Wang, "Plasmon Bragg reflectors and nanocavities on flat metallic surfaces," *Applied Physics Letters*, vol. 87, p. 013107, 2005.
- [6] J. Chen, Z. Li, M. Lei, X. Fu, J. Xiao, and Q. Gong, "Plasmonic Y-splitters of high wavelength resolution based on strongly coupled-resonator effects," *Plasmonics*, vol. 7, pp. 441-445, 2012.
- [7] N. Nozhat and N. Granpayeh, "Switching power reduction in the ultra-compact Kerr nonlinear plasmonic directional coupler," *Optics Communications*, vol. 285, pp. 1555-1559, 2012.
- [8] Z. Lu and W. Zhao, "Nanoscale electro-optic modulators based on graphene-slot waveguides," *JOSA B*, vol. 29, pp. 1490-1496, 2012.
- [9] N. Nozhat and N. Granpayeh, "Analysis of the plasmonic power splitter and MUX/DEMUX suitable for photonic integrated circuits," *Optics Communications*, vol. 284, pp. 3449-3455, 2011.

- [10] H. Li, J. W. Noh, Y. Chen, and M. Li, "Enhanced optical forces in integrated hybrid plasmonic waveguides," *Optics express*, vol. 21, pp. 11839-11851, 2013.
- [11] N. Nozhat and N. Granpayeh, "All-optical nonlinear plasmonic ring resonator switches," *Journal of Modern Optics*, vol. 61, pp. 1690-1695, 2014.
- [12] J. Tao, Q. J. Wang, and X. G. Huang, "All-optical plasmonic switches based on coupled nano-disk cavity structures containing nonlinear material," *Plasmonics*, vol. 6, p. 753, 2011.
- [13] Y. Liu, F. Qin, Z.-M. Meng, F. Zhou, Q.-H. Mao, and Z.-Y. Li, "All-optical logic gates based on two-dimensional low-refractive-index nonlinear photonic crystal slabs," *Optics express*, vol. 19, pp. 1945-1953, 2011.
- [14] D. Pan, H. Wei, and H. Xu, "Optical interferometric logic gates based on metal slot waveguide network realizing whole fundamental logic operations," *Optics express*, vol. 21, pp. 9556-9562, 2013.
- [15] L. Wang, L. Yan, Y. Guo, K. Wen, W. Pan, and B. Luo, "Optical quasi logic gates based on polarization-dependent four-wave mixing in subwavelength metallic waveguides," *Optics express*, vol. 21, pp. 14442-14451, 2013.
- [16] Y. Bian and Q. Gong, "Compact all-optical interferometric logic gates based on one-dimensional metal–insulator–metal structures," *Optics Communications*, vol. 313, pp. 27-35, 2014.
- [17] K. J. Ooi, H. S. Chu, P. Bai, and L. K. Ang, "Electro-optical graphene plasmonic logic gates," *Optics letters*, vol. 39, pp. 1629-1632, 2014.
- [18] I. S. Maksymov, "Optical switching and logic gates with hybrid plasmonic–photonic crystal nanobeam cavities," *Physics Letters A*, vol. 375, pp. 918-921, 2011.

- [19] S. Kaur and R.-S. Kaler, "Ultrahigh speed reconfigurable logic operations based on single semiconductor optical amplifier," *Journal of the Optical Society of Korea*, vol. 16, pp. 13-16, 2012.
- [20] G.-Y. Oh, D. G. Kim, and Y.-W. Choi, "All-optical logic gate using waveguide-type SPR with Au/ZnO plasmon stack," in *OECC 2010 Technical Digest*, 2010, pp. 374-375.
- [21] Q. Xu and M. Lipson, "All-optical logic based on silicon micro-ring resonators," *Optics express*, vol. 15, pp. 924-929, 2007.
- [22] T. Liang, L. Nunes, M. Tsuchiya, K. Abedin, T. Miyazaki, D. V. Thourhout, *et al.*, "Nonlinear self-distortion of picosecond optical pulses in silicon wire waveguides," in *Quantum Electronics and Laser Science Conference*, 2006, p. JThC44.
- [23] J.-H. Kim, B.-K. Kang, Y.-H. Park, Y.-T. Byun, S. Lee, D.-H. Woo, *et al.*, "All-optical AND gate using XPM wavelength converter," *Journal of the Optical Society of Korea*, vol. 5, pp. 25-28, 2001.
- [24] H. Wei, Z. Wang, X. Tian, M. Käll, and H. Xu, "Cascaded logic gates in nanophotonic plasmon networks," *Nature communications*, vol. 2, pp. 1-5, 2011.
- [25] A. Dolatabady and N. Granpayeh, "All optical logic gates based on two dimensional plasmonic waveguides with nanodisk resonators," *Journal of the Optical Society of Korea*, vol. 16, pp. 432-442, 2012.
- [26] Y.-D. Wu, Y.-T. Hsueh, and T.-T. Shih, "Novel All-optical Logic Gates Based on Microring Metal-insulator-metal Plasmonic Waveguides," in *PIERS Proceedings*, 2013.
- [27] N. Nozhat and N. Granpayeh, "All-optical logic gates based on nonlinear plasmonic ring resonators," *Applied optics*, vol. 54, pp. 7944-7948, 2015.
- [28] A. Dolatabady and N. Granpayeh, "All-optical logic gates in plasmonic metal-insulator-metal nanowaveguide with slot cavity resonator," *Journal of Nanophotonics*, vol. 11, p. 026001, 2017.

- [29] Z. Liu, L. Ding, J. Yi, Z. Wei, and J. Guo, "Design of a multi-bits input optical logic device with high intensity contrast based on plasmonic waveguides structure," *Optics Communications*, vol. 430, pp. 112-118, 2019.
- [30] B. Lee, I.-M. Lee, S. Kim, D.-H. Oh, and L. Hesselink, "Review on subwavelength confinement of light with plasmonics," *Journal of Modern Optics*, vol. 57, pp. 1479-1497, 2010.
- [31] M. Li, S. K. Cushing, and N. Wu, "Plasmon-enhanced optical sensors: a review," *Analyst*, vol. 140, pp. 386-406, 2015.
- [32] F. Samadi, M. Akbari, M. R. Chaharmir, and A. Sebak, "Scatterer surface design for wave scattering application," *IEEE Transactions on Antennas and Propagation*, vol. 67, pp. 1202-1211, 2018.
- [33] R. A. Ammar and M. Lemerini, "Surface plasmon polariton in metal-insulator-metal configuration," 2017.
- [34] J. W. Haus, *Fundamentals and applications of nanophotonics*: Woodhead Publishing, 2016.
- [35] S. Unser, I. Bruzas, J. He, and L. Sagle, "Localized surface plasmon resonance biosensing: current challenges and approaches," *Sensors*, vol. 15, pp. 15684-15716, 2015.
- [36] T. V. Shahbazyan and M. I. Stockman, *Plasmonics: theory and applications*: Springer, 2013.
- [37] C. Caucheteur, T. Guo, and J. Albert, "Review of plasmonic fiber optic biochemical sensors: improving the limit of detection," *Analytical and bioanalytical chemistry*, vol. 407, pp. 3883-3897, 2015.
- [38] H. Xu, *Nanophotonics: Manipulating Light with Plasmons*: Pan Stanford, 2017.
- [39] P. K. Jain, X. Huang, I. H. El-Sayed, and M. A. El-Sayed, "Review of some interesting surface plasmon resonance-enhanced properties of

- noble metal nanoparticles and their applications to biosystems," *Plasmonics*, vol. 2, pp. 107-118, 2007.
- [40] E. Ozbay, "Plasmonics: merging photonics and electronics at nanoscale dimensions," *science*, vol. 311, pp. 189-193, 2006.
- [41] M. J. Kobrinsky, B. A. Block, J.-F. Zheng, B. C. Barnett, E. Mohammed, M. Reshotko, *et al.*, "On-Chip Optical Interconnects," *Intel Technology Journal*, vol. 8, 2004.
- [42] S. H. M. El, "DESIGN OPTIMIZATION AND MODELING OF PLASMONIC STRUCTURES," 2012.
- [43] A. Pratt, "Overview of the use of copper interconnects in the semiconductor industry," *Adv Energy Ind*, 2004.
- [44] A. Biberman and K. Bergman, "Optical interconnection networks for high-performance computing systems," *Reports on Progress in Physics*, vol. 75, p. 046402, 2012.
- [45] W. M. Green, M. J. Rooks, L. Sekaric, and Y. A. Vlasov, "Ultra-compact, low RF power, 10 Gb/s silicon Mach-Zehnder modulator," *Optics express*, vol. 15, pp. 17106-17113, 2007.
- [46] R. Zia, J. A. Schuller, A. Chandran, and M. L. Brongersma, "Plasmonics: the next chip-scale technology," *Materials today*, vol. 9, pp. 20-27, 2006.
- [47] D. K. Gramotnev and S. I. Bozhevolnyi, "Plasmonics beyond the diffraction limit," *Nature photonics*, vol. 4, p. 83, 2010.
- [48] W. L. Barnes, A. Dereux, and T. W. Ebbesen, "Surface plasmon subwavelength optics," *nature*, vol. 424, pp. 824-830, 2003.
- [49] D. Taillaert, P. Bienstman, and R. Baets, "Compact efficient broadband grating coupler for silicon-on-insulator waveguides," *Optics letters*, vol. 29, pp. 2749-2751, 2004.
- [50] F. Xia, M. Rooks, L. Sekaric, and Y. Vlasov, "Ultra-compact high order ring resonator filters using submicron silicon photonic wires for

- on-chip optical interconnects," *Optics express*, vol. 15, pp. 11934-11941, 2007.
- [51] Y. Morita, Y. Tsuji, and K. Hirayama, "Proposal for a compact resonant-coupling-type polarization splitter based on photonic crystal waveguide with absolute photonic bandgap," *IEEE photonics technology letters*, vol. 20, pp. 93-95, 2008.
- [52] W. Bogaerts, R. Baets, P. Dumon, V. Wiaux, S. Beckx, D. Taillaert, *et al.*, "Nanophotonic waveguides in silicon-on-insulator fabricated with CMOS technology," *Journal of Lightwave Technology*, vol. 23, pp. 401-412, 2005.
- [53] S. A. Maier, "Plasmonics: The promise of highly integrated optical devices," *IEEE Journal of selected topics in Quantum Electronics*, vol. 12, pp. 1671-1677, 2006.
- [54] M. L. Brongersma, "Introductory lecture: nanoplasmonics," *Faraday discussions*, vol. 178, pp. 9-36, 2015.
- [55] K. Hasegawa, J. U. Nöckel, and M. Deutsch, "Surface plasmon polariton propagation around bends at a metal–dielectric interface," *Applied physics letters*, vol. 84, pp. 1835-1837, 2004.
- [56] H. Baltar, K. Drozdowicz-Tomsia, and E. M. Goldys, "Propagating surface plasmons and dispersion relations for nanoscale multilayer metallic-dielectric films," *Plasmonics—Principles and Applications*, pp. 135-156, 2012.
- [57] P. B. Johnson and R.-W. Christy, "Optical constants of the noble metals," *Physical review B*, vol. 6, p. 4370, 1972.
- [58] L. Nickelson, "Plasmonics," in *Electromagnetic Theory and Plasmonics for Engineers*, ed: Springer, 2019, pp. 611-695.
- [59] R. Zia, M. D. Selker, P. B. Catrysse, and M. L. Brongersma, "Geometries and materials for subwavelength surface plasmon modes," *JOSA A*, vol. 21, pp. 2442-2446, 2004.

- [60] S. A. Maier, *Plasmonics: fundamentals and applications*: Springer Science & Business Media, 2007.
- [61] S. Aldawsari, "Comprehensive Theoretical Studies of Guided Modes in Multilayer Hybrid Plasmonic Waveguides," 2018.
- [62] M. Alam, "Hybrid plasmon waveguides: Theory and applications," 2012.
- [63] H. Wei, D. Pan, and H. Xu, "Routing of surface plasmons in silver nanowire networks controlled by polarization and coating," *Nanoscale*, vol. 7, pp. 19053-19059, 2015.
- [64] H. Wei, Z. Li, X. Tian, Z. Wang, F. Cong, N. Liu, *et al.*, "Quantum dot-based local field imaging reveals plasmon-based interferometric logic in silver nanowire networks," *Nano letters*, vol. 11, pp. 471-475, 2011.
- [65] W. Storr, "Basic Electronics tutorial site," *Website (<http://www.electronics-tutorials.ws>)*, 2013.
- [66] M. H. Rezaei, A. Zarifkar, and M. Miri, "Ultra-compact electro-optical graphene-based plasmonic multi-logic gate with high extinction ratio," *Optical Materials*, vol. 84, pp. 572-578, 2018.
- [67] W. Yang, X. Shi, H. Xing, and X. Chen, "All-optical logic gates based on metallic waveguide arrays," *Results in Physics*, vol. 11, pp. 837-841, 2018.
- [68] A. Singh, A. Pal, Y. Singh, and S. Sharma, "Design of optimized all-optical NAND gate using metal-insulator-metal waveguide," *Optik*, vol. 182, pp. 524-528, 2019.
- [69] S. Sharma, R. Zafar, M. H. Mahdieh, G. Singh, and M. Salim, "High Contrast Ratio Based All-Optical OR and NOR Plasmonic Logic Gate Operating at E Band," in *Optical and Wireless Technologies*, ed: Springer, 2020, pp. 325-332.

- [70] D. Sarid and W. A. Challener, *Modern introduction to surface plasmons: theory, Mathematica modeling, and applications*: Cambridge University Press, 2010.
- [71] K. M. McPeak, S. V. Jayanti, S. J. Kress, S. Meyer, S. Iotti, A. Rossinelli, *et al.*, "Plasmonic films can easily be better: rules and recipes," *ACS photonics*, vol. 2, pp. 326-333, 2015.
- [72] M. G. Blaber, M. D. Arnold, and M. J. Ford, "A review of the optical properties of alloys and intermetallics for plasmonics," *Journal of Physics: Condensed Matter*, vol. 22, p. 143201, 2010.
- [73] H. Xu, *Nanophotonics: Manipulating Light with Plasmons*: Pan Stanford, 2017.
- [74] S. A. Maier, *Plasmonics: fundamentals and applications*: Springer Science & Business Media, 2007.
- [75] T. Roney, *Applications of plasmonics in silicon based photonic devices*: University of Leeds, 2012.
- [76] S. A. Ramakrishna, "Physics of negative refractive index materials," *Reports on progress in physics*, vol. 68, p. 449, 2005.
- [77] P. B. Johnson and R.-W. Christy, "Optical constants of the noble metals," *Physical review B*, vol. 6, p. 4370, 1972.
- [78] M. Pelton and G. W. Bryant, *Introduction to metal-nanoparticle plasmonics* vol. 5: John Wiley & Sons, 2013.
- [79] S. Enoch and N. Bonod, *Plasmonics: from basics to advanced topics* vol. 167: Springer, 2012.
- [80] R. H. Ras, R. A. Schoonheydt, and C. T. Johnston, "Relation between s-polarized and p-polarized internal reflection spectra: application for the spectral resolution of perpendicular vibrational modes," *The Journal of Physical Chemistry A*, vol. 111, pp. 8787-8791, 2007.
- [81] S. Enoch and N. Bonod, *Plasmonics: from basics to advanced topics* vol. 167: Springer, 2012.

- [82] B. Hecht, H. Bielefeldt, L. Novotny, Y. Inouye, and D. Pohl, "Local excitation, scattering, and interference of surface plasmons," *Physical review letters*, vol. 77, p. 1889, 1996.
- [83] L. Salomon, G. Bassou, H. Aourag, J. Dufour, F. De Fornel, F. Carcenac, *et al.*, "Local excitation of surface plasmon polaritons at discontinuities of a metal film: Theoretical analysis and optical near-field measurements," *Physical Review B*, vol. 65, p. 125409, 2002.
- [84] A. Bouhelier and G. Wiederrecht, "Excitation of broadband surface plasmon polaritons: Plasmonic continuum spectroscopy," *Physical Review B*, vol. 71, p. 195406, 2005.
- [85] A. Bouhelier and G. Wiederrecht, "Excitation of broadband surface plasmon polaritons: Plasmonic continuum spectroscopy," *Physical Review B*, vol. 71, p. 195406, 2005.
- [86] Z. Han and S. I. Bozhevolnyi, "Radiation guiding with surface plasmon polaritons," *Reports on Progress in Physics*, vol. 76, p. 016402, 2012.
- [87] S. Jahani and Z. Jacob, "Transparent subdiffraction optics: nanoscale light confinement without metal," *Optica*, vol. 1, pp. 96-100, 2014.
- [88] R. Oulton, G. Bartal, D. Pile, and X. Zhang, "Confinement and propagation characteristics of subwavelength plasmonic modes," *New Journal of Physics*, vol. 10, p. 105018, 2008.
- [89] Y. Liu, T. Chang, and A. E. Craig, "Coupled mode theory for modeling microring resonators," *Optical Engineering*, vol. 44, p. 084601, 2005.
- [90] K. Okamoto, *Fundamentals of optical waveguides*: Academic press, 2006.
- [91] M. L. Brongersma and P. G. Kik, *Surface plasmon nanophotonics* vol. 131: Springer, 2007.

- [92] N. Panoiu, W. Sha, D. Lei, and G. Li, "Nonlinear optics in plasmonic nanostructures," *Journal of Optics*, vol. 20, p. 083001, 2018.
- [93] H. Simon, R. Benner, and J. Rako, "Optical second harmonic generation with surface plasmons in piezoelectric crystals," *Optics Communications*, vol. 23, pp. 245-248, 1977.
- [94] S. Palomba and L. Novotny, "Nonlinear excitation of surface plasmon polaritons by four-wave mixing," *Physical Review Letters*, vol. 101, p. 056802, 2008.
- [95] C. Chen, A. De Castro, Y. Shen, and F. DeMartini, "Surface coherent anti-Stokes Raman spectroscopy," *Physical Review Letters*, vol. 43, p. 946, 1979.
- [96] S. Palomba, H. Harutyunyan, J. Renger, R. Quidant, N. F. van Hulst, and L. Novotny, "Nonlinear plasmonics at planar metal surfaces," *Philosophical Transactions of the Royal Society A: Mathematical, Physical and Engineering Sciences*, vol. 369, pp. 3497-3509, 2011.
- [97] J. Renger, R. Quidant, N. Van Hulst, and L. Novotny, "Surface-enhanced nonlinear four-wave mixing," *Physical review letters*, vol. 104, p. 046803, 2010.
- [98] H. Harutyunyan, S. Palomba, J. Renger, R. Quidant, and L. Novotny, "Nonlinear dark-field microscopy," *Nano letters*, vol. 10, pp. 5076-5079, 2010.
- [99] S. H. Abdulnabi and M. N. Abbas, "All-optical logic gates based on nanoring insulator–metal–insulator plasmonic waveguides at optical communications band," *Journal of Nanophotonics*, vol. 13, p. 016009, 2019.
- [100] S. H. Abdulnabi and M. N. Abbas, "Design an all-optical combinational logic circuits based on nano-ring insulator-metal-insulator plasmonic waveguides," in *Photonics*, 2019, p. 30.

# Appendices

# **APPENDIX (A)**

## **DESCRIPTION OF SPPs IN METALLIC NANOSTRUCTURES WITH ELECTROMAGNETIC FIELDS**

### **A.1 The Optical Properties of Metals**

Before explaining Maxwell's equations and electromagnetic waves propagation in plasmonic structures, the behavior of metals in these structures must be demonstrated.

Metals behave in a variety of ways with respect to different parts of the electromagnetic spectrum of the input light wave. They are highly reflective for frequencies up to the visible part of the spectrum, preventing light from penetrating them, which is why, for lower frequencies, they are generally considered as good conductors [70]. On the other hand, for near infrared and higher frequencies, the amount of field penetration of the input light into metals increases significantly, resulting in increased absorption of the light. At ultraviolet frequencies, metals behave as dielectric media, allowing electromagnetic waves to propagate through them with different degrees of attenuation. For noble metals, such as gold or silver, strong absorption between electronic bands due to inter-band transition occur, which is why they tend to be very lossy in this regime. Table A.1 shows the quality factors and SPP propagation lengths for four common plasmonic metals that are the most commonly used in plasmonic nanostructures [71].

**Table A.1. The quality factors and SPP propagation lengths for four common plasmonic metals**

wavelength regime	metal	$Q_{LSPR}$ (%)	$Q_{SPP}$ (%)	$L_{SPP}$ ( $\mu\text{m}$ )
ultraviolet (280 nm)	Al	11	-12	2.5
visible (650 nm)	Ag	200	250	84
	Cu	120	130	24
	Au	32	38	20
near-infrared (1000 nm)	Ag	160	200	340
	Cu	100	93	190
	Au	51	61	190
telecom (1550 nm)	Ag	270	480	1200
	Cu	140	120	820
	Au	81	95	730

Where ( $Q_{LSPR}$  and  $L_{SPP}$ ) are Quality factor of Localized Surface Plasmon Resonance (LSPR) and Quality factor of SPP, respectively. These two factors are described by Equations (A.1) and (A.2), respectively [72]. While  $L_{SPP}$  is a propagation length of SPP which is described by Equation (A.3) [73, 74]

$$Q_{LSPR} = -\epsilon_{re}/\epsilon_{im} \quad (A.1)$$

$$Q_{LSPR} = -\epsilon_{re}^2/\epsilon_{im} \quad (A.2)$$

$$L_{SPP} = \frac{1}{2im[\beta]} = \frac{1}{2k_{spp\ im}} = \lambda_o \frac{\epsilon_{re}^2}{2\pi\epsilon_{im}} \left\{ \frac{\epsilon_{re} + \epsilon_{re}}{\epsilon_{re}\epsilon_2} \right\}^{3/2} \quad (A.3)$$

Where  $\epsilon_{re}$  is a real part of the complex dielectric function (permittivity) of the metal,  $\epsilon_{im}$  is an imaginary part of dielectric function (permittivity) of the metal,  $k_{spp\ im}$  is an imaginary part of propagation constant, and  $\epsilon_2$  is permittivity of dielectric medium. which is related to the conductivity  $\sigma$  as shown in Equation (A.4) [73].

dielectric function  $\epsilon(\omega)$  which is a function of frequency (wavelength), The dispersive properties of metals can be described by a complex has overcome

other metals in the same wavelength (1550 nm). Therefore, this thesis used this material (Silver). For these advantages it wavelengths as well as higher  $Q_{LSPR}$ ,  $Q_{SPP}$ , and  $LSPP$  than other metals. materials in both the visible, near-infrared (NIR) at telecommunication From Table A.1, Silver exhibits the lowest losses of current Appendix (D). The two factors ( $Q_{SPP}$  and  $LSPP$ ) are explained and defined in

$$\varepsilon(\omega) = 1 + \frac{i\sigma(K,\omega)}{\varepsilon_0\omega} \quad (A.4)$$

Where  $\omega$  is the angular frequency of an incident plane wave,  $K$  is the wavevector and  $\varepsilon_0$  is permittivity of the vacuum.  $\varepsilon(\omega)$  can be separated into real and imaginary parts,  $\varepsilon_{re}$  and  $\varepsilon_{im}$  as shown in Equation(A.5) related to the complex refractive index  $n(\omega)$  as shown in Equation (A.6) .

$$\varepsilon(\omega) = \varepsilon_{re} + i\varepsilon_{im} \quad (A.5)$$

$$\varepsilon(\omega) = n(\omega)^2 = (n_{re}(\omega) + ik_{im}(\omega))^2 \quad (A.6)$$

From the above two equations, the derivation of the following four relationships between the real part of  $\varepsilon(\omega)$  and  $n(\omega)$ , and the imaginary part of them is easy [75].

$$\varepsilon_{re} = n_{re}^2 - k_{im}^2 \quad (A.7)$$

$$\varepsilon_{im} = 2n_{re}k_{im} \quad (A.8)$$

$$n_{re} = \sqrt{\frac{\varepsilon_{re}}{2}} + \frac{1}{2}\sqrt{\varepsilon_{re}^2 + \varepsilon_{im}^2} \quad (A.9)$$

$$k_{im} = \frac{\varepsilon_{im}}{2n_{re}} \quad (A.10)$$

Where  $k_{im}$  is the extinction coefficient which determines the amount of optical absorption of the EM waves propagating through the medium. It is useful to study the permittivity of the metal for different frequency regimes with respect to the plasma frequency: i.e for  $\omega < \omega_p$  and  $\omega > \omega_p$  For high frequencies close to  $\omega_p$ , the permittivity is predominantly real as in

Equation A.11:

$$\varepsilon(\omega) = 1 - \frac{\omega_p^2}{\omega^2} \quad (\text{A.11})$$

It can be noted from the above equation that at frequencies less than the plasma frequency  $\omega_p$ , the dielectric permittivity of the metals is negative, i.e. the plasma of the excited electrons protects the interior of metals from the external applied field. Thus, metals (such as silver) in this regime tend to provide very low resistance to the external field, and therefore have a good conductivity [76]. However, when the frequencies of the incident plane wave are larger than the plasma frequency, metals behave as a dielectric material with real and positive permittivity.

This thesis used Johnson and Christy data to describe the permittivity of the metal used (Silver) because it is more practical than the analytical equation of other models (such as Drude Model) which depend on practical points to describe the permittivity of the metal (Rounding and fitting do not occur). In Drude model, the rounding and fitting process will occur and this leads to an approximation in the value of permittivity at given point of wavelength or frequency, which results in a high approximation in the final results. In addition, this thesis worked on frequency domain (FEM method) and the accuracy of describing the permittivity is a very important factor since these points vary with frequency or rather with wavelength. Moreover, according to [77], when the dimensions of the parts of the structure become less than 50 nm, the Drude model becomes inefficient in these dimensions while Johnson and Christy data were designed for dimensions which reach to a few of Angstroms [77].

## A.2 Maxwell's Equations and Electromagnetic Wave Propagation

Maxwell's equations describe the electromagnetic field for a given system through four vectors which are strength of the electric field ( $E$ ), the displacement ( $D$ ), the strength of magnetic field ( $H$ ), and the flux density ( $B$ ) with the external charge and current densities  $\rho_{ext}$  and  $J_{ext}$  [78]. The Maxwell's equations are described in the following four Equations:

$$\nabla \cdot D = \rho_{ext} \quad (A.12)$$

$$\nabla \cdot B = 0 \quad (A.13)$$

$$\nabla \times E = -\partial B / \partial t \quad (A.14)$$

$$\nabla \times H = J_{ext} + \partial D / \partial t \quad (A.15)$$

The four fields are further linked via the polarization  $P$  and magnetization  $M$  by [79]:

$$D = \varepsilon_0 E + P \quad (A.16)$$

$$H = \frac{1}{\mu_0} B - M \quad (A.17)$$

Where  $\varepsilon_0$  and  $\mu_0$  are the electric permittivity and magnetic permeability of the vacuum, respectively.  $P$  describes the electric dipole moment per unit volume inside the material, caused by the alignment of microscopic dipoles with the electric field.

The great advantage of this approach is that the macroscopic electric field includes all polarization effects. the following limits them to linear, isotropic and nonmagnetic media. One can define the constitutive relations [74].

$$D = \varepsilon_0 \varepsilon_r E \quad (A.18)$$

$$D = \mu_0 \mu_r H \quad (A.19)$$

Where  $\epsilon_r$  and  $\mu_r$  are electric permittivity and magnetic permeability of the material.

In order to investigate the physical properties of surface plasmon polaritons (SPPs), one must apply Maxwell's equations (A.12 to A.15) to the flat interface between a metal and a dielectric. To present this discussion most clearly, it is advantageous to present the equations first in a general form applicable to the guiding of electromagnetic waves, the wave equation. In the absence of external charge and current densities, the curl equations (A.14, A.15) can be combined to yield Equation (A.20)

$$\nabla \times \nabla \times \mathbf{E} = -\mu_0 \partial^2 \mathbf{D} / \partial t^2 \quad (\text{A.20})$$

Using the identities  $\nabla \times \nabla \times \mathbf{E} = \nabla (\nabla \cdot \mathbf{E}) - \nabla^2 \mathbf{E}$  as well as  $\nabla \cdot (\epsilon \mathbf{E}) = \mathbf{E} \cdot \nabla \epsilon + \epsilon \nabla \cdot \mathbf{E}$ , and remembering that due to the absence of external source  $\nabla \cdot \mathbf{D} = 0$ , Eq. A.20 can be rewritten as [74]:

$$\nabla(-(\mathbf{E} \nabla \epsilon) / \epsilon) - \nabla^2 \mathbf{E} = -\mu_0 \epsilon_0 \epsilon_r \mathbf{E} / \partial t^2 \quad (\text{A.21})$$

For negligible variation of the dielectric profile  $\epsilon(r)$  over distances about one optical wavelength, Eq. A.21 simplifies the central equation of electromagnetic wave theory [74].

$$\nabla^2 \mathbf{E} - (\epsilon_r / c^2) \partial^2 \mathbf{E} / \partial t^2 = 0 \quad (\text{A.22})$$

Practically, this equation has to be solved separately in regions of constant  $\epsilon_r$ , and the obtained solutions have to be matched using appropriate boundary conditions. Eq. A.22 can be represented in a form suitable for the description of confined propagating wave, there is two steps. First, assume in all generality a harmonic time dependence.  $\mathbf{E}(\mathbf{r}, t) = \mathbf{E}(\mathbf{r}) \exp(-i\omega t)$  of the electric field, where  $\mathbf{r}$  represents position vector. Insert into Eq. A.22 to yield [74]:

$$\nabla^2 \mathbf{E} + K_0^2 \epsilon_r \mathbf{E} = 0 \quad (\text{A.23})$$

Where  $K_0 = \frac{\omega}{c} = 2\pi\lambda_0$  is the wave vector of the propagating wave in vacuum. Where  $c$  is speed of light in free space and frequency of input light. Eq. A.23 is known as the Helmholtz equation. The propagation geometry is shown in Figure (A.1). Assume for simplicity a one-dimensional problem, i.e. depends only on one spatial coordinate. Specifically, the waves propagate along the  $x$ -direction of a Cartesian coordinate system, and show no spatial variation in the perpendicular in-plane  $y$ -direction (see Figure A.1) [74].

In order to find the surface plasmons which are waves bound to the interfaces ( $x$ - $z$  plane of input light), the magnitudes of the electric and magnetic pharos fields can be written as [80]:

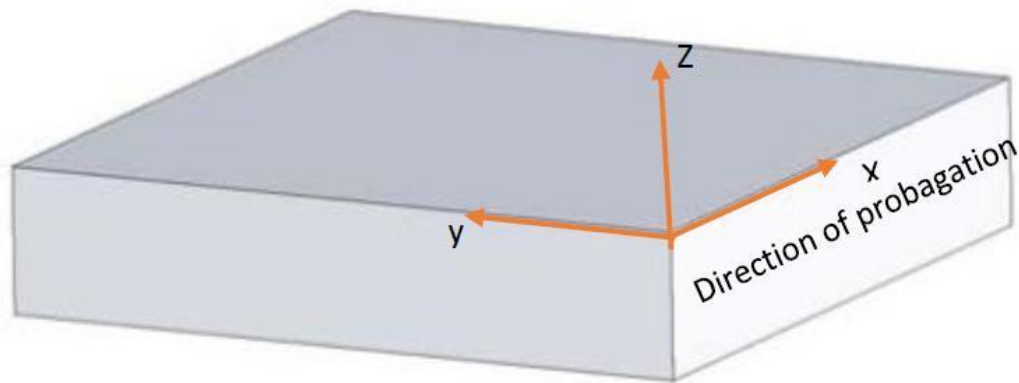


**Figure (A.1) Definition of a planar waveguide geometry. The waves propagate along the  $x$ -direction in a Cartesian coordinate system [81]**

$$(r) = (x, z) = (z)e^{i\beta x} \quad (A.24)$$

$$(r) = (x, z) = (z)e^{i\beta x} \quad (A.25)$$

Where  $\beta$  is propagation constant, in the  $x$  direction. Creating surface plasmon polariton depends on the type of polarization. Therefore  $\epsilon_r = (z)$ . Applied to electromagnetic surface problems, the plane  $z = 0$  coincides with the interface sustaining the propagating waves. In this case, the differential operators with respect to the coordinates  $x$  and  $y$  can be written as [80].

$$\frac{\partial}{\partial x} = i\beta \quad (\text{A.26})$$

$$\frac{\partial}{\partial y} = 0 \quad (\text{A.27})$$

This makes it possible to express the Laplacian of any of the fields as [80]:

$$\partial^2 F(x, z) = \partial^2 F(x, z) / \partial z^2 - \beta^2 F(x, z) = 0 \quad (\text{A.28})$$

The Laplacian in Eq. (A.28) and the fields in Eq. A.24 can be used to simplify the Helmholtz's equations to one dimension [80].

$$\partial^2 E(z) / \partial z^2 + (K_0^2 \epsilon_r - \beta^2) E(z) = 0 \quad (\text{A.29})$$

Naturally, a similar equation exists for the magnetic field  $H$ . Eq. A.29 is the starting point for the general analysis of guided electromagnetic modes in waveguides, and an extended discussion of its properties and applications and similar treatments of photonics and optoelectronics. In order to use the wave equation for determining the spatial field profile and dispersion of propagating waves, now there is a need to find explicit expressions for the different field components of  $\mathbf{E}$  and  $\mathbf{H}$ . This can be achieved in a straight forward way using the curl equations (A.14, A.15). Harmonic time dependence  $\partial / \partial t = -i\omega$  will arrive at the following set of coupled equations [74].

$$\partial E_z / \partial y - \partial E_y / \partial z = i\omega\mu_0 H_x \quad (\text{A.30})$$

$$\partial E_x / \partial z - \partial E_z / \partial x = i\omega\mu_0 H_y \quad (\text{A.31})$$

$$\partial E_y / \partial x - \partial E_x / \partial y = i\omega\mu_0 H_z \quad (\text{A.32})$$

$$\partial H_z / \partial y - \partial H_y / \partial z = i\omega\mu_0 E_x \quad (\text{A.33})$$

$$\partial H_x / \partial z - \partial H_z / \partial x = i\omega\mu_0 E_y \quad (\text{A.34})$$

$$\partial H_y / \partial x - \partial H_x / \partial y = i\omega\mu_0 E_z \quad (\text{A.35})$$

For propagation along the x-direction  $\partial/\partial x = i\beta$  and homogeneity in the y-direction  $\partial/\partial y = 0$ , this system of equation is simplified to [74]:

$$\partial E_x/\partial z = -i\omega\mu_0 H_x \quad (\text{A. 36})$$

$$\partial E_x/\partial z - i\beta E_z = i\omega\mu_0 H_x \quad (\text{A. 37})$$

$$i\beta E_z = i\omega\mu_0 H_z \quad (\text{A. 38})$$

$$\partial H_y/\partial z = i\omega\epsilon_0\epsilon_r E_x \quad (\text{A. 39})$$

$$\partial H_x/\partial z - i\beta H_z = -i\omega\epsilon_0\epsilon_r E_x \quad (\text{A. 40})$$

$$i\beta H_y = -i\omega\epsilon_0\epsilon_r E_z \quad (\text{A. 41})$$

It can easily be shown that this system allows two sets of self-consistent solutions with different polarization properties of the propagating waves. The first set are the Transverse Magnetic (TM or P-Polarized) modes, where only the field components  $E_x, E_z$  and  $H_y$  are nonzero, and in the second set, the Transverse Electric (TE or S-Polarized) modes, only  $H_x, H_z$  and  $E_y$  are nonzero. For TM modes, the system of governing Equations (A.36-A.41) is reduced to [74]:

$$E_x = -(i\partial H_y/\partial z)/\omega\epsilon_0\epsilon_r \quad (\text{A. 41})$$

$$E_z = -\beta H_y/\omega\epsilon_0\epsilon_r \quad (\text{A. 42})$$

In addition, the wave equation for TM modes is:

$$\partial^2 H_y(z)/\partial z^2 + (K_0^2\epsilon_r - \beta^2)H_y(z) = 0 \quad (\text{A. 44})$$

For TE modes the analogous set is

$$H_x = (i\partial E_y/\partial z)/\omega\mu_0 \quad (\text{A. 45})$$

$$H_z = \beta E_y/\omega\mu_0 \quad (\text{A. 46})$$

In addition, the TE wave equation is:

$$\partial^2 E_y(z)/\partial z^2 + (K_0^2\epsilon_r - \beta^2)E_y(z) = 0 \quad (\text{A. 47})$$

# **APPENDIX (B)**

## APPENDIX (B)

### THE POLARIZATION OF INPUT LIGHT

#### B.1 Polarization of Input light

In which the plane of incidence can be defined as the  $x$ - $z$  plane. In these conditions, for a plane wave propagating in the  $x$ - $z$  plane, the magnitudes of the pharos fields are dependent on the coordinates  $x$  and  $z$ , but constant along the  $y$  direction. The creating surface plasmon polariton is dependent on the type of light polarization (S or P) [80].

##### 1. S-polarization or TE-polarization

The incident electromagnetic wave which is the electric field component  $E$  is perpendicular to the plane of incidence, this type of polarization is called S-Polarized, and results in an evanescent wave  $E_y$ , parallel with the  $y$  coordinate. The component of the  $E$ -field that lies in the  $x$ - $y$  plane is continuous as moving across the plane of the interface. Here, all  $E$ -fields are in the  $y$ -direction, which is in the plane of the interface [80]. This case is shown in Figure (B.1).

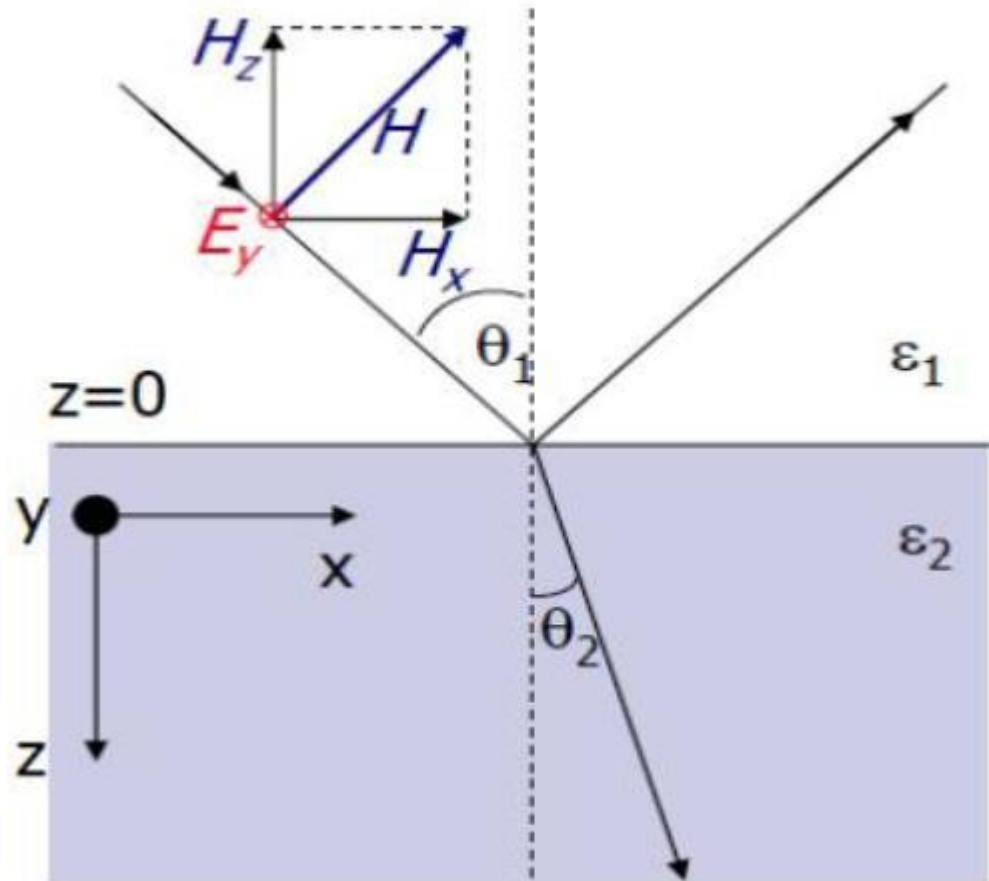


Figure (B.1) S-Polarization [80]

## 2. P-polarization or TM-polarization

The incident electromagnetic wave which is the magnetic field component  $H$  is perpendicular to the plane of incidence. This type of polarization is called P-Polarized. The component of the E-field which lies in the  $x-z$  plane is continuous as moving parallel to the plane of the interface. Here, all E-fields are in the parallel to incident plane, which is in the plane of the interface [80]. This case shown in Figure (B.2).

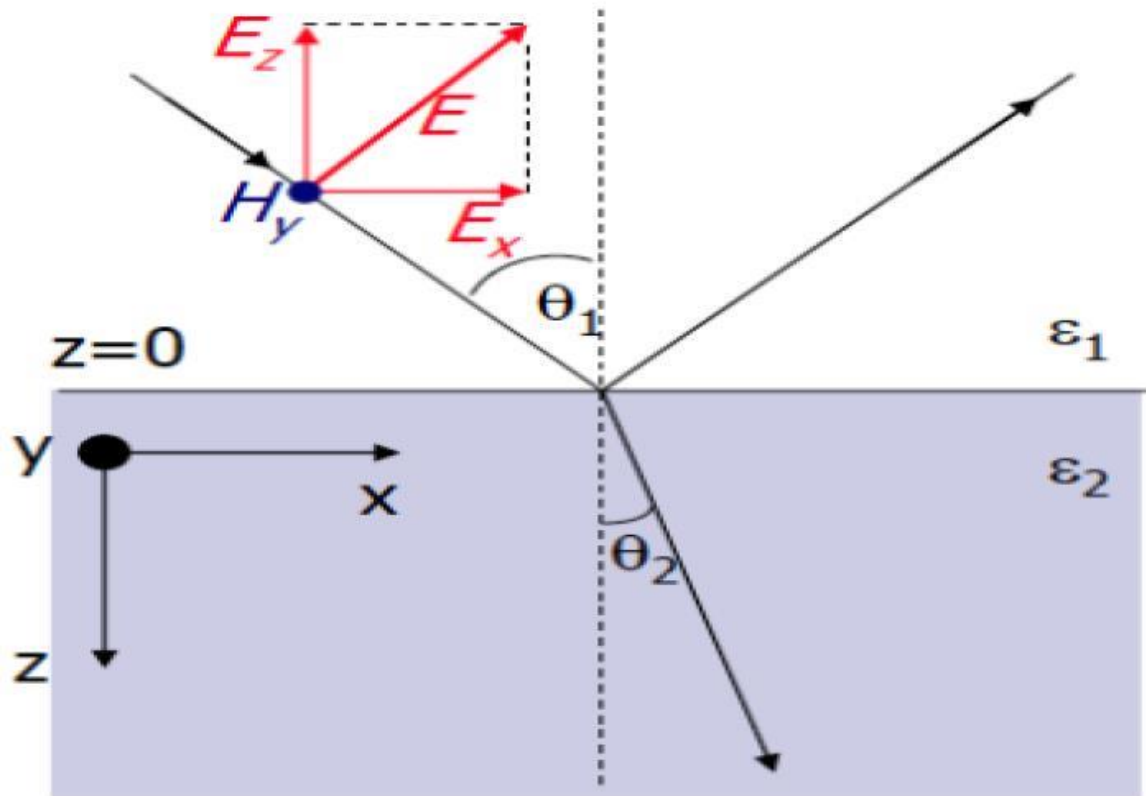
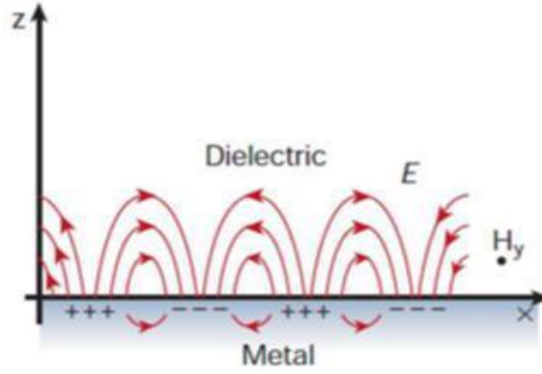


Figure (B.2) P-polarization [80]

## B.2 Existence of SPPs in Which Mode

The most simple geometry sustaining SPPs is that of a single, flat interface as shown in Figure (B.3) between a dielectric, non-absorbing half space ( $z > 0$ ) with positive real dielectric constant and an adjacent conducting half space ( $z < 0$ ) described via a dielectric function  $\epsilon_m(\omega)$ . The requirement of metallic character implies that  $\text{Re}[\epsilon_m] < 0$ . For metals, this condition is fulfilled at frequencies below the bulk plasmon frequency  $\omega_p$  needed to look for propagating wave solutions confined to the interface, i.e. with evanescent decay in the perpendicular  $z$ -direction.



**Figure (B.3) Geometry for SPP propagation at a single interface between a metal and a dielectric**

At first look at TM solutions. Using the equation set (A.42-A.44) in both half spaces yields [74].

For  $z > 0$  and

$$H_y(z) = A_d \exp(i\beta_x) \exp(-k_d z) \quad (B.1)$$

$$E_x(z) = iA_d \frac{1}{\omega \epsilon_0 \epsilon_d} k_d \exp(i\beta_x) \exp(-k_d z) \quad (B.2)$$

$$E_z(z) = -A_d \frac{\beta}{\omega \epsilon_0 \epsilon_d} \exp(i\beta_x) \exp(-k_d z) \quad (B.3)$$

For  $z < 0$  and

$$H_y(z) = A_m \exp(i\beta_x) \exp(k_m z) \quad (B.4)$$

$$E_x(z) = -iA_m \frac{1}{\omega \epsilon_0 \epsilon_d} k_m \exp(i\beta_x) \exp(k_m z) \quad (B.5)$$

$$E_z(z) = -A_m \frac{> \beta}{\omega \epsilon_0 \epsilon_d} \exp(i\beta_x) \exp(k_m z) \quad (B.6)$$

For  $z < 0$ .  $k_i \equiv k_z$  ( $i = m, d$ ) is the component of the wave vector perpendicular to the interface in the two media. and are the amplitude of electric and magnetic fields in the metal and dielectric, respectively. Its a

reciprocal value,  $Z = 1/|k_z|$ , which defines the evanescent decay length of the fields perpendicular to the interface [74].

This quantifies the confinement of the wave. Continuity of  $E_y$  and  $H_x$  at the interface requires that  $A_d = A_m$  and. Thus

$$k_d/k_m = -\varepsilon_d/\varepsilon_m \quad (B.7)$$

Note that with the convention of the signs in the exponents in (B.1-B.3) and (B.4-B.6), confinement to the surface demands  $\text{Re}[\varepsilon_m] < 0$  if  $\varepsilon_d > 0$ . The surface waves exist only at interfaces between materials with opposite signs of the real part of their dielectric permittivity, i.e. between a conductor and an insulator. The expression for  $H_y$  further has to fulfill the wave Equation Eq. (A.44), yielding [74]:

$$K_m^2 = \beta^2 - K_0^2 \varepsilon_m \quad (B.8)$$

$$K_d^2 = \beta^2 - K_0^2 \varepsilon_d \quad (B.9)$$

Combining Equations (B.8 and B.9) with Eq. B.7 will arrive at the central result of this section. The dispersion relation of SPPs propagates at the interface between the two half spaces that is:

$$\beta = K_0 \sqrt{\frac{\varepsilon_m \varepsilon_d}{\varepsilon_m \varepsilon_d}} \quad (B.10)$$

This expression is valid for both real and complex  $\varepsilon_m$ , i.e. for conductors without and with attenuation. For (TE) modes, the corresponding fields can be written as:

For  $z > 0$  and

$$E_y(z) = A_d \exp(i\beta_x z) \exp(-k_d z) \quad (B.11)$$

$$H_x(z) = -iA_d \frac{1}{\omega\mu_0} k_d \exp(i\beta_x) \exp(-k_d z) \quad (B.12)$$

$$H_z(z) = A_d \frac{\beta}{\omega\mu_0} \exp(i\beta_x) \exp(-k_d z) \quad (B.13)$$

For  $z > 0$  and

$$E_y(z) = A_m \exp(i\beta_x) \exp(-k_m z) \quad (B.14)$$

$$H_x(z) = iA_m \frac{1}{\omega\mu_0} k_m \exp(i\beta_x) \exp(k_m z) \quad (B.15)$$

$$H_z(z) = iA_m \frac{\beta}{\omega\mu_0} \exp(i\beta_x) \exp(k_m z) \quad (B.16)$$

A gain from the boundary condition (continuity of  $E_y$  and  $H_x$ ) at the interface may yield:

$$C (K_d + K_m) = 0 \quad (B.17)$$

Where  $C$  is a constant. As the surface waves require that  $\text{Re} [k_d] > 0$  and  $\text{Re} [k_m] > 0$ , so Eq. (B.17) is obtained only when ( $A_d = 0$ ) and because ( $A_d = A_m = 0$ ). It means no surface wave can exist for (TE) modes. As a result, existence of SPPs is only possible with TM polarization. The following flowchart shown in Figure (B.4) describes the equations, on which SPP is dependent.

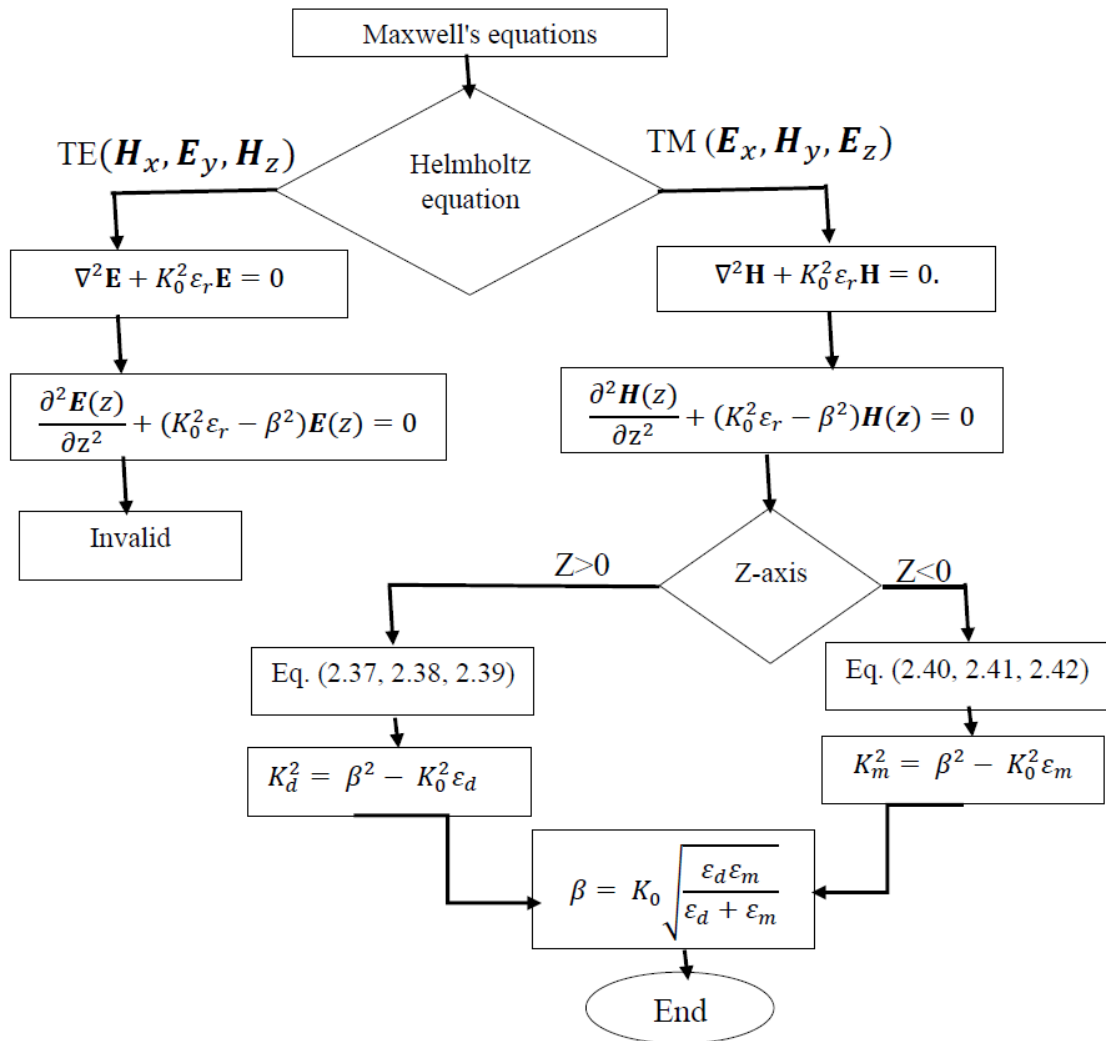


Figure (B.4) Flowchart for describing the equations, on which SPP is dependent

# **APPENDIX (C)**

## APPENDIX (C)

### SPPS EXCITATIONS MECHANISMS

#### C.1 SPPs Excitations Methods

The mechanisms of SPPs excitation are explained in the following sections.

##### A. Prism coupling

This technique, also known as attenuated total internal reflection, involves the coupling of the SPPs to the evanescent electro-magnetic field established upon total internal reflection of a light beam at a surface in an optically dense medium [74]. Two different geometries for prism coupling are possible as shown in Figure (C.1). In the Kretschmann configuration, the metal film is steamed on top of a glass prism. The film is illuminated through the dielectric prism at an angle of incidence greater than the angle of total internal reflection. The wave vector of light is increased in the optically dense medium [74]. At a certain angle of incidence where the in-plane component of the photon wave vector in the prism synchronizes with the SPP wave vector on an air-metal surface, resonant light tunneling through the metal film occurs and light is coupled to the surface polaritons as depicted in Equation (C.1) [74].

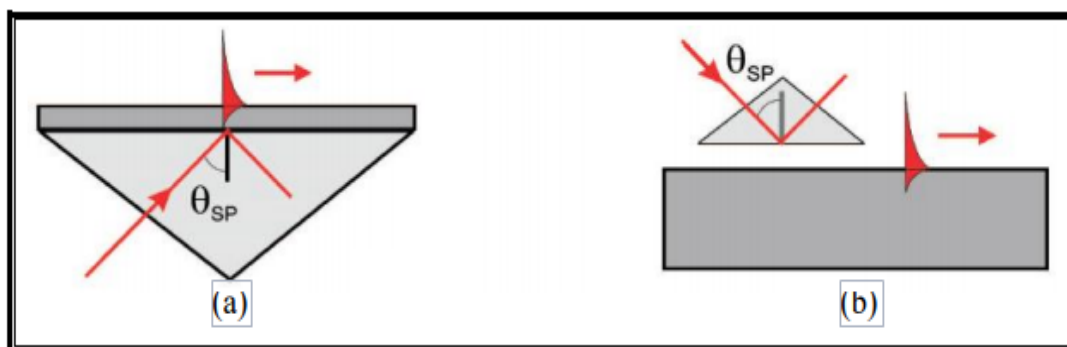


**Figure (C.1) Prism coupling: (a) Kretschmann, (b) Otto configuration [74]**

$$\beta = \frac{\omega}{c} \sqrt{\epsilon_{prism}} \sin \theta \quad (C. 1)$$

Under these resonant conditions, a sharp minimum is observed in the reflectivity from the prism interface as light can be coupled to SPPs with almost 100% efficiency [74]. When increasing the metal film thickness, the efficiency of the SPP excitation reduces as the tunneling distance increases [74]. SPP on an interface between the prism and metal cannot be excited in this geometry because the wave vector of SPP at this interface is larger than the photon wave vector in the prism at all incident angles. To be able to excite SPP on the internal metal interface, an additional dielectric layer with a refractive index smaller than of the prism should be deposited between the prism and the metal film [74]. In such a two-layer geometry, the photon tunneling through this additional dielectric layer can provide resonant excitation of SPP on the inner interface. Thus, both SPP modes (on the surface and the interface) can be excited in such a configuration at different angles of illumination [74].

When the thickness of metal (or surfaces of bulk metal) is increased, the Kretschmann configuration cannot be used, SPP can be excited in the Otto configuration. Here, the prism where total internal reflection happens is placed close to the metal surface, so that photon tunneling occurs through the air gap between the prism and the surface [74]. The resonant conditions are analogous to those in the Kretschmann configuration. This configuration is also favored when direct contact with the metal surface is unwanted, e.g. for studying the surface quality [74].

## B. Grating coupling

The mismatch in wave vector between the in-plane momentum  $k_x = k \sin\theta$  of impinging photons and  $\beta$  can also be overcome by using diffraction effects at a grating pattern on the metal surface [74]. For a one-dimensional grating of

grooves with lattice constant  $a$ , as depicted in Figure (C.2), phase-matching takes place whenever the condition in Equation (C.2) is fulfilled [74].

$$\beta = k \sin \theta \pm nG \quad (\text{C.2})$$

Where  $G = 2\pi/a$  is the reciprocal vector of the grating and  $n = 1, 2, 3, \dots$ . As with prism coupling, excitation of SPPs is detected as a minimum in the reflected light [74]

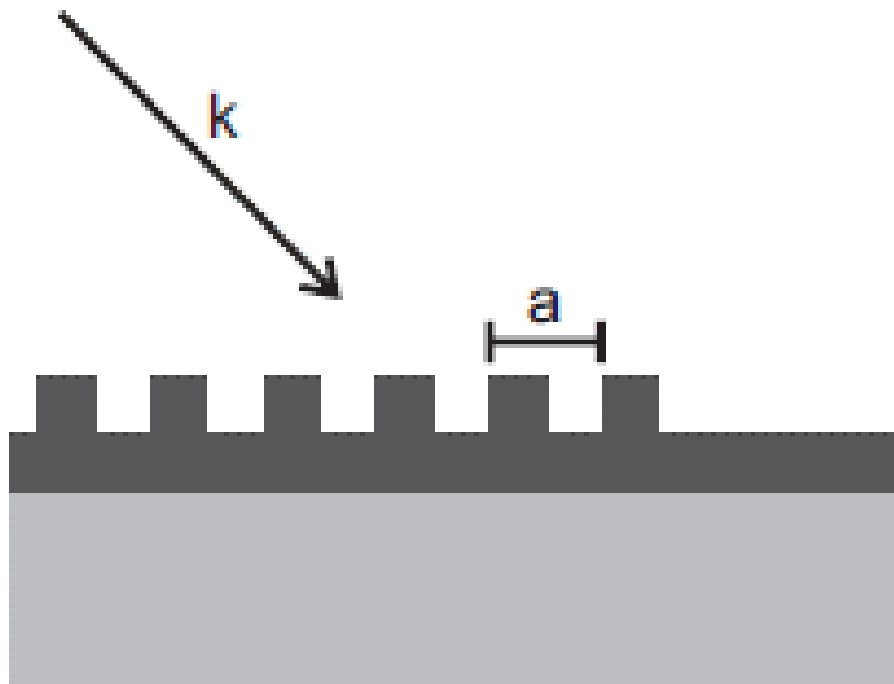
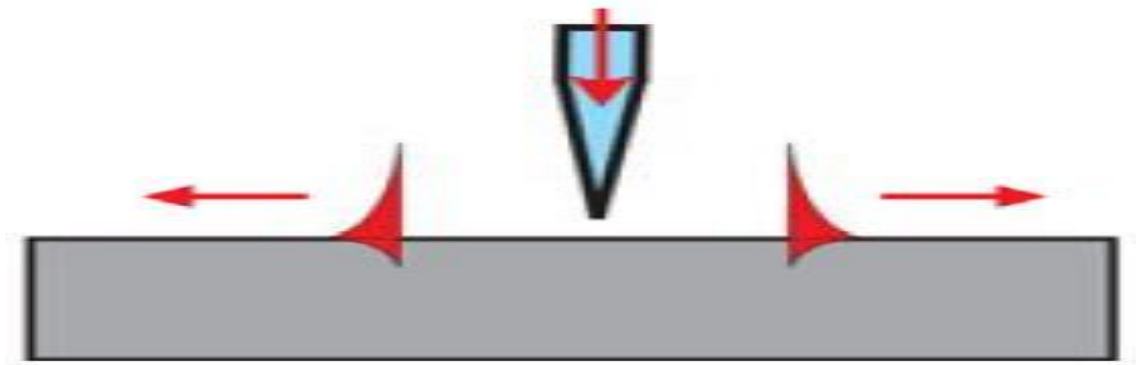


Figure (C.2) Grating coupling of a light with wave vector  $k$  impinging on a metal grating surface of period  $a$  [74]

## C. Near field excitation mechanism

In contrast to the macroscopic SPPs excitation schemes such as prism or grating coupling, near-field optical microscopy represents a point source to provide local excitation of SPPs over a subwavelength area [82]. In the typical near-field SPPs excitation configuration depicted in Fig. C.3, the illumination light from a small probe tip of aperture size ( $a$ ) ( $a \leq \lambda_{SPP} \leq \lambda_0$ ) has wave vectors  $k_0 \leq k_{SPP} \leq k$ , thus allowing a nearfield coupling of the phase-matched subwavelength aperture diffracted light into SPPs. Using such probes in near-field scanning optical microscopy (NSOM), SPPs at different positions of the metal surface can be locally excited.



**Figure (C.3) Excitation with a near-field scanning optical microscopy (NSOM)**

**Probe**

#### **D. Excitation using surface features diffraction**

When the surface is randomly rough in the near-field region, the diffracted light components possess all wave vectors and thus SPPs can be excited by conventional illumination without any special arrangements. Unlike using the diffraction grating, this is a non-resonant excitation. Similarly, SPPs can also be optically excited through light diffraction from surface features as shown in Figure (C.4) [83]

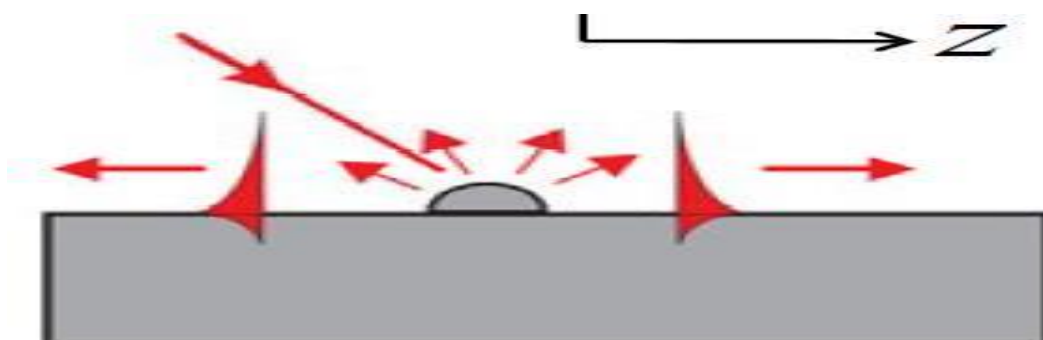


Figure (C.4) Diffraction on surface features [84]

### E. Excitation using highly focused optical beams

A typical setup of using highly focused optical beams for SPP excitation is sketched in Figure C.5. Instead of using a prism to satisfy the total internal reflection and SPP resonance condition, a high numerical index, which matched oil-immersion microscope objective, is brought into contact with the glass substrate, on which a thin metal film is deposited. Owing to the high numerical aperture of the lens, the broad angular spread of the focused illumination beam is large enough to have the resonance wave vector for SPP excitation at the metal-air interface. The highly focused illumination beam provides localized SPPs excitation over a diffraction-limited area

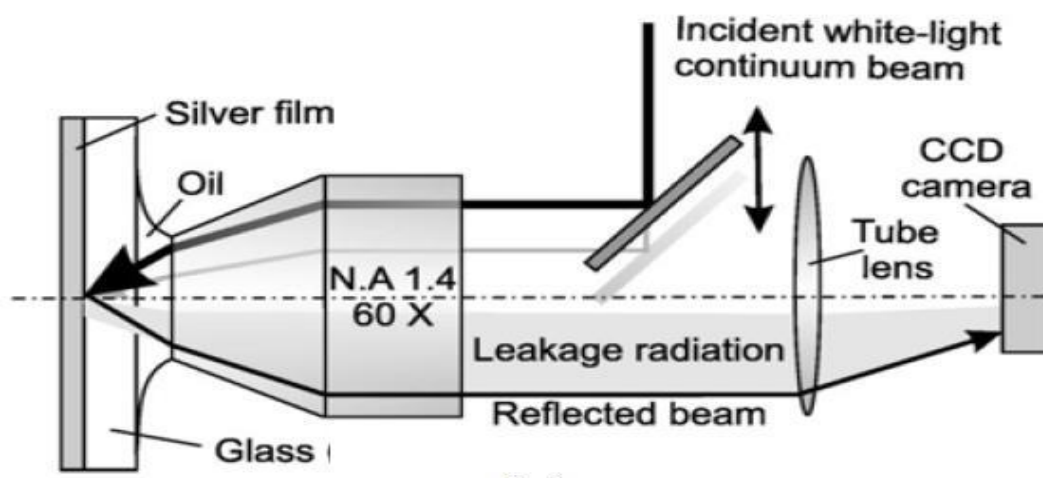


Figure (C.5) Excitation with highly focused optical beams [85]

# **APPENDIX (D)**

**APPENDIX (D)**

**PARAMETERS PERFORMANCE OF PLASMONIC**

**WAVEGUIDES**

**D.1 Definition of Confinement, Propagation Length, Quality Factor  
and Figure of Merit**

**A. Definition of confinement**

The rapid evolution of PWs with strongly confined SPPs demonstrated their ability to achieve the sub-wavelength of the conventional DWs [86]. Basically, the sub-wavelength confinement of light in the plasmonic waveguide is associated with engineering the evanescent fields outside the core of the waveguide. When an optical ray traverses a flat interface between two different dielectrics which can be seen in Figure (D.1 (a)), the light is partially reflected back to the core medium and is partly refracted in the cladding medium. Snell's law governs the angle of reflection and refraction. If  $n_1 > n_2$  ( $n_1$  and  $n_2$

are the refractive index of the two dielectrics) and the incident angle is greater than the critical angle  $\theta_c$ , as shown in Equation (D.1), light is totally reflected

back to the core medium and evanescently decays in the cladding medium. This process is known as total internal reflection (TIR)

$$\theta_c = \sin^{-1} \frac{n_2}{n_1} \quad (D.1)$$

However, if the cladding is a metal (e.g. Au or Ag), the SPP can be excited when certain phase matching conditions are met, and the energy from the excitatory light wave can be transferred to the free electron to form an SPP which spreads at the metal - insulator surface. SPP has a shorter wavelength than a free excited light. Moreover, a very small skin depth can be achieved

where the energy is rapidly degraded in the metal as can be seen in Figure D.1 (b). In a more complicated sandwich structure, the dielectric waveguide (Figure D.1 (c)) could not achieve sub-wavelength of light confinement because the diffraction limit phenomenon. For the plasmonic waveguide as shown in Figure (D.1 (d)), which can be described as a MIM structure. In this type of structure, the wavelength of the resonance, the thickness of the core layer and the skin depth of the evanescent waves in the cladding medium achieve the sub-wavelength light confinement in the waveguide core. While, the confinement factor in IMI PWs is less in MIM PWs as shown in the comparison between them

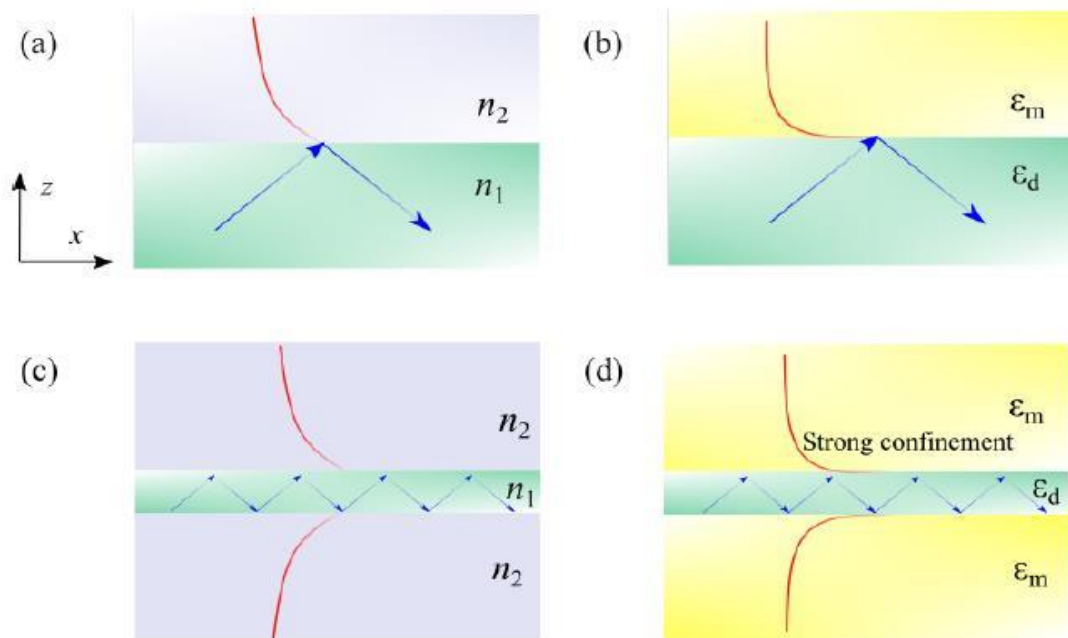


**Figure (D.1) (a) TIR happens when  $n_1 > n_2$  (b) In a One dimensional**

subwavelength light confinement in a metal-dielectric interface,  $\epsilon_m$  is the permittivity of the metal and  $\epsilon_d$  is the permittivity of the dielectric (c) Two-dimensional light confinement in a sandwiched DW (d) Two dimensional sub-wavelength light confinement in a sandwiched PW [87]

## B. Definition of propagation length

The propagation length is defined as the distance space where a mode can travel before the energy density decays to 1/e of its original value [88]. It is described by Equation (A.3) in Appendix A.

## C. Definition of quality factor

The quality factor is the ratio of twice propagation length to the resonance wavelength of SPPs. It is described in Equation (D.2) in addition to previous description in Equation (A.2).

$$Q_{SPP} = 2\pi L_{spp} / \lambda_{spp} \quad (D.2)$$

## D. Definition of figure of merit

The figure of merit (FoM) is a quality measure for surface plasmon waveguides. It is defined as benefit-to-cost ratio where the benefit is confinement and the cost is attenuation for a particular mode. It can be described by Equations below

$$FoM_{\text{confinment}} = \lambda_0 / \delta \quad (D.3)$$

Where  $\delta$  is a skin depth of the medium in meters

$$FoM_{\text{propagation}} = L_{spp} / \lambda_{spp} \quad (D.4)$$

Substituting Eq. (D.2) in Eq. (D.4), yields:

$$FoM_{\text{propagation}} = Q_{SPP} / 2\pi \quad (D.5)$$

When applying the definition of FoM, the result is the following equations:

$$FoM = FoM_{\text{confinment}} / FoM_{\text{propagation}} \quad (D.6)$$

$$FoM = (\lambda_0 / \delta) / (L_{spp} / \lambda_{spp}) = (\lambda_0 \lambda_{spp}) / (\delta L_{spp}) = (2\pi \lambda_0) / (\delta Q_{SPP}) \quad (D.7)$$

## الخلاصة

تعتمد أنظمة الاتصالات حاليًا على الأجهزة الإلكترونية أو الأجهزة الضوئية. مع ذلك ، فإن الحاجة المتزايدة لنقل ساعات أكبر من المعلومات بسرور نقل فائقة إضافة إلى تقليص الأجهزة ، جعل الأجهزة الإلكترونية والضوئية تواجه العديد من المحددات. نظرًا لأدائها وأحجامها غير المتطابقة ، فإنه من الصعب جدًا الحصول على معدل نقل بيانات عالي جدًا إضافة إلى تقليل حجم هذه الأجهزة التقليدية. لذلك طور الباحثون تقنية جديدة تدعى تقنية plasmonics والتي تعتبر بمثابة سقالة بين الأجهزة الضوئية و الأجهزة الإلكترونية كما أن تردددها يعادل تقريبًا تردد الضوء كما أن قدرتها على التعامل مع الأجهزة الإلكترونية المتناهية في الصغر عالية جدًا. تقنية Plasmonics هي مجال بحثي جديد و متطور في علم البصريات يتعامل مع ما يدعى surface plasmon polariton التي لها تطبيقات واسعة جدًا في مجال معالجة الإشارة الضوئية بالكامل. في هذا العمل ، تم استخدام التركيب التالي (عازل-موصل-عازل) وذلك لغرض تحقيق البوابات المنطقية plasmonic من التصميم المقترح الأساسي الذي يحتوي على حلقات نانوية وموجهات موجية مستقيمة من خلال توظيف ظاهرة التداخل البناء والاتلافي.

يحتوي التصميم الأساسي لهذا العمل على حلقة نانوية واحدة مع موجيين مستقيمين ، ويعتبر هذا التصميم بمثابة التصميم الأساسي للتصاميم المتبقية حيث من خلال إضافة حلقات نانوية جديدة و موجهات مستقيمة إلى التصميم الأساسي بنفس الأبعاد ، من خلال ذلك تم تحقيق البوابات المنطقة الضوئية ذات الإدخالين إضافة للبوابات المنطقة متعددة الإدخالات.

تم تحقيق بوابة NOT الضوئية بالكامل باستخدام هيكلين مختلفين للتحقيق في تأثير تغيير أبعاد الهيكل على نتائج الإخراج ؛ ابعاد التصميم الأول هو (180 نانومتر × 200 نانومتر) يعمل بطول موجي (1550 نانومتر) ، ابعاد التصميم الثاني هو (350 نانومتر × 350 نانومتر) ، حد عتبة الإرسال هي (0.5) لكل من الهياكل ، نتائج المحاكاة أظهرت فرق طفيف جدًا بين الهياكلين.

بوابات AND ، OR ، NAND ، NOR ، EX-OR ، EX-NOR تم تحقيقها بالكامل في التصميم الثالث من هذا العمل و بنفس ابعاد التصميم الثاني (350 نانومتر × 350 نانومتر) تعمل هذه البوابات بطول موجي (1550 نانومتر) و حد عتبة الإرسال (0.5).

البوابات المنطقة الضوئية متعددة الإدخالات AND و NAND و NOR و EX-NOR تم تحقيقها في التصميم الرابع من هذا العمل بأبعاد (400 نانومتر × 400 نانومتر) مع طول موجي (1550 نانومتر) و حد عتبة الإرسال (0.26).

أظهرت نتائج المحاكاة ان العوامل التي من شأنها التأثير على النتائج النهائية للتصميم هي ؛ الابعاد الهندسية للتصميم ، تناظرية التصميم ، انواع المعادن والعوازل المستخدمة في التصميم ، وتوزيع منفذ البوابات المنطقة الخاصة بالتصميم.

تم اختبار أداء البوابات المنطقية البلازمية البصرية المصممة بالكامل والتحقيق فيها استناداً إلى الإرسال المعياري ونسبة التباين بين الحالات المعاكسة للبوابة المحددة. تظهر نتائج المحاكاة انتقالاً طبيعياً ممتازاً في بعض الحالات المصممة مثل بوابة OR ، حيث يساوي الإرسال المقاس في هذه البوابة (127%) اي انه اعلى من النسبة الكلية (100%) و ذلك نتيجة لعملية التداخل البناء بين الإشارات الضوئية. من ناحية أخرى ، تظهر بعض البوابات المصممة نسبة تباين جيدة جداً بين حالة (ON) و (OFF) للبوابة المحددة والتي تعطي مؤشراً حول الأداء المثالي للبوابة ، على سبيل المثال ، نسبة التباين للإدخال المتعدد NAND البوابة هي (14.6 ديسيبيل).

تعتبر البوابات المنطقية الضوئية المقترحة هي لبنات البناء الأساسية في تحقيق الدوائر المتكاملة البصرية بالكامل ومعالجة الإشارات الضوئية بالكامل.



وزارة التعليم العالي والبحث العلمي

جامعة بغداد

معهد الليزر للدراسات العليا

# تصميم و تحليل البوابات الرقمية الضوئية البلازمونية في حزمة انظمة الاتصالات الضوئية

أطروحة مقدمة الى

معهد الليزر للدراسات العليا / جامعة بغداد / لاستكمال متطلبات نيل شهادة دكتوراه فلسفه في

الليزر / الهندسة الالكترونية والاتصالات

من قبل

حسن فلاح محسن فخرالدين

بكالوريوس هندسة الاتصالات - 2010

ماجستير هندسة الالكترونيك والاتصالات - 2014

باشراف

الاستاذ المساعد الدكتوراة تحرير صفاء منصور